OPTIMIZATION OF PHOTOLUMINESCENCE-FOLLOWING ELECTRON-TRANSFER WITH TRIS(2,2'-BIPYRIDYL)OS(III) AND APPLICATION TO THE DETERMINATION OF DOPAMINE, SEROTONIN AND CARBIDOPA IN BRAIN MICRODIALYSATE

by

Moon Chul Jung

BS, Seoul National University, Korea, 1995

MS, Seoul National University, Korea, 1997

Submitted to the Graduate Faculty of

Arts and Sciences in partial fulfillment

of the requirements for the degree of

Doctor of Philosophy

University of Pittsburgh

2006

UNIVERSITY OF PITTSBURGH

FACULTY OF ARTS AND SCIENCES

This dissertation was presented

by

Moon Chul Jung

It was defended on

July 1, 2005

and approved by

Adrian C. Michael

David H. Waldeck

Jeffrey K. Yao

Stephen G. Weber
Dissertation Director

OPTIMIZATION OF PHOTOLUMINESCENCE-FOLLOWING ELECTRON-TRANSFER WITH TRIS(2,2'-BIPYRIDYL)OS(III) AND APPLICATION TO THE DETERMINATION OF DOPAMINE, SEROTONIN AND CARBIDOPA IN BRAIN MICRODIALYSATE

Moon Chul Jung, PhD

University of Pittsburgh, 2006

Biogenic monoamines such as dopamine and serotonin play important roles as major neurotransmitters. Simultaneous determination of the concentration changes is thus crucial to understand brain function. We have developed a capillary HPLC combined with a redox-based postcolumn reaction method, the photoluminescence-following electron-transfer (PFET) technique, for the determination of certain neurotransmitters and their metabolites.

Tris(2,2'-bipyridine)osmium was the postcolumn oxidant. The spectroscopic properties of the oxidant changed upon a redox reaction. The change was measured using a laser-induced fluorescence setup to quantify electrochemically active analytes from the chromatographic eluent. Spectroscopic and electrochemical properties of the complex, along with its reaction kinetics were studied in detail to optimize the postcolumn reaction efficiency. The complex was capable of oxidizing and detecting catechols. The spectroscopic properties of the complex were not very advantageous, but careful control of the detection system and reaction conditions enabled sensitive detection of monoamine neurotransmitters in rat brain dialysates. The extent of the postcolumn reaction was predicted by the second-order reaction kinetics in fluidic conditions and experimentally verified. Efficient mixing and reaction of the postcolumn reagent was achieved in a radial diffusion mixer without significant band broadening.

The optimized system was capable of detecting biogenic monoamines, such as dopamine, serotonin and 3-methoxytyramine, at about 200 pM concentrations in 500 nL samples. Typical analysis time was less than 10 min. We used this method to monitor neurotransmitter concentrations in rat brain dialysates when the rat was given tetrodotoxin or nomifensine. Changes in neurotransmitter concentrations were observed. Another application of this method was detecting carbidopa in rat brain microdialysates, to study the damage in brain tissues by a microdialysis probe. We observed that carbidopa was present in striatal dialysates after the rat was given i.p. injection of carbidopa.

TABLE OF CONTENTS

LIST OF TABLES

LIST OF FIGURES

PREFACE

"I seem to have been only like a boy playing on the sea-shore, and diverting myself in now and then finding a smoother pebble or a prettier shell, whilest the great ocean of truth lay all undiscovered before me." – Sir Isaac Newton

As I look back upon my years in graduate school, I realize it was a great time to learn a variety of new things. At the same time I realize how little my understanding on nature is, compared to the great ocean of truth. The most valuable thing I've learned and experienced in graduate school is not only scientific facts, but the way of learning and thinking.

In this regard, I would like to thank to my research advisor, Prof. Stephen Weber. It was a great pleasure to have a chance to work with him. I learned many things from him. His teachings included not just chemistry, but most importantly, logical thinking. His patience allowed time for me and my fellow graduate students to think over problems inside out. The time of pondering was not fun at first, but it later provided a lot of insight. The fruits of pondering were openly discussed in the group meeting hours, which were more of a brainstorming time. With his vast knowledge of science he always provided proper guidance and little discouragement. So we could walk away from his office with whole new perspectives (and most likely a valuable key to the answer). His love of science and life (including blues music) is another teaching from him which I appreciate a lot.

I also would like to thank to all the Weber group members – fellow graduate students, postdocs and undergraduates: especially Michele Monaco, Xu Zhang, Amy Beisler, Rong Meng, Hong Zhao, Imants Zudans, Brad Lambie and Yifat Guy. They have been good friends in many ways. We were more of a family rather than a research group. The warm and caring atmosphere is something I cannot forget.

I also would like to thank to Prof. Adrian Michael and his research group. The collaboration with the Michael group was surely a productive and fun experience. I extend my gratitude to Prof. David Waldeck and Dr. Jeffrey Yao for their valuable time and comments as my dissertation committee members. People from the machine shop, electronic shop and glass shop gladly shared their expertise with me. Most of my research would have been impossible without their help.

I am truly indebted to so many people in the Pittsburgh Korean community. Although I was several thousand miles away from my home country, Korea, I felt at home when I was with them.

Finally, I would like to thank my parents for their continued support for my entire life.

1. Introduction

The history of the chromatographic detector dates back to the first days of liquid chromatography when Tswett first reported the separation of plant pigments.[1, 2] His detector was simple human eyes, which observed and confirmed the successful separation of the analytes by differences in color. Visual observation as a chromatographic detection is simple yet convenient for many analytes. This detection technique is still widely used in thin layer chromatography. However, the utility of human eyes as a systematic chromatographic detector is limited: human eyes only respond to a certain wavelength rage. They do not easily distinguish slight changes in light intensity, which is essential in quantitative measurements.

Early quantitative liquid chromatographic detection was achieved by offline analysis. Collected fractions were then analyzed, or distilled to collect the analytes. This practice is not only time-consuming, but also very insensitive. Resolution may be limited by the fraction collector.

Online liquid chromatographic detection was made possible when the conductivity detector[3] and refractive index detector[4, 5] became available. These detection methods are categorized as bulk property detectors. Unlike detectors sensitive to the specific solutes, the bulk property detectors measure the changes in the physical property of the column effluent. Changes caused by dissolved solute are generally very small, especially when the solute concentration is low. Bulk property detectors are sensitive to environmental changes such as ambient temperature fluctuations and flow rate fluctuations. Thus the sensitivity of the bulk property detector is generally not very high.[5]

Nevertheless, the development of online detectors provided feedback to the advancement of the chromatographic system. The availability of online detectors enabled the precise

measurements of solute peak shapes which could be compared to theoretical predictions. Such findings served as the basis for the more efficient chromatography. Increased efficiency decreased peak volumes and increased peak capacity. Thus the increased performance of chromatographic system in turn requires the development of a more sensitive detection method with a small inner volume. The development of a detector and that of the chromatographic system always go hand in hand.

One possible way to improve detection sensitivity and selectivity is by coupling chromatography and chemical reactions. A chromatographic sample can be converted to a product which yields high response to a detector. The selectivity of the detector can be also improved from chemical reactions, where only a certain set of sample components are reacted. Such chemical reactions can be coupled to chromatography either before the separation (precolumn) or after (postcolumn). Precolumn reaction is often preferred due to its easy implementation in a chromatographic system. However, precolumn reaction may change the chromatographic properties of the analytes. Large molecules with multiple reaction sites such as proteins or peptides yielded several reaction products, resulting in multiple chromatographic peaks.[6, 7] Postcolumn reactions do not have such problems. One concern with postcolumn reactions is that reactions can compromise the chromatographic efficiency, as extra volume is added after the separation.

The dissertation is mainly focused on the optimization and the application of a sensitive and selective postcolumn detection method coupled to a capillary high-performance liquid-chromatographic (capillary HPLC) system. The postcolumn reaction used in this study is the photoluminescence-following electron-transfer technique (PFET). This technique is a combination of two widely used detection techniques for capillary HPLC: electrochemical

detection and laser-induced photoluminescence detection. PFET detection is based on the electrochemical activity of analytes. The analytes react homogeneously with a soluble oxidant. The spectroscopic properties of the oxidant are changed upon reduction. The changes include the presence of photoluminescence at the reduced state, which is measured after laser excitation. The PFET detection technique has several advantages over electrochemical detection: the electron-transfer reaction is in liquid phase, thus no surface fouling compromises the stability of detection method.

The mutual dependency of the detector technology and the chromatography system development is also valid here. The PFET technique was initially applied to a small bore column HPLC system (1 mm in column diameter) at a flow rate of 50 μL/min.[8-10] The theoretical calculation revealed that the efficient mixing of the PFET reagent and the analytes occurs in a much smaller volumetric flow rate condition. Thus the HPLC system was naturally transitioned into a capillary HPLC system, with 100 μm id capillary columns at a flow rate of 1 μL/min.

As the total fluidic volume of the system gets small, the effect of a postcolumn volume on the chromatographic efficiency becomes large. The postcolumn capillary Taylor reactor, used in our system to homogenize the PFET reagent and the chromatographic analytes, is not an exception. Earlier papers by Beisler et al. describe the performance and the band-broadening effect of the reactor when the reaction is relatively fast.[11, 12] Chapter 3 of the dissertation is an extension of that work by taking a kinetically slow reaction into consideration. The length of the reactor was minimized to achieve a reasonable PFET reaction by both theoretical analysis and experiments. An optimized reactor configuration was found for the detection of catecholamines.

It became obvious from the reactor optimization process that the properties of the PFET reagent also influence the detector performance. The reagent in this study,

tris(2,2'-bipyridyl)osmium(III) serves as an oxidant and a luminophore. The electrochemical and optical properties of the reagent were examined. Reaction conditions, such as pH and temperature, were also optimized to decrease PFET detection limits. The findings on the optical property were applied to the development of optical setup. The optimization on the reaction condition specific to the reagent is discussed in Chapter 2. The detailed aligning procedure for the detection optics is presented in Appendix.

The optimized detector was applied to the detection of biological monoamines such as dopamine, serotonin and 3-methoxytyramine in rat brain dialysates samples, which is discussed in Chapter 4. The chromatographic separation was optimized by changing the solvent strength and the concentration of ion interaction reagent. The performance of the PFET system was compared with fluorescence detection and electrochemical detection in terms of the mass/concentration sensitivity, sample volume, analysis time and the variety of analytes detected on a single run.

Chapter 5 describes the application of the PFET system in answering the biologically challenging questions. Microdialysis sampling in brain was so far believed to be semi-invasive.[13, 14] Recent studies shows that the brain tissue damage caused by inserting the microdialysis probe depends on many factors: the amount of recovery time after the insertion, probe dimensions, probe material, perfusion fluid and so on.[15, 16] The damage in rat brain tissues is monitored in this study: a synthetic drug, carbidopa, which is normally absent in brain is injected into the rat body. When there is no damage to the brain tissue, the drug does not enter into brain. Microdialysis samples were analyzed to determine quantitatively carbidopa in rat brain. The carbidopa concentrations in dialysis samples were analyzed with a temporal resolution of 10 min to monitor its time-dependent change.

2. Use of Tris(2,2'-bipyridine)osmium as a Postcolumn Photoluminescence-Following Electron-Transfer Reagent for Postcolumn Detection in Capillary High-Performance Liquid Chromatography

This work is published in *Anal. Chem.*, **2006**, *78*, 1761-1768;

2.1. Abstract

The photoluminescence-following electron-transfer (PFET) technique, developed in our laboratory, is a sensitive chromatographic detection method for oxidizable analytes. Because the oxidations are homogeneous, the technique avoids the problem of electrode fouling. A liquid-phase oxidant reacts with the electrochemically active analytes after separation, becoming capable of photoluminescence. Laser-induced photoluminescence is measured to quantitate the analytes. Thus, the electrochemical properties of the oxidant determine the detection selectivity and the spectroscopic properties define the sensitivity.

The properties of tris(2,2'-bipyridine)osmium (**1**) were investigated for use as the liquid-phase oxidant in the PFET system. The redox potential of the complex is less positive than that of tris(2,2'-bipyridine)ruthenium (**2**), thus on-line generation of $\mathbf{1}^{3+}$ by reaction with PbO_2, and selective oxidation of catechols by $\mathbf{1}^{3+}$ was possible. The mild oxidizing power of $\mathbf{1}^{3+}$ led to lower background signal (compared to $\mathbf{2}^{3+}$) when mixed with acidic mobile phases. Photoluminescence from $\mathbf{1}^{2+}$ was much weaker than that from $\mathbf{2}^{2+}$, nonetheless the system achieved subnanomolar detection limits for dopamine, 3-methoxytyramine and serotonin. Dopamine and 3-methoxytyramine in rat brain striatal dialysates were determined before and after the injection of nomifensine.

The pH of the mobile phase can govern the detection selectivity, since oxidation of most organic is accompanied by proton-transfer. Reaction of **1** with catechols showed pH-dependent sensitivity resulting from pH-dependent reaction rate changes. Since the reaction rate is also temperature dependent, increased temperature at the mixer resulted in higher sensitivity.

However, the noise level also increased at elevated temperature, thus the detection limit did not improve.

2.2. Introduction

High-performance liquid chromatography with electrochemical detection (HPLC-EC) is a sensitive and selective technique for the quantitative determination of small biomolecules.[17] It has been widely used to determine peptides,[18] proteins,[19, 20] and neurotransmitters.[21] One advantage of HPLC-EC is its sensitivity and selectivity. A limitation of HPLC-EC comes from the fact that the reaction always occurs at the electrode surface. Substances in biological samples compromise the electrode surface. Attention to the surface has been a major issue in HPLC-EC.

There are several ways to create an optical signal from an analyte's electrochemical activity. Chemiluminescence detection is an alternative means of obtaining a quantitative signal from a redox reaction. Oxidizable drugs,[22-26] amines,[27, 28] and other species[29-31] yield signals. A chemical derivatization step before the chemiluminescent reaction permits determination of neurotransmitters and related species such as catecholamines and hydroxyindoles.[32-34]

Similarly, electrogenerated chemiluminescence (ECL) has been successful in detection schemes, for example for ascorbate,[35, 36] amines,[37-39] and biopolymers.[40, 41] The mechanism of the production of ECL in schemes based on ruthenium complexes is now understood.[42, 43] This mechanistic understanding shines light on the strong dependence of the ECL signal on the analyte properties. A clever way to use ECL that avoids this problem is to require analytes and an ECL-active solution to compete for current.[44] This microfluidic based approach essentially replaces the current measurement in an electrochemical detector with ECL. While simpler from an instrumentation point of view than electrochemical detection, it suffers from poor sensitivity.

The photoluminescence-following-electron-transfer (PFET) technique, developed in our laboratory[9, 10], is another useful detection scheme for generating an optical signal from electrochemically active molecules. A fluid stream containing a homogeneous oxidant is mixed with chromatographic effluent in a diffusion-controlled mixer.[11, 12, 45] The oxidant is subsequently reduced to produce photoluminescence upon optical excitation, which is measured quantitatively and recorded. The chemistry involved is much simpler than in the techniques of chemiluminescent detection or ECL described above. PFET does not include derivatization steps, only an electron transfer reaction. Thus, the optically detected species in PFET is always the same: namely, the reduced form of the oxidant.

To date PFET applications to peptides[10] and explosives[9] have used $Ru(bpy)_3^{3+/2+}$ (bpy = 2,2'-bipyridine) as the reagent/photoluminescor. While having certain advantages, it is by no means perfect. It has a rather long lifetime, and thus is susceptible to quenching.[46] This could lead to inaccuracy when using it as the basis for PFET. It is also an aggressive oxidant. The selectivity advantage of electrochemical detection is most obvious at modest potentials. The analogous situation must hold for PFET. Electrochemical detection has the potentiostat; PFET does not. It is imperative to demonstrate alternatives to the aggressive $Ru(bpy)_3^{3+}$ as a reagent.

Tris(2,2'-bipyridine)osmium ($Os(bpy)_3$, **1**) may be a valuable PFET reagent. It has a fast electron-transfer rate and is stable in oxidation state (III) and (II). As a result, it has been used as a mediator[47-50] for many electrochemical studies. It happens to be ECL active, as well.[51, 52] Like many similar bipyridine or phenanthroline metal complexes, **1** changes its spectroscopic properties according to the oxidation state: $\mathbf{1}^{2+}$ is photoluminescent while the $\mathbf{1}^{3+}$ complex is not. Interestingly, $\mathbf{1}^{2+}$ has a similar absorbance spectrum to $Ru(bpy)_3^{2+}$ ($\mathbf{2}^{2+}$) so that the same laser line can be used to excite both complexes. Also favoring its application to PFET is its short

lifetime[53] which will minimize quenching interferences. Most importantly, its reduction potential is about 0.4 V less positive than the analogous ruthenium complex. Therefore, this complex seems to fulfill a need for a less aggressive reagent than $\mathbf{2}^{3+}$. Unfortunately, $\mathbf{1}^{2+}$ is a very poor luminophore. Furthermore, its luminescence occurs in the far red region of the electronic spectrum necessitating the use of a photocathode with a low work function. Photomultipliers based on low work-function photocathodes, of course, suffer from higher dark current than their higher work function counterparts. Thus it is not clear at the outset that $\mathbf{1}^{3+/2+}$ will be an effective PFET reagent. The purpose of this chapter is to determine the utility of $\mathbf{1}^{3+/2+}$ as a PFET reagent.

2.3. Experimental Section

2.3.1. Reagents

All chemicals from commercial sources were used as received without further purification except where noted. Reagent and sources were as follows: trifluoroacetic acid (TFA) from Acros (Geel, Belgium); monochloroacetic acid from Mallinckrodt (St. Louis, MO); acetonitrile, 2-propanol, and sodium acetate from EMD (Gibbstown, NJ); 1-propanol, lead dioxide, sodium hydroxide, glacial acetic acid, and disodium EDTA from J.T. Baker (Phillipsburg, NJ); ruthenium(III) chloride, tris(2,2'-bipyridine)ruthenium dichloride hexahydrate, glycine and sodium perchlorate from Aldrich (Milwaukee, WI); 4,7-diphenyl-1,10-phenanthroline, 4,7-bis(4-sulfophenyl)-1,10-phenanthroline from GFS Chemicals (Powell, OH); chloral hydrate, nomifensine, dopamine (DA) hydrochloride, 3, 4-dihydroxyphenylacetic acid (DOPAC), serotonin (5HT) hydrochloride, 3-methoxytyramine (3MT) hydrochloride, 5-hydroxyindole-3-acetic acid (5HIAA) and sodium 1-octanesulfonate from Sigma (St. Louis, MO). Maleic acid is from Fisher (Fair Lawn, NJ) and

recrystallized once from water. Sodium perchlorate was recrystallized from methanol once to remove chloride. All aqueous solutions were prepared with deionized water (18.2 MΩ resistivity) from a Millipore Milli-Q Synthesis A10 system (Billerica, MA).

2.3.2. Preparation of metal polypyridyl complexes

1, tris(4,7-diphenyl-1,10-phenanthroline)ruthenium(**3**), and tris(4,7-bis(4-sulfophenyl)-1,10-phenanthroline)ruthenium(**4**) were prepared and recrystallized in our laboratory according to previously reported procedures.[54, 55] A slight modification of the procedure was required for **4** due to its solubility. 4,7-bis(4-sulfophenyl)-1,10-phenanthroline was dissolved in water to be added to the ethanol solution of $RuCl_3$. The reaction product was recrystaillized from a methanol-ethanol mixture. Figure 2-1 shows the complexes. Crystals of complexes were dissolved in acetonitrile(**1**, **2** and **3**) or in water(**4**), to make 1.0 mM stock solutions. Aliquots of the stock solution were diluted in an acidic electrolyte solution (0.2% TFA and 0.1 M $NaClO_4$ in acetonitrile or water) to prepare the PFET reagent solution. The resulting solution was used accordingly after passing a disposable 0.45 μm PTFE/PP syringe filter (Chrom Tech, Apple Valley, MN).

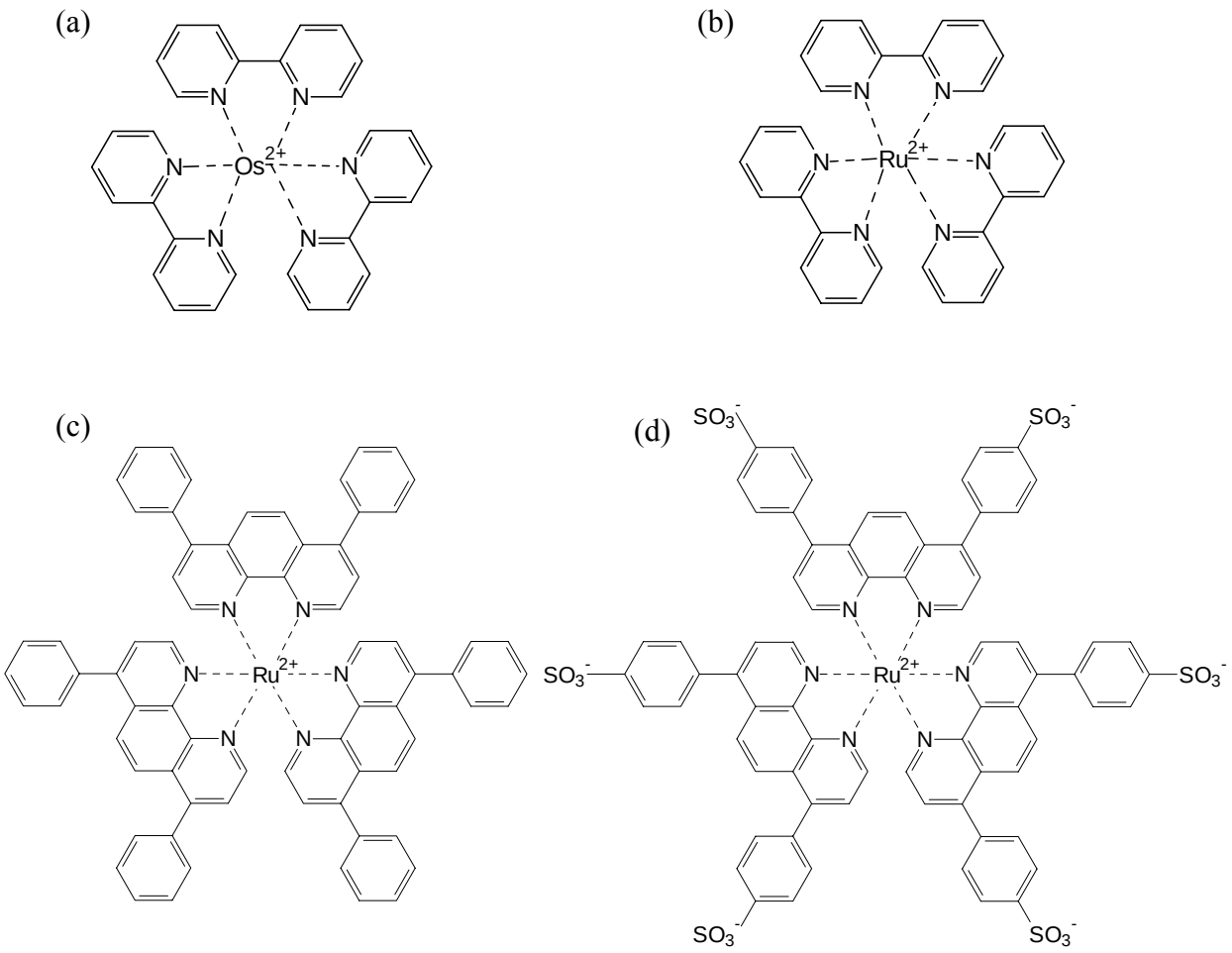

Figure 2–1. Bipyridine and phenanathroline complexes.
(a) 1^{2+}, (b) 2^{2+}, (c) 3^{2+} and (d) 4^{2+}

2.3.3. Absorbance and photoluminescence measurements

The absorbance of each complex was measured using an Agilent 8453 UV-visible spectrometer (Agilent Technologies, Wilmington, DE), and corresponding photoluminescence was measured using a fluorometer (Jobin-Yvon, Edison, NJ). Typically, 20 μM complexes in the acidic electrolyte solutions are mixed with 0.1% TFA in water (50:50) to mimic the postcolumn reaction in a chromatographic system. The final concentration of the complex is thus 10 μM. To

check the reactivity with a solid oxidant, PbO_2, complexes were mixed with PbO_2 particles and stirred. The resulting slurry was passed through a syringe filter to retain the PbO_2 particles, and absorbance and photoluminescence were measured.

2.3.4. Cyclic voltammetry

All cyclic voltammograms were obtained using an AIS electrochemical analyzer (AIS model DLK-100A, Flemington, NJ) with a glassy carbon working electrode and a Ag/AgCl reference electrode. All analytes were prepared in the acidic electrolyte solution (in acetonitrile)-water mixture (50:50) as described before. The analyte concentrations were 1 mM. Each cyclic voltammogram was obtained at the scan rate of 50 mV/sec.

2.3.5. Stability of $\mathbf{1}^{3+}$

10 μM $\mathbf{1}^{2+}$ in the acidic electrolyte solution (acetonitrile) was mixed with PbO_2 particles, and then transferred into quartz cuvettes. An aliquot was prepared by taking the supernatant (without filtration), and another by passing it through the disposable syringe filter (with filtration). UV-vis absorption spectra were measured for 3000 sec with an interval of 10 sec. Absorbances at 480 nm were corrected for simple baseline shifts by subtracting the absorbance at 800 nm. Corrected absorbances at 480 nm were compared to the absorbance of $\mathbf{1}^{2+}$ at 480 nm to calculate the amount of reconversion from $\mathbf{1}^{3+}$ to $\mathbf{1}^{2+}$.

The pH dependent reversion of $\mathbf{1}^{3+}$ was measured in a flow-injection system. $\mathbf{1}^{3+}$ was prepared on-line by passing a solution of $\mathbf{1}^{2+}$ through a packed bed of PbO_2, which was mixed

with buffers at various pH. Mixtures of monochloroacetic acid and acetic acid (combined concentration of 100 mM) made pH 2.00 to 3.00 buffers. The pH of this mixture was adjusted with concentrated sodium hydroxide solution. For pH 4.00 to 5.00 buffers, 100 mM sodium acetate solution was titrated with glacial acetic acid. 100 mM maleate solutions were titrated with concentrated sodium hydroxide solution to adjust pH 6.00 to 7.00. A 100 mM glycine solution with concentrated sodium hydroxide was used to make a pH 9.00 buffer.

2.3.6. Second-order reaction rate constant measurements

The procedure to measure the second order reaction rate constants of $\mathbf{1}^{3+}$ with solutes has been reported.[45] Briefly, clear filtrate of $\mathbf{1}^{3+}$ was mixed with reactant solutions of the same volume in the fluorometer at room temperature. The reactant solutions contained either dopamine or DOPAC at pH ranging from 3.00 to 5.00. pH of the solutions are buffered with monochloroacetic acid/acetic acid (pH 3.00 and 3.50) or with acetic acid (pH 4.00 to 5.00). The mixture was optically excited at 470 nm, and the photoluminescence was monitored at 722 nm for 60 s with an integration time of 0.01 s. Traces of signal intensity versus time were converted to product-time traces and fit into a second-order reaction kinetics model with the reaction rate constant as a variable. The SOLVER function in the Microsoft Excel spreadsheet found the optimum value of the variable, which gave the minimum sum of squared deviations.

.

2.3.7. Chromatographic system

Two HPLC pumps (Waters 590 and 600/626S, Milford, MA) or a syringe pump (ISCO 100DM, Lincoln, NE) with simple tees as flow splits delivered solutions at ~1 μL/min. The flow rate from each source was frequently checked by measuring the volume of solutions delivered in a specific time, to ensure the correct flow rate was maintained during experiments.

Homemade capillary columns were packed by previously described techniques[56] using 100 μm i.d., 360 μm o.d. fused-silica capillaries as the column blank. The column was slurry packed with reversed-phase particles at 3000-4000 psi using a constaMetric III metering pump (LDC Analytical, Riveria Beach, FL)[11] and connected directly to an Upchurch loop microinjector (Oak Harbor, WA), which introduced 0.5 μL of each sample into the column.

A capillary Taylor reactor (CTR) was used to mix the chromatographic effluents and the postcolumn PFET solution. They were prepared according to the previously reported procedure.[11, 45, 57] The ends of two 18-μm tungsten wires (Goodfellow, Devon, PA) were each threaded into two 50-μm fused-silica capillaries (Polymicro Technologies, Phoenix, AZ). The other ends were both threaded into another 50-μm fused-silica capillary to form a Y-shaped device. The third capillary was transparent coated. The junction between three capillaries was placed in a piece of dual shrink/melt tubing (Small Parts, Miami Lakes, FL). After sufficient heating, the device was allowed to cool and the tungsten wires were removed to create fluid conduits of 18-μm diameter between 50-μm capillaries. It is important to gently tug the wire at the initial stages of the cooling process, or else the wire will stick. The reaction length was set at 8 cm from the confluence according to the previous study.[45]

2.3.8. Optical detector setup

Figure 2-2 is the diagram of optical detector setup. A laser beam from a 30-mW variable-power blue-line argon ion laser (Cyonics/Uniphase 2201-30BL, San Jose, CA) passed through a 488-nm band-pass filter and was focused onto an optically transparent capillary (Polymicro Technologies, Phoenix, AZ). Photoluminescence from $\mathbf{1}^{2+}$ was measured using an epifluorescence: a microscopic objective lens (Carl-Zeiss, Plan Neofluar 20x, NA 0.5, Thornwood, NY) focused the optical emission from the capillary and a combination of a dichroic mirror (cutoff at 500 nm) and optical filters (a 600-nm long-pass filter and a 750-nm band-pass filter, angle tuned) allowed the photoluminescence into an IR-sensitive photomultiplier tube (Hamamatsu R374, Bridgewater, NJ). A Keithley 6485 picoammeter (Cleveland, OH) converted photocurrent from the photomultiplier tube to a dc voltage signal. An IBM-compatible computer with a PeakSimple Chromatographic Data System (SRI Instruments, Torrance, CA) collected the dc signal after a 0.4-Hz eight-pole low-pass filter (Wavetek 852 Dual filter, San Diego, CA).

2.3.9. Chromatographic conditions for separation of catechols and indoleamines

Separation of catechols and 5-hydroxyindoleamines was achieved using an acidic mobile phase: aqueous buffer containing 100 mM sodium acetate, 0.15 mM disodium EDTA, and 0.15 mM sodium salt of 1-octanesulfonic acid (pH was adjusted to 4.70 with glacial acetic acid) was mixed with methanol (90:10, v/v) and passed through a Nylon filter with 0.45 μm pores (Osmonics, Minnetonka, MN). The column was slurry packed to 9.5 cm with 3 μm AlltimaC_{18} (Alltech, Deerfield, IL) reversed phase material.

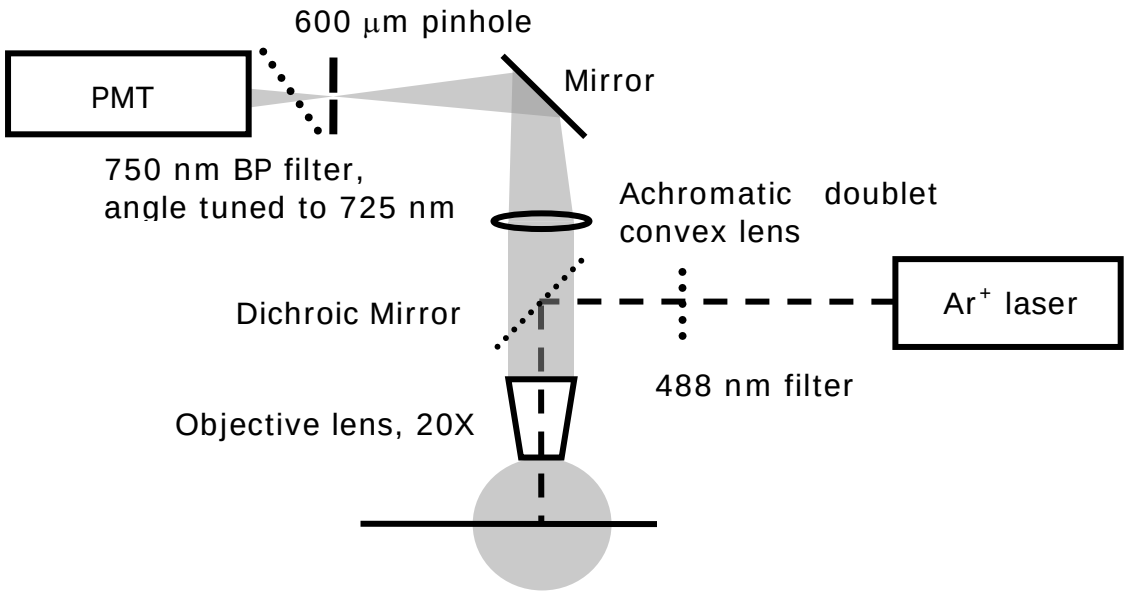

Figure 2–2. Optical parts of the detection system.

2.3.10. Chromatographic standard samples

Stock solutions of 1.0 mM catechols and standards were prepared in 0.1 M acetic acid and stored frozen. The frozen stock solutions were thawed before each use and were diluted to desired concentrations in degassed solutions. Typically, successive 10 fold dilutions were made using 0.1 M acetic acid except the final dilution, where artificial cerebrospinal fluid (aCSF) was used to mimic the sample matrix of the microdialysis samples. The aCSF contained 145.0 mM NaCl, 2.7 mM KCl, 1.0 mM $MgCl_2$, 1.2 mM $CaCl_2$, 0.45 mM NaH_2PO_4 and 1.55 mM Na_2HPO_4 at pH 7.40.

2.3.11. Chromatographic conditions for temperature-controlled reaction kinetics experiments

An acidic mobile phase was used to attenuate the reaction kinetics in the CTR. An aqueous buffer containing 85 mM monochloroacetic acid, 15 mM sodium acetate, 0.15 mM disodium EDTA, 10.0 mM SOS, (pH was adjusted to 2.40 with concentrated sodium hydroxide solution) was mixed with acetonitrile (89:11, v/v) and passed through a Nylon filter. The column was slurry packed to 7.6 cm with 2.6 μm XTerra MS-C_{18} (Waters, Milford, MA) reversed phase particles. Injection samples contained dopamine and serotonin, each at 100 nM, and 0.11 M acetic acid in aCSF.

2.3.12. Temperature effect on detection sensitivity

A homemade heating block controlled the temperature of the CTR. A Minco PID controller (Model CT15122, Minneapolis, MN) drove two square-shaped silicon rubber heaters (Omega SRFG-202/10, 5 x 5 cm^2, 2.5 W/in^2, Stamford, CT). An aluminum block directly on top of the heaters transferred heat to the confluence end of the CTR. Between the CTR and the aluminum block were silicon rubber sheets (0.10" thickness, McMaster-Carr, Cleveland, OH) to enhance the thermal contact. All the heating assembly is placed inside of insulator blocks made from calcium silicate (McMaster-Carr). The insulator assembly helped to stabilize the temperature of the heating block. An elastomer-coated temperature sensor (Minco, S665PDZ24A) in the insulator assembly monitored the actual temperature, and this information was used as a feedback to the PID controller.

For each new temperature setting, enough thermal equilibration time was given. Once the temperature became stable, a blank injection with aCSF was made to determine the baseline noise level. The baseline signal from 1 to 4 minutes was analyzed with Microsoft Excel's REGRESSION function. After a linear regression was made for a given data set, the standard deviation of Y-residual values was taken as the noise level. Thus, the noise figure contains both high frequency noise and low frequency noise (drift), but not linear drift.

2.3.13. Animal and surgical procedures

All procedures involving animals were conducted with approval of the Institutional Animal Care and Use Committee of the University of Pittsburgh. Male Sprague–Dawley rats (250–375 g, Hilltop, Scottdale, PA, USA) were anesthetized with chloral hydrate (initial dose of 300 mg/kg i.p. with additional doses of 50 mg/kg i.p. as needed to maintain anesthesia) and wrapped in a homeothermic blanket (EKEG Electronics, Vancouver, BC, Canada). The rats were placed in a stereotaxic frame (David Kopf Instruments, Tujunga, CA, USA) with the incisor bar set at 5 mm above the interaural line[58] and appropriately placed holes were drilled through the skull.

2.3.14. Microdialysis

Vertical concentric microdialysis probes (220 μm o.d., 4 mm long) were constructed with hollow fiber dialysis membrane (Spectra-Por RC Hollow Fiber, MWCO: 13,000, 160 μm i.d., Spectrum Laboratories Inc., Rancho Dominguez, CA) and fused silica outlet lines (150 μm o.d., 75μm i.d., Polymicro Technologies, Phoenix, AZ). The microdialysis probe was implanted into the brain over a period of 30 min to the following coordinates: 2.5 mm anterior to bregma, 2.5 mm lateral

from midline and 7.0 mm below dura. The probe was perfused at 0.586 μL/min. Nomifensine (20 mg/kg, i.p.) was prepared in PBS and administrated. All brain dialysates were collected in vials containing 10% (v/v) 0.1 M acetic acid.

2.4. Results and Discussion

2.4.1. Optical properties of complexes

Figure 2-3 shows absorbance spectra of the complexes. Compared to its ruthenium-analogs, **1** has a smaller molar absorptivity(ε) in the (II) oxidation state. Compounds **3** and **4** show a much higher ε than **1**. The experimentally found results are compared to literature values,[46] and summarized in Table 2-1. Photoluminescence intensity from **1** is much smaller than its ruthenium analogs by 20-50 fold as can be found in Figure 2-4 and Table 2-2, corresponds to the reported quantum efficiency difference. To compensate for the smaller photoluminescence intensity, an epifluorescence setup was employed. The optical setup is shown in Figure 2-2.[59]

Table 2–1. Absorbance of the complexes.

Complex	Literature Value			Experimental Value		
	ε ($cm^{-1}M^{-1}$)	λ_{max} (nm)	solution	ε ($cm^{-1}M^{-1}$)	λ_{max} (nm)	solution
1	11100 12000	478 480	ACN Water	11900	483	ACN/ water
2	14600	452	Water	14200	451	ACN/ water
3	29500 28600	460 463	Water MeOH/ EtOH	31100	464	ACN/ water
4	-	-		18800	463	Water

Table 2–2. Photoluminescence of the complexes.

Complex	Literature Value			Experimental Value	
	ϕ	λ_{Em} (nm)	solution	λ_{Em} (nm)	solution
1	0.005	743 715	ACN Water	722	ACN/ water
2	0.042	613	Water	606	ACN/ water
3	- 0.366	610 618	Water MeOH/ EtOH	612	ACN/ water
4	-	-		614	Water

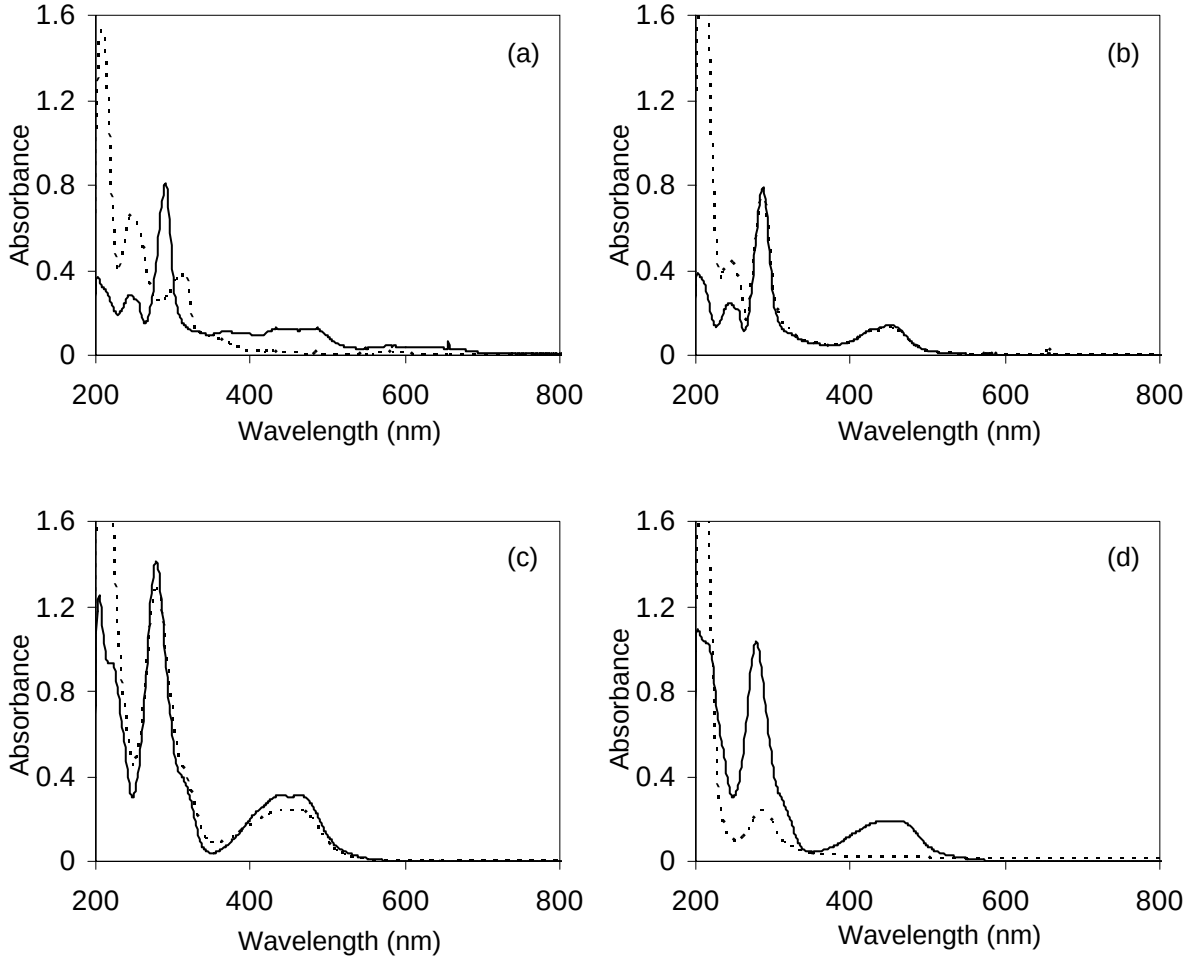

Figure 2–3. UV absorbance spectra of complexes.

(a) 1, (b) 2, (c) 3 and (d) 4. Solid lines show spectra of the complexes' original absorbance, while dashed line shows the absorbance when the complexes were mixed with PbO_2 particle and subsequently filtered. Complex concentration in the solution is 10 μM, in 50:50 mixture of acetonitrile and water (1-3) or in 100% water (4), containing electrolytes.

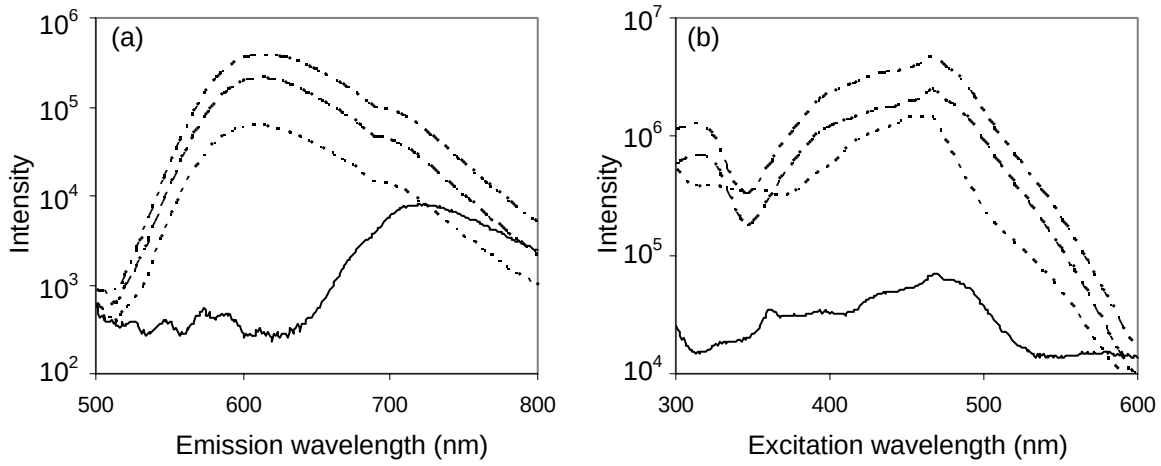

Figure 2–4. Emission and excitation photoluminescence spectra of complexes.

(a) Emission spectra were measured when complex was optically excited at 488 nm. (b) Excitation spectra were measured at their maximum emission wavelength while the wavelength of excitation.

2.4.2. Electrochemical properties

Since the $\mathbf{1}^{3+}$ is the oxidant in PFET, the electrochemical properties of **1** are important. Its redox potential basically defines an electrochemical potential window for detectable analytes, thus the detection selectivity.

Table 2-3 shows the electrochemical properties of various species. The redox potential of $\mathbf{1}^{2+/3+}$ is about 0.76 V. It can be seen that the ability of $\mathbf{1}^{3+}$ to detect compounds is not clearly related to the anodic peak potential of the analytes investigated. $\mathbf{1}^{3+}$ oxidizes ferrocene, ferrocene carboxylic acid and hydroquinone as well as the catechols dopamine, DOPAC, carbidopa, norepinephrine and the indoles serotonin and 5-hydroxyindole acetic acid.[45] These oxidations may be expected based on a consideration of the peak potentials in cyclic voltammetry for the analytes. However, it is not always possible to use cyclic voltammetric behavior to infer reactivity of a particular analyte. Just as in standard electrochemical detection, it is probably

necessary to test potential analytes experimentally. For example, we note that phenol, bromide, nitrite and chlorite have rather high peak potentials, yet nitrite and chlorite give signals while phenol and bromide do not. We have not investigated this in detail, but we can say a few things about these reactions. The reduction potential for phenol should be approximately 1.0 V (Ag/AgCl, 3 M NaCl) based on the data of Harriman.[60] This is significantly more positive than the reduction potential for the reagent. Bromide, on the other hand, has the more modest reduction potential of about 0.86 V (Ag/AgCl, 3 M NaCl)[61] yet it does not give a signal. This is likely due to the mechanism of the oxidation. The reduction potential for bromide/bromine radical is about 2 V (Ag/AgCl, 3 M NaCl).[61] It is the dimerization of two bromine radicals from bromine that lowers the free energy significantly. This is a second order reaction, thus its rate is diminished in homogeneous solution at low concentrations. The solutes nitrite and chlorite react with $\mathbf{1}^{3+}$ but show very positive anodic peak potentials. No relevant literature could be found on chlorite, but it has been reported that nitrite is oxidized in a catalytic wave by Ce(IV)EDTA.[62] The wave is near 0.75 V (Ag/AgCl, 3 M NaCl). This is consistent with its oxidation by $\mathbf{1}^{3+}$. Thus, the selectivity of PFET detection is governed not only by thermodynamics but also by kinetics. This is generally true for electrochemical detection as well. However, it cannot be assumed that the selectivities of the two approaches are the same.

Table 2–3. Electrochemical properties of various analytes.

Electrolyte solutions contain 0.1 M $NaClO_4$ and 0.05% trifluoroacetic acid in 50:50 water/acetonitrile mixture to mimic the detection condition in the PFET system. All potentials are reported versus Ag/AgCl reference electrode.

Species	E_{pa}	E_{pc}	$\frac{E_{pa}+E_{pc}}{2}$	Reaction with $\mathbf{1}^{3+}$
$\mathbf{1}^{2+}$	.790	.736	0.763	-
Br^-	1.12	.671	0.896	N
phenol	1.18	-	-	N
Fe^{2+}	.803	.315	0.559	Y
Ferrocene carboxylic acid	.566	.492	0.529	Y
p-hydroquinone	.638	.117	0.378	Y
ClO_2^-	> 1.3	-	-	Y
NO_2^-	> 1.3	-	-	Y

2.4.3. Oxidation of the complexes by PbO_2

The oxidized complex is used as a homogeneous oxidant in the PFET system. Previous studies[9, 10] utilized a packed-bed porous carbon electrode, but this is complicated. It requires a potentiostat and strategic placement of the auxiliary electrode to avoid reconversion of the oxidized product back to the reduced starting material. Any strongly oxidizing redox couple can achieve the same result more simply. PbO_2 has been used by Rubenstein and Bard for oxidizing **2**.[63] Figures 2-3 and 2-5 show the UV-vis and photoluminescence spectra of complexes after they were mixed with solid particles of PbO_2 (dashed lines). Both spectroscopic measurements lead to the same conclusion **1** and **4** are virtually completely oxidized by PbO_2, while **2** was not oxidized at all under our conditions. Spectra of **3** are, in both UV-vis and photoluminescence, in between complete and incomplete oxidation, which indicates its redox potential is in between those of **1** and **2** as reported previously.[46, 64]

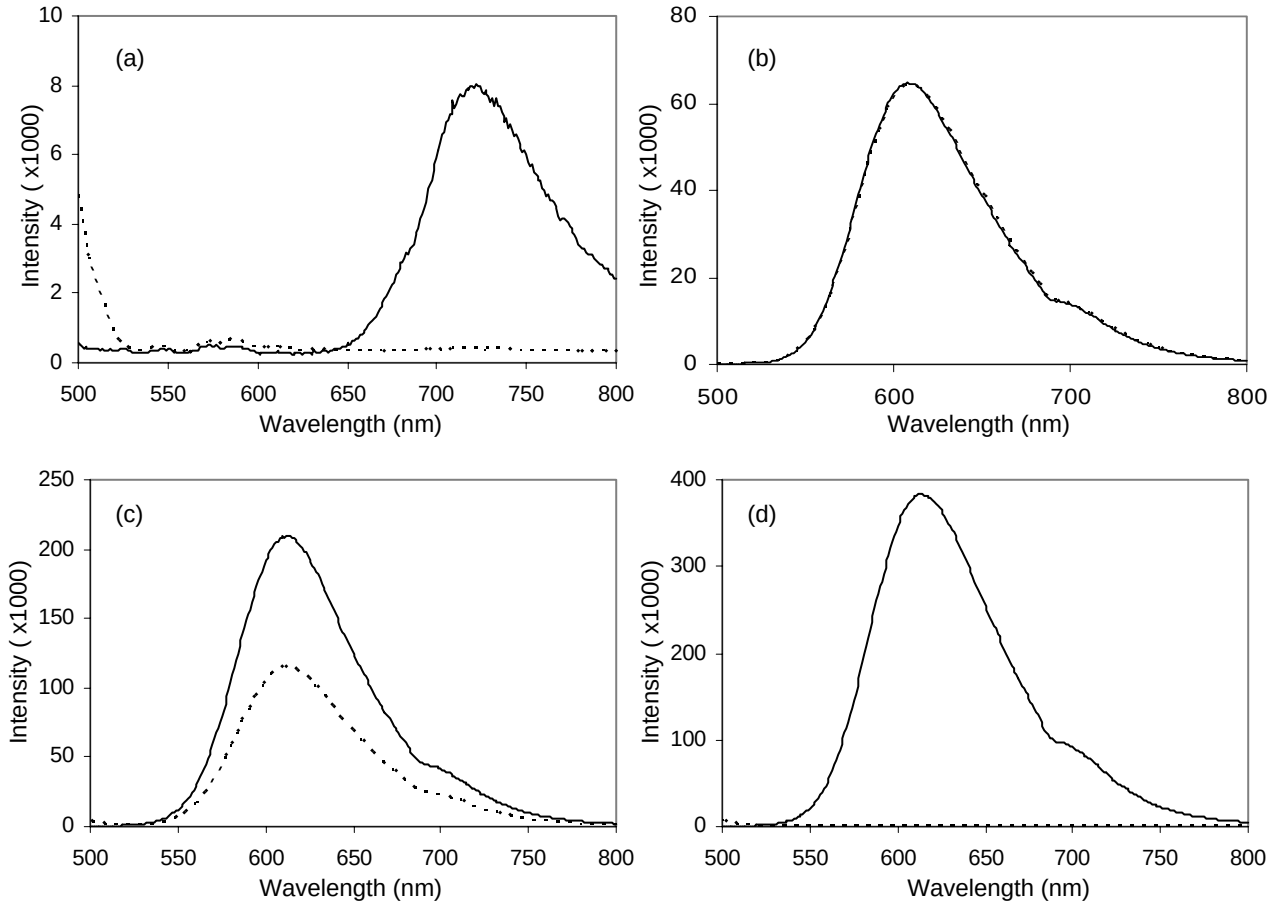

Figure 2–5. Photoluminescence of complexes.

(a) 1, (b) 2, (c) 3 and (d) 4. Intensity on the y-axis is arbitrary. Solid lines show spectra of the complexes' original photoluminescence, while dashed line shows the photoluminescence when the complexes were mixed with PbO_2 particle and subsequently filtered. Complex concentration in the solution is 10 μM, in 50:50 mixture of acetonitrile and water (1-3) or in 100% water (4), containing electrolytes.

Although clean $\mathbf{1}^{3+}$ can be prepared by simple oxidation with PbO_2, it is possible $\mathbf{1}^{3+}$ can be converted back to $\mathbf{1}^{2+}$ through the oxidation of residual impurities. The residual amount of $\mathbf{1}^{2+}$ is very important in chromatographic applications, since the level of residual $\mathbf{1}^{2+}$ defines the baseline of PFET detection. Figure 2-6 shows the reversion of $\mathbf{1}^{3+}$ in 0.2% TFA, 0.1 M $NaClO_4$ in acetonitrile. This is the same composition as the reagent stream before mixing with the HPLC eluent. $\mathbf{1}^{3+}$ was prepared by reaction with PbO_2 particles, and the absorbances at 480 nm were continuously measured to monitor the degree of reversion. Excess PbO_2 particles were removed

from $\mathbf{1}^{3+}$ by two methods: the solution was filtered by a syringe filter or only the supernatant was taken. The absorbance changes in the two solutions are quite different. The filtered solution showed steady reversion of $\mathbf{1}^{3+}$ over the 20 minutes, while in the supernatant solution the reversion stopped after about 500 s. We found that the supernatant solution contained fine particles of PbO_2, thus they were continuously oxidizing $\mathbf{1}^{2+}$. To prevent PbO_2 particles from entering the detection system in chromatography, commercial PEEK frits with a pore size of 0.45 μm (Upchurch, Oak Harbor, WA) were used. In the PFET system, the residence time of $\mathbf{1}^{3+}$ is in the order of 10 s, thus it is expected that the reversion of $\mathbf{1}^{3+}$ is small in its application in the detection system.

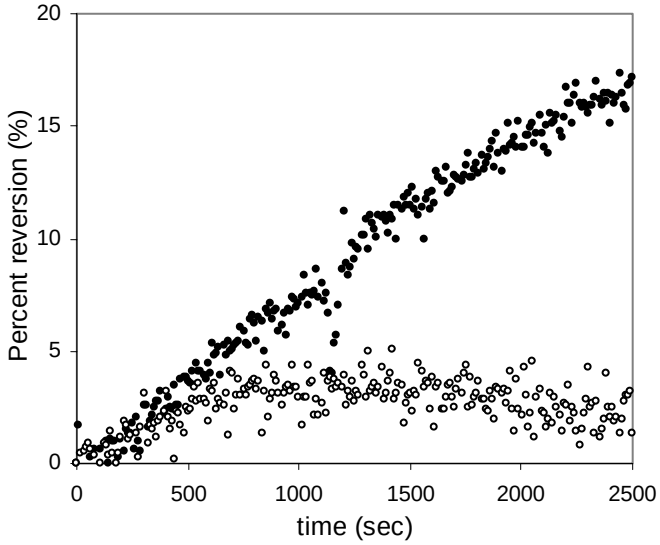

Figure 2–6. Reversion of 1^{3+}.

1^{3+} was prepared from a reaction of 1^{2+} with PbO_2. Reversion was calculated by measuring absorbances of the solution at 480 nm. Solid circles are from the filtered mixture, and open circles are from the supernatant. Concentration of 1 is 10 μM in 0.2% TFA, 0.1 M $NaClO_4$ acetonitrile solution.

When $\mathbf{1}^{3+}$ is in the PFET system, however, there is another source of the increased baseline: the introduction of mobile phase. The baseline increase due to the mobile phase was

previously reported in a similar system with $\mathbf{2}^{3+}$ as the oxidant.[10] Figure 2-7 shows the reversion of oxidized complexes, **1** and **2**, when the PFET reagents are mixed with mobile phases at various pHs. It is clear that the reversion increases as the mobile phase becomes more basic. The increased reversion, thus the baseline, can be due to water or hydroxide ion oxidation.[51, 65, 66] Oxidizable impurities are another possibility. To achieve a baseline with less than 10% reversion of $\mathbf{1}^{3+}$, the pH should be less than 6, while that for to $\mathbf{2}^{3+}$ is pH below 4. This result is also consistent with the difference in the redox potentials of complexes.[46, 64]

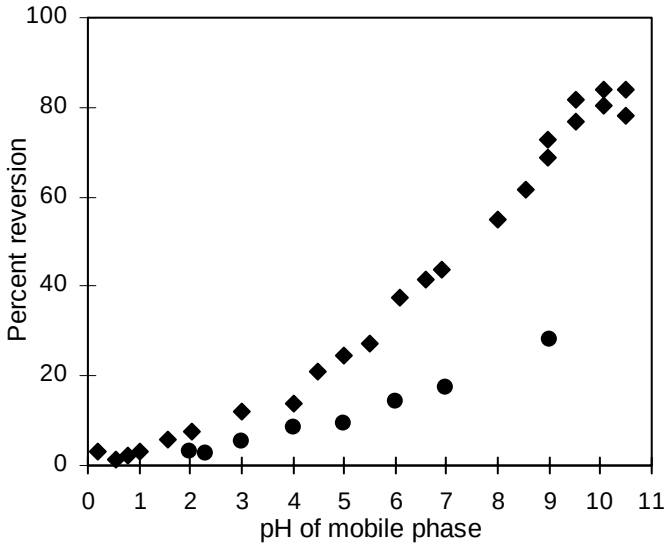

Figure 2–7. Reversion of $\mathbf{1}^{3+}$ (●) and $\mathbf{2}^{3+}$ (◆) after being mixed with buffer solutions at various pHs in a flow-injection system.

2.4.4. Control over sensitivity and selectivity

Most organic redox reactions are accompanied by proton transfer steps, while the reduction of $\mathbf{1}^{3+}$ is not. Therefore, the difference in E^0 between solutes and $\mathbf{1}^{3+}$ may be pH sensitive. Thus, a thermodynamic control exists. There may also be a kinetic means of control by the same route.

The second order rate constants of $\mathbf{1}^{3+}$ with DA and DOPAC were measured in a fluorometer at various pHs. Figure 2-8 shows that the second order rate constants at pHs below 4.0 decreased as pH decreased. At pH 4.5 and 5.0, the reaction rates are pH invariant for both species. The pKa for the redox-active functional group is certainly higher than the range of pH 4. This result can be explained by the "scheme of squares".[67-70] Catechols and similar hydroquinone analogues are known to undergo a proton-coupled 2-electron oxidation. It was found from previous studies that the oxidation of catechols follows an eHHe mechanism at pH 4-6, while the mechanism changes to an eHeH mechanism at lower pHs.[67, 69] Rate-determining steps are mostly electron-transfer steps. However, deprotonation at low pH is thermodynamically not favorable, thus making the overall reaction slow at low pH.

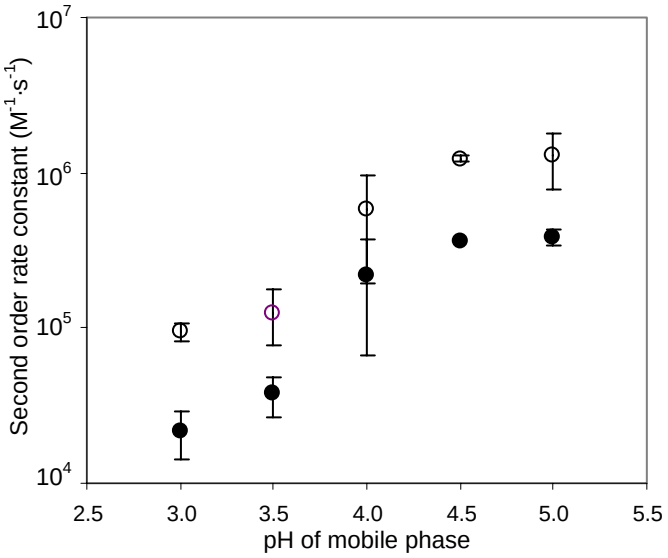

Figure 2–8. Change of second order reaction rate constants as a function of mobile phase pH.

Rate constants of reactions between 1^{3+} and dopamine (●) and DOPAC(○) were measured in a fluorometer. The error bars on the figure represents the standard errors of the mean.

It is therefore generally desirable to operate the PFET detection system at a relatively high pH in proton coupled electron transfer reactions. For separation of certain compounds, however, acidic mobile phases may be beneficial. It was reported that metabolic acids such as DOPAC and amono acids with pK_a of ~2, exhibit more retention at pH values below 2.[71] In such cases, in principle, increased temperature can increase the sensitivity.

The temperature dependence of the sensitivity was thus studied by analyzing chromatographic peaks of DA and 5HT at various temperatures. The reactor, but not the column, was heated. Figure 2-9 shows the results. The peak height (a) and the peak area (b) for DA increased at high temperatures. The peak height and area for 5HT remained constant. The concentration of each species was much lower than that of $\mathbf{1}^{3+}$: 100 nM of solutes compared to 10 μM $\mathbf{1}^{3+}$(before mixing). DA was reported previously to undergo slow reaction with $\mathbf{1}^{3+}$ at similar reaction conditions.[45] We infer from this that the reaction with 5HT is not kinetically limited on the ~seconds timescale, where the reaction with DA is. Panel (c) in the same figure shows that, despite the increase in sensitivity, the detection limit does not change or decrease as temperature increases: the baseline, as well as its noise level, increased even more at elevated temperature. The overall effect was similar or worse detection limits at high temperatures. The reason for the increase in baseline and background noise at high temperature is not certain. It might infer the presence of oxidizable impurities or oxidation of water or hydroxide ion. The dependence of the noise on the background level is a clear indication that the presence of "background" $\mathbf{1}^{2+}$ is the determining factor in establishing detection limits.

Figure 2-9 (a) shows that the peak area of 5HT did not change much with temperature, while that of DA does change with temperature. The concentration of each species was much lower than that of $\mathbf{1}^{3+}$: 100 nM of solutes compared to 10 μM $\mathbf{1}^{3+}$(before mixing). DA was

reported previously to undergo slow reaction with $\mathbf{1}^{3+}$ at similar reaction conditions.[45] Therefore one can expect that the reaction rate of DA, and thus the peak area of DA, will increase with temperature. On the other hand, the reaction of $\mathbf{1}^{3+}$ and 5HT might be fast enough to complete the oxidation of 5HT in the given reaction length (8 cm) at room temperature. As a result, the increase of reaction rate by heat is almost negligible. The reason for the increase in baseline and background noise at high temperature, on the other hand, is not certain. It might imply the presence of oxidizable impurities or oxidation of water or hydroxide ion.

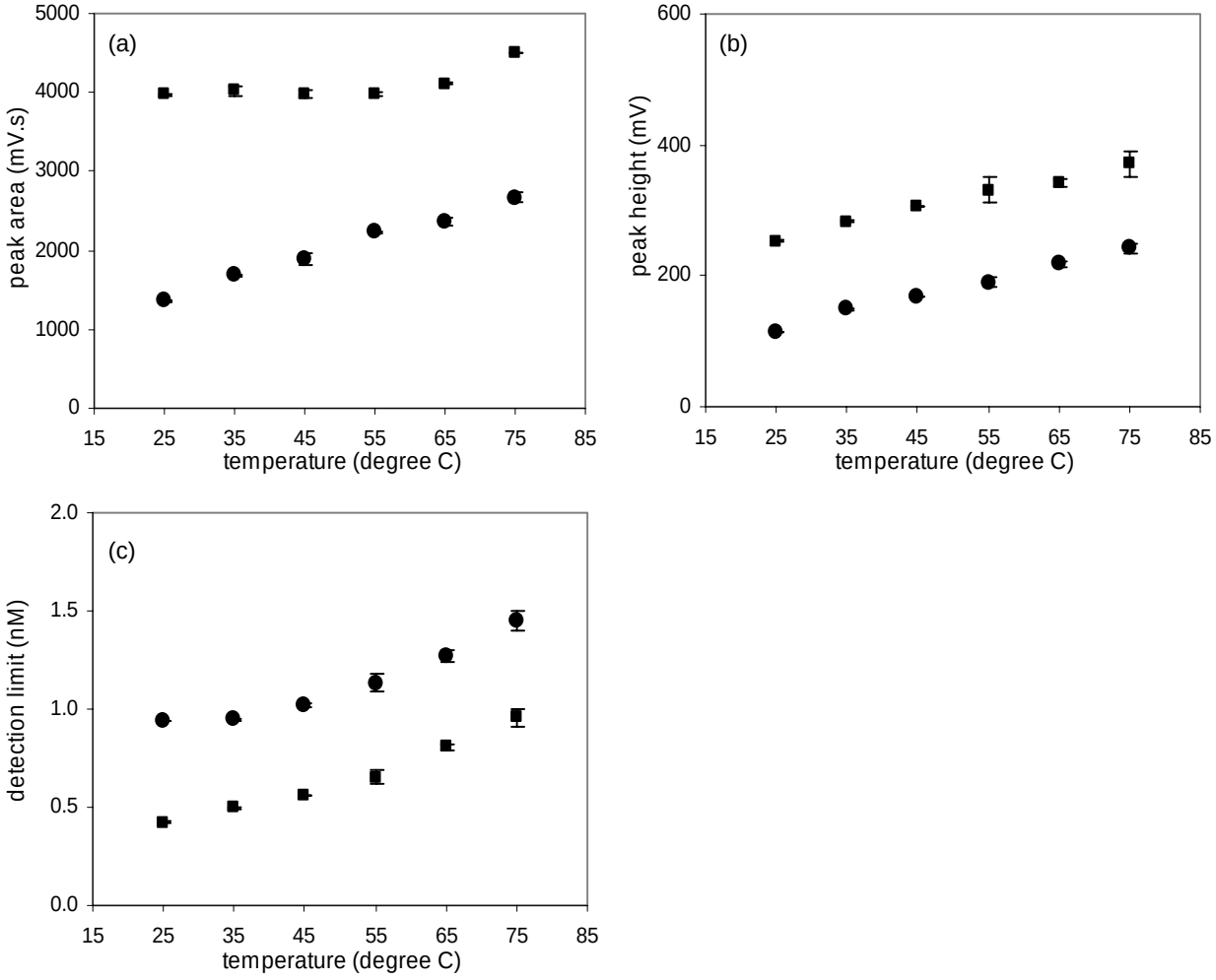

Figure 2–9. Reaction of 1^{3+} with monoamines at various temperatures.

(a) Peak area, (b) peak height and (c) detection limit are compared for chromatographic peaks of dopamine (●) and serotonin (■).The error bars on the figure represents the standard errors of the mean.

2.4.5. Applications to biological separation

The PFET system was applied to detect biogenic monoamines; DA, 3MT and 5HT. Figure 2-10 (a) shows a chromatogram of a standard solution containing 100 nM of DOPAC, DA, 5-HIAA, 3MT and 5HT. Detection limits (signal to noise ratio of 3) for DA, 3MT and 5HT are 0.66, 1.1, 0.58 nM at 500 nL injection volume (thus, 330, 550, 290 amol mass detection limits), respectively. Detection limits for DOPAC and 5-HIAA are much lower, at 0.50 and 0.26 nM. The HPLC-PFET system was stable for ~6 hours without changes in sensitivity.

Rat brain microdialysis samples were analyzed. The basal levels of DA and its metabolite, 3MT, were 16 and 10 nM, respectively (Figure 2-10 (b)). Upon the injection of nomifensine, a DA uptake blocker, extracellular concentrations of DA and 3MT increased significantly (56 and 15 nM, respectively. Figure 2-10(c)).[72]

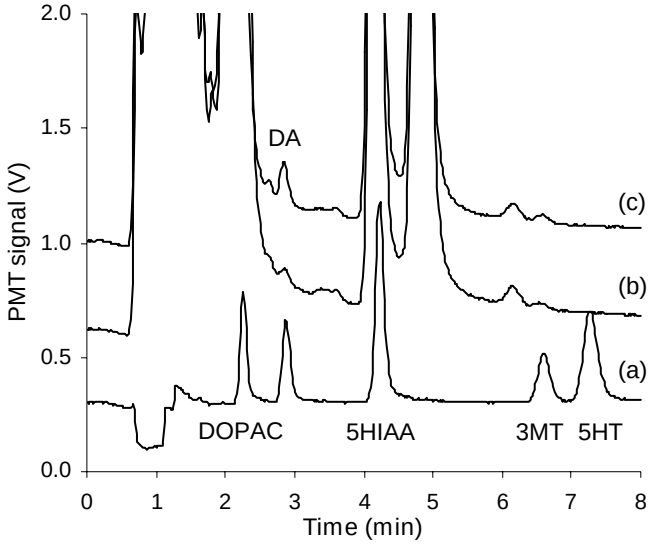

Figure 2–10. Chromatograms of monoamines.

(a) 100 nM standard mixture, brain microdialysis sample from an anesthetized rat (b) before and (c) after injection of nomifensine. Separation conditions were as follows. Mobile phase: pH 4.70 aqueous buffer containing 100 mM sodium acetate aqueous buffer with 0.15 mM disodium EDTA and 0.15 mM sodium 1-octanesulfonate, mixed with methanol (90:10, v/v). Column: 100 μm i.d., 9.5 cm length capillary column packed with 3 μm AlltimaC_{18} reversed phase material. Flow rate: 1 μL/min. Injection volume: 500 nL.

2.5. Conclusions

The reagent $\mathbf{1}^{3+}$ is effective despite its low quantum yield and the use of a red-sensitive photocathode. Having a pair of reagent (**1** and **2**) that can operate with the same optical and spectroscopic parameters adds to the flexibility and applicability of PFET. The PFET technique, as demonstrated herein and in the next chapters, is highly suited to the quantitative determination of neurotransmitters in rat brain microdialysates. The major limitation of the technique is nonspecific reduction of the reagent to the photoluminescent form. This is equivalent to background current in electrochemical detection. Major advantages are compatibility with capillary separations, day-to-day reproducibility, selectivity, sensitivity and the lack of a need to create derivatives of the analytes. Compared to ECL, the breadth of application is far greater.

3. Influence of Chemical Kinetics on Postcolumn Reaction in a Capillary Taylor Reactor with Catechol Analytes and Photoluminescence-Following Electron-Transfer

This work is published in *Anal. Chem.*, **2005**, *77*, 974-982;

3.1. Abstract

Postcolumn derivatization reactions can enhance detector sensitivity and selectivity, but their successful combination with capillary liquid chromatography has been limited because of the small peak volumes in capillary chromatography. A capillary Taylor reactor (CTR), developed in our lab, provides simple and effective mixing and reaction in a 25 μm radius postcolumn capillary. Homogenization of reactant streams occurs by radial diffusion, and a chemical reaction follows. Three characteristic times for a given reaction process can be predicted using simple physical and chemical parameters. Two of these times are the homogenization time, which governs how long it takes the molecules in the analyte and reagent streams to mix, and the reaction time, which governs how long the molecules in a homogeneous solution take to react. The third characteristic time is an adjustment to the reaction time called the start time which represents an estimate of the average time the analyte stream spends without exposure to reagent.

In this study, laser-induced fluorescence monitored the extent of the postcolumn reaction (reduction of $Os(bpy)_3^{3+}$ by analyte to the photoluminescent $Os(bpy)_3^{2+}$) in a CTR. The reaction time depends on the reaction rates. Analysis of product vs. time data yielded second-order reaction rate constants between the PFET reagent, tris(2,2'-bypyridine)osmium, and standards ((ferrocenylmethyl)trimethylammonium cation and *p*-hydroquinone) or catechols (dopamine, epinephrine, norepinephrine and 3, 4-dihydroxy-phenylacetic acid. The extent of the reactions in a CTR were then predicted from initial reaction conditions, and compared to experimental results. Both the theory and experimental results suggested the reactions of catechols were generally kinetically controlled, while those of the standards were controlled by mixing time (1-2 s). Thus, the extent of homogenization can be monitored in a CTR using the relatively fast

reaction of the reagent and *p*-hydroquinone. Kinetically controlled reactions of catechols, however, could be also completed in a reasonable time at increased reagent concentration.

A satisfactory reactor, operating at 1.7 cm/s (2 μL/min) velocity with solutes having diffusion coefficients in the 5 x 10^{-6} cm^2/s range, can be constructed from 8.0 cm of 25 μm radius capillary. Slower reactions require longer reaction times, but theoretical calculations expect that a CTR does not broaden a chromatographic peak (N=14000) from a 100 μm capillary chromatography column by 10% if the pseudo-first-order rate constant is larger than 0.1 s^{-1}.

3.2. Introduction

Among various quantitative detection methods used in capillary HPLC,[56, 73] electrochemical (EC)[56] and laser-induced fluorescence (LIF)[74] approaches are two frequently used techniques due to the ease of miniaturization. LIF has lower mass detection limits than EC, detecting down to a single molecule. The challenge associated with LIF detection, however, is that not all analytes are fluorescent in a specific optical range: few combinations of analytes can be detected simultaneously with a single-source excitation and a set of detection optics.

Because of this major limitation, derivatization of analytes is often necessary. The derivatization step is either before the separation (precolumn) or after (postcolumn). Precolumn derivatization is often preferred to avoid problems associated with reaction kinetics and band spreading. However, derivatization changes the chemical properties of analytes and the sample matrix, thus optimal separation conditions are often different before and after derivatization. The problem of multiple peaks due to multiple reactive sites in peptides or proteins is another concern.[6, 7] Postcolumn derivatization methods do not have such problems. A successful

postcolumn derivatization method, however, should satisfy following criteria: (1) The reagent itself must not be detected. (2) The reagent and the reaction product must be stable during the experiment. (3) The reaction yield should be high and unrelated to the analyte concentration. (4) The reaction must be fast so that no significant band broadening occurs during the derivatization.[75]

The photoluminescence-following electron-transfer (PFET) technique, developed in our lab, is a useful postcolumn derivatization scheme which satisfies the above criteria, and is useful in chromatography.[9, 10] The PFET reagent used in this study is tris(2,2'-bypyridine)osmium (**1**), which changes its spectroscopic properties according to the oxidation state[64]: when excited at 483 nm, $\mathbf{1}^{2+}$ luminesces at 723 nm while $\mathbf{1}^{3+}$ is not photoluminescent. The molar absorptivity (ε) of $\mathbf{1}^{2+}$ is 11900 $cm^{-1} \cdot M^{-1}$ in a 50:50 water/acetonitrile mixture and the quantum yield (ϕ) in acetonitrile is 0.005 [64]. The redox potential of $\mathbf{1}^{3+}/\mathbf{1}^{2+}$ couple is 0.84 V versus NHE,[76] about 0.4 V less positive than that of similar but more widely studied complex, tris(2,2'-bypyridine)ruthenium. Many studies used **1** as a mediator[47-50, 76] because of its fast electron transfer rate[50, 77] and stability in both oxidation states. With all these properties, **1** is a good electron-transfer postcolumn derivatization reagent: $\mathbf{1}^{3+}$ oxidizes analytes in column effluents, creating $\mathbf{1}^{2+}$, which is optically detected.

Having a good reagent is only one requirement for success. The column effluent and derivatization reagent must mix before a reaction can occur. There have been many ingenious approaches to achieve efficient fluid mixing and reaction in micrometer-sized devices (micromixers), for example, coaxial reactors,[78, 79] gap-junction reactors,[80, 81] and sheath flow reactors.[82-84] Most studies, however, focus mainly on the workability of devices, but not much on their efficiency of reaction. Excessive dilution of analytes during reaction often occurs,[79] or not

all analytes reacts with a derivatizing reagent.[80] Low reproducibility is another problem. For example, a coaxial reactor does not function well if the two tubes are slightly off-axis.[85]

Increasing interest in micromixers is not solely from analytical chemists. Increasing demands on microfluidic devices initiated rigorous theoretical studies by chemical and mechanical engineers.[85-87] Their main focus is, however, on fast mixing of fluids, which often includes turbulent mixing.[88] Another interesting application of micromixers utilizes fast convective flow to prevent fluid mixing, allowing only small molecules in the fluids to diffuse across the interface.[89, 90] These approaches are, in any case, not preferable for a postcolumn reactor coupled with a capillary HPLC. A publication from the Whitesides group showed a mixer made by soft-lithography.[91] Its imprinted patterns on the wall create radial chaotic flow to enhance radial mixing while minimizing axial broadening at a wide range of flow conditions. Despite its good performance, fabricating such devices is still not trivial, thus a simple device with a comparable performance is desirable.

A particularly simple postcolumn reactor is the 'capillary Taylor reactor (CTR)'.[57] Previous studies of postcolumn copper complexation with enkephalins showed successful mixing of two fluid streams by radial diffusion alone. Convective dispersion in a fluoropolymer mixer followed by a simple open tube capillary reactor is experimentally indistinguishable from a simple capillary.[11, 12] In this study, we show that a simple fluoropolymer/silica CTR creates effective radial mixing of two fluid streams. PFET can be achieved with **1** as a postcolumn reagent. The extent of reaction generally depends on the reaction kinetics, and the limitation of low signal intensity due to slow reaction kinetics can be avoided by careful selection of postcolumn derivatization reagent conditions.

3.3. Experimental Section

3.3.1. Reagents

All commercial chemicals were used as received without further purification except where noted. Reagents and sources were as follows: trifluoroacetic acid (TFA) from Acros (Geel, Belgium); acetonitrile, 2-propanol, sodium acetate from EMD (Gibbstown, NJ); 1-propanol, lead dioxide, glacial acetic acid, disodium EDTA from J.T.Baker (Phillipsburg, NJ); (ferrocenylmethyl)trimethylammonium iodide from Lancaster Synthesis (Windham, NH); *p*-hydroquinone, 1-heptanesulfonic acid sodium salt monohydrate, anhydrous sodium iodide, sodium perchlorate from Aldrich (Milwaukee, WI); dopamine, 3, 4-dihydroxy-phenylacetic acid (DOPAC), epinephrine, norepinephrine from Sigma (St. Louis, MO). Sodium perchlorate was recrystallized in methanol once to remove chloride. All aqueous solutions were prepared with deionized water (18.2 MΩ·cm resistivity) from a Millipore Milli-Q Synthesis A10 system (Billerica, MA).

$Os(bpy)_3(PF_6)_2$ (**1**) was synthesized in our lab according to a previously reported procedure.[54] Crystals of the osmium complex were dissolved in acetonitrile to make a 1.0 mM stock solution. Aliquots of the stock solution were diluted in an acidic electrolyte solution (0.2% TFA and 0.1 M $NaClO_4$ in acetonitrile) to prepare the postcolumn derivatization reagent. The resulting postcolumn derivatization reagent was introduced into the system after passing a 0.45 μm PTFE/PP syringe filter (Chrom Tech, Apple Valley, MN). Stock solutions of 1.0 mM catechols and standards were prepared in 0.1 M acetic acid and stored frozen. The frozen stock

solutions were thawed before each use and were diluted to desired concentrations in degassed flow-injection solutions.

3.3.2. Optical setup

A laser beam from a 30 mW variable power blue-line argon-ion laser (Cyonics/Uniphase 2201-30BL, San Jose, CA) passed through a 488 nm band-pass filter and was focused onto an optically transparent capillary. Photoluminescence from $\mathbf{1}^{2+}$ was measured using an epifluorescence optical setup: a microscopic objective lens (Carl-Zeiss Plan Neofluar 20x, NA 0.5, Thornwood, NY) focused the optical emission from the capillary and a combination of a dichroic mirror (cutoff at 500 nm) and optical filters (a 600 nm long-pass filter and a 750 nm band-pass filter, angle tuned) allowed the photoluminescence into an IR-sensitive photomultiplier tube (Hamamatsu R374, Bridgewater, NJ).

3.3.3. General flow injection apparatus

Two HPLC pumps (Waters 590 and 600/626S, Milford, MA) with simple tees as flow splits, or a dual syringe pump (Model 11VPF, Harvard Apparatus, Holliston, MA) delivered solutions at about 1 μL/min. The flowrate from each source was frequently checked by measuring the volume of solutions delivered in a specific time, to ensure the correct flowrate is maintained during experiments.

3.3.4. Capillary Taylor reactor construction

Reactors were prepared according to the previously reported procedure.[57] The ends of two 18 μm tungsten wires (Goodfellow, Devon, PA) were each threaded into two 50 μm fused-silica capillaries (Polymicro Technologies, Phoenix, AZ). The other ends were both threaded into another 50 μm fused-silica capillary to form a Y-shaped device. The third capillary was either polyimide-coated (normal CTR) or transparent (transparent CTR). When the third capillary was a polyimide-coated one, an optical window of 1 cm width was made by burning off the coating. The junction between three capillaries was placed in a piece of dual shrink/melt tubing (Small Parts, Miami Lakes, FL). After heat-shrinking, the device was allowed to cool, the tungsten wires were removed to create fluid conduits of 18 μm diameter between 50 μm capillaries.

3.3.5. Determination of reaction rate constant of $\mathbf{1}^{3+}$ with analytes

$\mathbf{1}^{3+}$ was prepared before each use as follows: electrolyte solutions containing $\mathbf{1}^{2+}$ were mixed with a solid oxidant, PbO_2, and stirred. The resulting slurry was passed through a disposable syringe filter with a pore size of 0.45 μm. The clear filtrate was quickly mixed with analyte solutions of the same volume in a quartz fluorometer cell seated in a fluorometer (Jobin-Yvon, Edison, NJ) at room temperature. The analyte solutions were pH 4.00 acetate buffers containing analyte. Typical concentrations of reactants were as follows: 2.0 ~ 20 μM $\mathbf{1}^{3+}$ with 3.0 ~ 40.0 μM (ferrocenylmethyl)trimethylammonium cation (**5**) where **5** was always in excess, 2.0 μM $\mathbf{1}^{3+}$ with 1.5 μM *p*-hydroquinone and 20.0 μM $\mathbf{1}^{3+}$ with 20.0 μM catechols. The mixture was optically excited at 470 nm and the photoluminescence was monitored at 722 nm for 60 s with an

integration time of 0.01 s. Traces of signal intensity versus time were converted to product-time traces and fit into a second-order reaction kinetics model with the reaction rate constant as a variable. The SOLVER function in the Microsoft Excel spreadsheet found the optimum value of the variable which gave the minimum sum of squared deviations.

3.3.6. Flow-injection system with continuous analyte flow

A 2.0 μM solution of $\mathbf{1}^{2+}$ was divided into two aliquots. An excess of PbO_2 oxidant particles was added into one, producing a 2.0 μM solution of $\mathbf{1}^{3+}$. A dual syringe pump delivered a 10.0 μM *p*-hydroquinone in aqueous 0.1% TFA solution and either $\mathbf{1}^{2+}$ or $\mathbf{1}^{3+}$ at a flowrate of 1 μL/min into a transparent CTR. The photoluminescence was monitored at various detection points along the length of transparent capillary. Random selection of detection points helped minimize the possible time-dependent signal changes. Focusing on the capillary was carefully checked to achieve a maximum signal after each move of the detection point.

3.3.7. Flow-injection system with analyte bands

A packed bed of PbO_2 converted $\mathbf{1}^{2+}$ into $\mathbf{1}^{3+}$. The online conversion of **1** is efficient; up to 99.8% of $\mathbf{1}^{2+}$ was converted. Typically, the conversion is about 98%. A Rheodyne 7125 injector (Rohnert Park, CA) connected the PbO_2–packed column into the system for fast and easy start/stop control of $\mathbf{1}^{3+}$ generation. An HPLC pump with a split delivered this reagent at 1 μL/min to one arm of a CTR.

Each analyte was prepared in the flow-injection buffer at various concentrations ranging from 0.25 to 2.5 μM. The flow-injection buffer, which represents the HPLC eluent, was made as follows: aqueous buffer containing 50 mM sodium acetate, 0.15 mM disodium EDTA and 0.4 mM sodium salt of 1-heptanesulfonic acid (pH was adjusted to 4.00 with glacial acetic acid) was mixed with acetonitrile (95:5, v/v) and passed through a Nylon filter with 0.45 μm pores (Osmonics, Minnetonka, MN). This solution was pumped by another HPLC pump with a split and delivered to the other arm of the CTR. An Upchurch loop microinjector (Oak Harbor, WA) introduced 4 μL of each analyte into the system. Resulting photoluminescence was detected in a CTR either 3.0 or 8.0 cm from the confluence.

3.3.8. Data collection

A Keithley 6485 picoammeter (Cleveland, OH) converted photocurrent from the photomultiplier tube to a DC voltage signal. An IBM-compatible computer with a PeakSimple Chromatographic Data System (SRI Instruments, Torrance, CA) collected the DC signal after a 0.4 Hz 8-pole low-pass filter (Wavetek 852 Dual filter, San Diego, CA).

3.4. Results and Discussion

3.4.1. Determination of reaction rate constants

In order to make quantitative estimates of the required length of a postcolumn reaction, knowledge of rate constants is necessary. The reaction rate constant of a reaction between $\mathbf{1}^{3+}$

and (ferrocenylmethyl)trimethylammonium cation (**5**), a 1-electron transfer standard,[10] was calculated from the Marcus outer-sphere electron-transfer theory[92] with known parameters.[50, 77, 93] The calculated rate constant of 1.7 x 10^9 $M^{-1} \cdot s^{-1}$ suggests the reaction is fast. The reaction time for such a 1-electron oxidation reaction can be predicted from a simple second-order reaction kinetics model,

$$A + B \rightarrow P \qquad (1a)$$

$$d[P]/dt = k_1 \cdot [A] \cdot [B] \qquad (1b)$$

where k_1 is a second-order reaction rate constant ($M^{-1} \cdot s^{-1}$). Solving the above differential equation for the time variable, *t*, gives,

$$t = \frac{1}{k_1} \frac{1}{[B]_i - [A]_i} \ln \frac{[A]_i \cdot ([B]_i - x)}{[B]_i \cdot ([A]_i - x)} \qquad (2)$$

where $[C]_i$ is the initial concentration of a solute C, and *x* is the concentration of the product([P]) at time *t.* A value of the reaction time can be determined in any particular case with knowledge of the starting concentrations, the rate constant, and an assumption about the necessary extent of reaction (e.g., 50%, 80%, 95%).

Hydroquinone analogs such as *p*-hydroquinone and catechols generally undergo a 2-election oxidation. The oxidation reaction follows the 'scheme of squares',[67-69] and application of the Marcus theory is not straightforward. It is also known that the actual mechanism varies according to reaction conditions.[94] Earlier work showed that the oxidation of *p*-hydroquinone or catechols on a platinum and a carbon paste electrode[67, 69] follows an eHHe mechanism at pH 4.0, where the first electron-transfer reaction is the rate-determining step. Thus the reaction can be approximated as second-order. The reaction rate laws shown in equations (1), (2) need small modifications,

$$2 \cdot \mathbf{1}^{3+} + H_2Q \rightarrow 2 \cdot \mathbf{1}^{2+} + Q + 2H^+ \quad (3a)$$

$$-d[\mathbf{1}^{3+}]/dt = k_2 \cdot [\mathbf{1}^{3+}] \cdot [H_2Q] \quad (3b)$$

where H_2Q /Q denotes the redox pair of hydroquinone analogs and k_2 is a second-order reaction rate constant ($M^{-1} \cdot s^{-1}$).

$$t = \frac{1}{k_2} \frac{1}{[\mathbf{1}^{3+}]_i - 2 \cdot [H_2Q]_i} \ln \frac{[H_2Q]_i \cdot ([\mathbf{1}^{3+}]_i - 2 \cdot x)}{[\mathbf{1}^{3+}]_i \cdot ([H_2Q]_i - x)} \quad (4)$$

$$[\mathbf{1}^{2+}] = \frac{2 \cdot [H_2Q]_i \cdot [\mathbf{1}^{3+}]_i \cdot (F - 1)}{[\mathbf{1}^{3+}]_i \cdot F - 2 \cdot [H_2Q]_i} \quad (5)$$

where $F = \exp[\, k_2 \cdot t \cdot ([\mathbf{1}^{3+}]_i - 2\,[H_2Q]_i)]$.

Direct measurement of the photoluminescence in a spectrofluorometer as a function of time following mixing of reagent and analytes can reveal the reaction rate constants of $\mathbf{1}^{3+}$ with *p*-hydroquinone and catechols. Figure 3-1 is a typical trace of such measurements, where the photoluminescence was converted to the concentration of product. The typical rise time of the photoluminescence signal varied from 1 to 4 s, according to the reaction rate. A reaction of a blank pH 4.00 buffer with 20.0 μM $\mathbf{1}^{3+}$ as a control experiment showed the signal increased by less than 1% in the initial 5 s. Another control experiment of mixing **5** with $\mathbf{1}^{2+}$, the photoluminescent form of the reagent, revealed the mixing time in a fluorometer cell to be about 0.5 s.

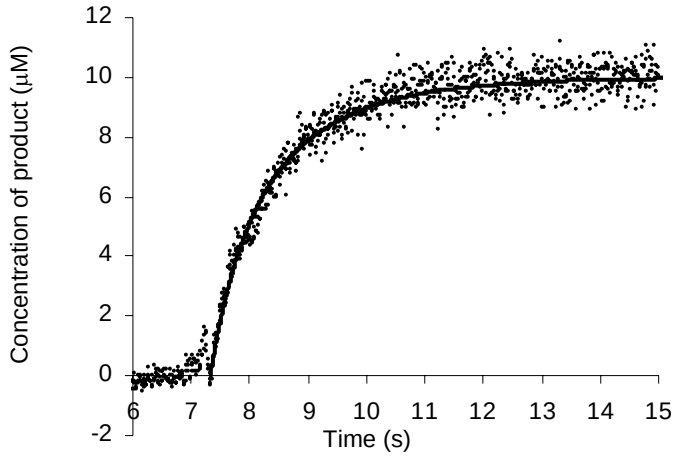

Figure 3–1. A typical photoluminescence change upon the reaction of 20 μM 1^{3+} with 20 μM dopamine.

The rise time of the signal here is about 4 s, which varied from 1 to 4 s depending on the analytes. The resulting photoluminescence intensity was converted to the amount of 1^{2+} produced (points). Nonlinear fitting of data (solid line) revealed the reaction rate constants.

Table 3–1. Rate constants of analytes for second-order reactions with 1^{3+}.

Experimental errors in standard errors of the mean (SEM) with numbers of replicates in parentheses. * calculated using the Marcus theory

Analyte	k ($M^{-1} \cdot s^{-1}$)	Error (n)	Relative Error (%)
5	1.7×10^{9} *	-	-
p-hydroquinone	8.04×10^{5}	3.4×10^{4} (5)	4.3
dopamine	6.88×10^{4}	3.3×10^{3} (6)	4.8
DOPAC	1.93×10^{5}	5.4×10^{3} (3)	2.8
norepinephrine	7.97×10^{4}	3.5×10^{3} (4)	4.4

Experiments of $\mathbf{1}^{3+}$ with **5** at various reactant concentrations showed the rise time of about 0.5 s, almost same as in the control mixing experiment. Reproducible fitting was thus not

possible, and this suggests that the reaction of $\mathbf{1}^{3+}$ and **5** is indeed fast. Table 3-1 is the summary of measured reaction rate constants and corresponding standard errors of the mean (SEM).

Nonlinear fit of the reaction between $\mathbf{1}^{3+}$ and epinephrine was not successful using the simple second-order reaction kinetics model because in this case the absorbance increased linearly and reached a plateau (data not shown). The oxidation of epinephrine is complex because adrenalinequinone, the 2-electron oxidation product of epinephrine, regenerates epinephrine after a series of reactions including cyclization.[95]

3.4.2. Theoretical considerations on mixing

The column effluent and derivatization reagent must mix before a reaction can occur. There is a range of specific experimental conditions known as the Taylor dispersion regime, in which the radial concentration gradient of a solute due to the parabolic velocity profile of a laminar flow in a tube is relaxed to form a radially homogeneous Gaussian band. The resulting concentration dispersion relative to a plane moving with a mean linear velocity, v, resembles the concentration distribution resulting from molecular diffusion with the Taylor dispersion coefficient, $\mathcal{D}$, replacing the molecular diffusion coefficient, D.

$$\mathcal{D} = v^2 \cdot a^2 / 48D \qquad (6)$$

where a is the radius of the tube.

Although the idea of Taylor dispersion was originally developed using a narrow band of a single component in laminar flow, it is evident that two parallel fluid streams created by the confluence of a reagent stream and an analyte stream in a single tube will be completely homogenized when the flow is in the Taylor dispersion regime.

The Taylor regime has two criteria; (1) the axial molecular diffusion is negligible compared with the dispersion effect, and (2) the cylindrical tube is long enough for a solute to have enough time to relax the radial concentration gradient established by the flow profile. Writing the first criterion in a mathematical form gives,

$$D << \mathcal{D} \tag{7}$$

which can be rearranged using the Peclet number, *Pe*, a ratio of mass transported by linear convection and by radial diffusion,

$$Pe^2 = (v \cdot a/D)^2 >> 48 \tag{8a}$$

$$Pe >> 7 \tag{8b}$$

Rephrasing the second criterion states that the time it takes a solute to diffuse in the radial direction is shorter than or equal to the residence time of a solute. The radial diffusion time of a solute in a tube with a radius a, is $t_D = a^2/4D$, and the residence time for a tube of length L, is $t_L = L/v$. The mathematical expression of the second criterion is thus,[96]

$$t_D << t_L \tag{9a}$$

$$Pe << 4 \cdot L/a \tag{9b}$$

If we use, somewhat arbitrarily, a factor of ten to be "much greater than", then we arrive at the criteria in equation (10).

$$Pe > 70 \tag{10a}$$

$$Pe < 0.4 \cdot L/a \tag{10b}$$

Figure 3-2 shows the resultant inequalities in a plane of log *Pe* versus log *L/a*.[96] The arrow on the diagram indicates where on the graph capillaries (a = 25 μm, v = 1.7 cm/s and $D(\mathbf{1})$ = 3.5 x 10^{-6} cm^2/s [97], which is $Pe \sim 1200$) of increasing length are. Note the wide range of the transition region, which satisfies $0.4 \cdot L/a < Pe < 10 \cdot L/a$. Precise theoretical prediction of

minimum mixing length is not possible. The flow in a CTR is expected to be in the Taylor dispersion regime after about 8 cm ($Pe < 0.4 \cdot L/a$), but a shorter length might work as well. Some authors define the Taylor regime based on the less tight criterion of $Pe < L/a$,[91, 98] which in our case would be $L > 3.0$ cm.

3.4.3. Determination of the mixing length

As seen from the previous section, theoretical calculations give estimates of the mixing length in a capillary tube. Precise estimation of the mixing length, however, is not possible by theoretical calculations only, because the boundaries in Figure 3-2 are somewhat arbitrary. A simple experiment was devised to monitor the mixing in our system. Photoluminescence intensity was measured from combined equal flow rate solutions of 2.0 μM $\mathbf{1}^{2+}$, the photoluminescent form of the reagent, and 10.0 μM *p*-hydroquinone at various detection lengths. Measured values can be referred to the photoluminescence from pure 1.0 μM $\mathbf{1}^{2+}$, its expected final concentration after complete homogenization. The result is in Figure 3-3. There is a decrease in the signal as detection length increases to reach a steady-state after about 3 cm (~ 1.8 s).

A comparison with a similar experiment using $\mathbf{1}^{3+}$ instead of $\mathbf{1}^{2+}$ can assess the extent of reaction. An excess of analyte rather than reagent was used to make the reaction fast and to remove ambiguity about the extent of the reaction. The experimental photoluminescence signal along the reaction length is overlaid in Figure 3-3. The signal reached a maximum at around 1.5 cm (~ 0.9 s) and stabilized also at a steady-state after about 3 cm (~ 1.8 s). The experiments with $\mathbf{1}^{3+}$ and $\mathbf{1}^{2+}$ gave the same steady-state signal, confirming that the extent of the chemical reaction of $\mathbf{1}^{3+}$ approached 100%.

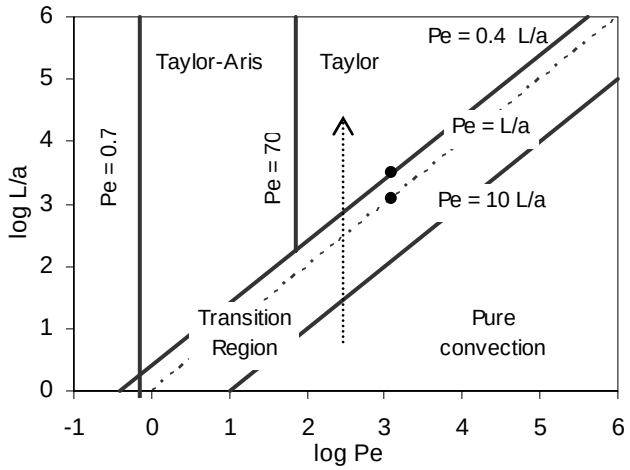

Figure 3–2. Diagrammatic representation of various solution dispersion regimes.

The arrow indicates the positions for the mixed flow in our experiments, traveling at 1.7 cm/s along a 50 μm capillary (*Pe* ~ 1200). Two dots are at lengths of 3.0 and 8.0 cm, respectively. Adapted and modified from Figure 4.6.5.[96]

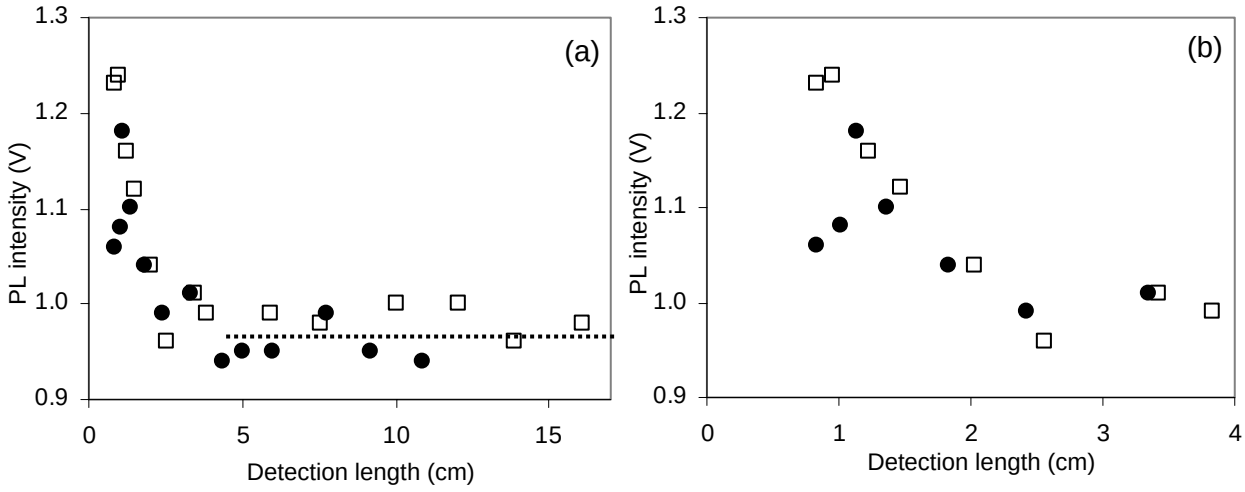

Figure 3–3. Photoluminescence (PL) signal intensity at different detection lengths.

A stream containing 10.0 μM *p*-hydroquinone was mixed with 2.0 μM 1^{2+} (□, dashed line) and 1^{3+} (●, solid line) in a flow system, (a) overall, (b) blow-up. Both 1^{2+}/1^{3+} show photoluminescence decreasing to the same steady-state value (dotted line in panel (a))

3.4.4. Determining the extent of derivatization at low reactant concentration

The reaction of 2 μM $\mathbf{1}^{3+}$ with 10 μM *p*-hydroquinone in the fluoropolymer/silica CTR was completed in ~ 3 cm (~ 1.8 sec), but it should be noted that the analyte was in excess. The reaction of analytes at low concentration, however, is different, and is important in the context of improving detection limits in chromatography. Figure 3-4 shows the signals from bands of four catechols and two standards, at two reaction lengths at a single concentration of reagent. The use of analyte bands instead of a continuous flow was for the experimental convenience. **5** is expected to react very fast with $\mathbf{1}^{3+}$ with 1:1 stoichiometry. From the experiment, however, 2 μM of **5** showed only 81% of the maximum signal at 3.0 cm reaction length. The extent of the reaction at 8.0 cm was close to 100%.

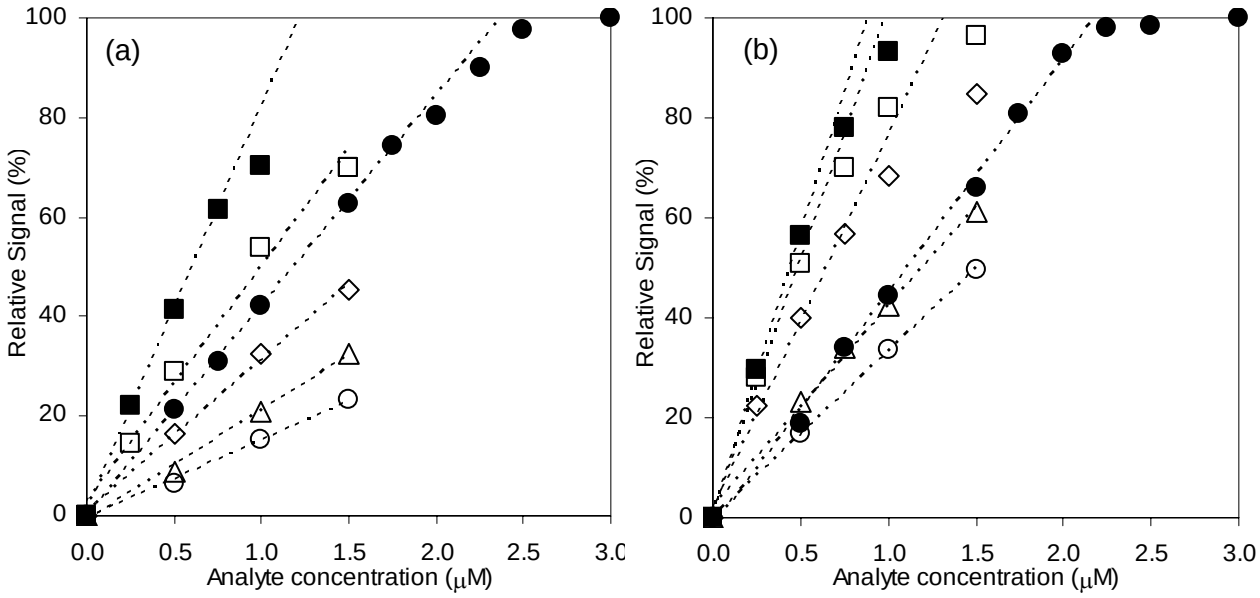

Figure 3–4. Relative signal intensity for slow reactions.

2.0 μM 1^{2+} was combined with standards and catechols: 5 (●), *p*-hydroquinone (■), dopamine (○), DOPAC (□), epinephrine (◇) and norepinephrine (△). Straight lines are least-square fittings on the linear ranges. Detection length was (a) 3.0 cm, and (b) 8.0 cm, respectively.

A rate law predicts that the reaction rate will slow down as a reagent depletes. The slope of signal intensity versus each analyte concentration on the graphs is linear at low analyte concentrations with typical R^2 values higher than 0.995, and slowly decreases to zero at higher concentrations. The slopes of the linear range, when compared with that of a standard, are the observed number of electrons transferred (n_{obs}). Table 3-2 shows n_{obs} values for the reaction with $\mathbf{1}^{3+}$. It is clear that *p*-hydroquinone undergoes a 2 electron oxidation. The n_{obs} values of catechols, however, are in general less than or equal to *p*-hydroquinone. Values of n_{obs} increase as the reaction length increases. It is clear that n_{obs} increases as *k*: slow kinetics results in small apparent n_{obs}, and consequently decreased photoluminescence signal.

Since the reactions of $\mathbf{1}^{3+}$ and catechols follow second-order reaction kinetics, increasing $\mathbf{1}^{3+}$ concentration makes the reactions faster. The reaction kinetics can be approximated as pseudo-first order at high $\mathbf{1}^{3+}$ concentration. Using a high concentration of $\mathbf{1}^{3+}$ has also the advantage of a larger linear dynamic range in chromatographic applications. Figure 3-5 shows data for a single reaction length and three concentrations of reagent. Corresponding n_{obs} are summarized in Table 3-2. As expected, n_{obs} approaches 2 for all catechols except epinephrine, which approaches 3.3. This larger value of n_{obs} is again due to the regeneration of epinephrine. Regeneration of catechols includes a cyclization of the corresponding oxidation product as the rate-determining step. The first-order reaction rate of this step for epinephrine at pH 4.00 is much higher than those of other catechols.[95]

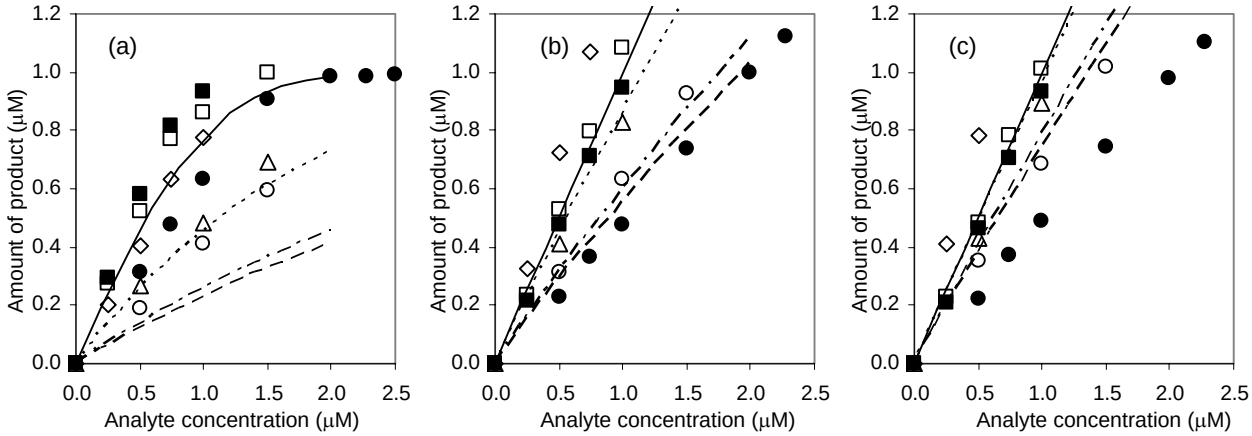

Figure 3–5. Increase of reaction rates with 1^{3+} concentration.

Amounts of products when (a) 2.0 μM, (b) 6.0 μM, and (c) 10.0 μM of 1^{3+} were reacted with various analytes. Detection length was 8.0 cm. Points denote experimental data and lines denote theoretical calculations with a 4.4 s reaction time. 5 (●), *p*-hydroquinone (■, solid line), dopamine (○, broken line), DOPAC (□, dashed line), epinephrine (◇) and norepinephrine (△, broken/dotted line)

Table 3–2. Observed numbers of electrons transferred (n_{obs}) of analytes for a reaction with 1^{3+}

Detection length	3.0 cm	8.0 cm	8.0 cm	8.0 cm
$\mathbf{1}^{3+}$ concentration	2.0 μM	2.0 μM	6.0 μM	10.0 μM
5	1.0	1.0	1.0	1.0
p-hydroquinone	1.9	1.8	1.9	1.9
dopamine	0.4	0.6	1.2	1.4
DOPAC	1.3	1.6	2.2	2.1
epinephrine	0.7	1.3	2.9	3.3
norepinephrine	0.5	0.8	1.6	1.9

We note as an aside that **5** in our experiments has iodide as a counterion. The redox potential of iodide falls in the oxidizable range by $\mathbf{1}^{3+}$. (E^0 = 0.5355 V vs. NHE for $I_2 + 2e = 2I^-$, E^0 = 0.536 V for $I_3^- + 2e = 3I^-$) However, injection of sodium iodide at micromolar concentrations did not yield any photoluminescence, while millimolar concentrations produced a small photoluminescence. This inactivity of iodide in the flow-injection system is due to the slow kinetics of the reaction. Previous studies showed that $\mathbf{1}^{3+}$ undergoes a series of reactions with iodide as follows,[99]

$$\mathbf{1}^{3+} + I^- \leftrightarrows \mathbf{1}^{2+} + I\bullet \quad (11a)$$

$$\mathbf{1}^{3+} + 2I^- \leftrightarrows \mathbf{1}^{2+} + I_2^- \quad (11b)$$

$$I\bullet + I^- \leftrightarrows I_2^- \quad (11c)$$

$$\mathbf{1}^{3+} + I_2^- \leftrightarrows \mathbf{1}^{2+} + I_2 \quad (11d)$$

where the forward direction rate constants for reactions are 1.7 x 10^1, 9.2 x 10^3, 7.6 x 10^9 and 2.9 x 10^{10} $M^{-2} \cdot s^{-1}$, respectively.[99] Because the equilibrium constants for first two steps are far less than unity (7.7 x 10^{-10} and 9.2 x 10^{-5} M^{-1}, respectively), fast reactions (11c) and/or (11d) do not occur significantly. Thus the effect of iodide in the experiments was ignored.

3.4.5. Bridging theoretical calculations and the experimental results

The mixing length was evaluated from calculations and experiments in the previous sections. Theoretical calculation predicted the mixing length will be shorter than 8 cm from equation (10b) ($Pe < 0.4 \cdot L/a$), but precise prediction was not possible due to the uncertainties in boundaries. The experimentally found mixing length is about 3 cm in a 50 μm capillary. The length corresponds

to the minimum length for a flow in the Taylor regime when the criterion $Pe < L/a$ was applied, and we define this as L_H, the length of homogenization.

Homogenization of two fluid streams, however, does not mean that all the reactants are converted to products. The characteristic length at which the signal-producing species has been formed from the analyte and the reagent we define as L_R. L_R is thus greater than or equal to L_H. The difference of two lengths is related to the reaction time, t_K.

The time at which the streams first meet cannot be taken as $t = 0$ because the reagents are not completely mixed as soon as the two separate streams come into contact. On the other hand, the homogenization length specifies the time at which mixing is fairly complete. Certainly the "starting time" for the reaction is between these two values. We have developed a very approximate method to specify an average start time for the reaction. We consider the solutes in a plane perpendicular to the flow direction and moving with the average velocity. At short times, the solutes are distributed radially from $r = 0$ to $r = a/\sqrt{2}$ (Figure 3-6) (reagent occupies half of this circle from $\theta = 0$ to π, while the analyte occupies the other "D-shaped" half of the circle for $\theta = \pi$ to 2π). In order to determine an average time for mixing, we use the simple, one dimensional Einstein equation, $t \sim l^2/2D$. However, we must average the squared distances (l_1, l_2 …) diffused to arrive at the average time at which analyte, A, and reagent, R, are mixed to a significant degree in this plane.

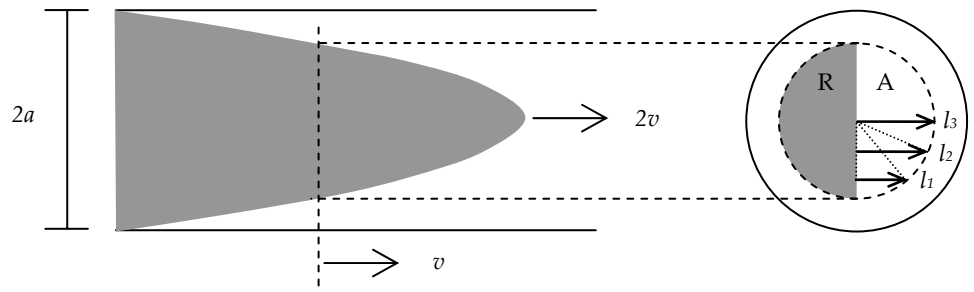

Figure 3–6. The parabolic shape of an analyte in a laminar flow inside a tube.

The flow travels at an average linear velocity of *v*, with maximum velocity of 2*v* in the center. There is a plane which travels at *v*, and this plane is taken as a representative plane of analytes moving as a parabola (denoted as a dashed circle). The radius of the dashed circle is $a/\sqrt{2}$ where the reagent, R, occupies half of this circle, and the analyte, A, occupies the other half. The average diffusional relaxation time in the disc is calculated using equation (9), where *r* is the radial distance from the center of the tube.

From simple geometry, the lengths (l_1, l_2 … see Figure 3-6) are dependent on the distance from the center line.

$$l^2(r) = \left(\frac{a^2}{2} - r^2 \right) \tag{12}$$

The mean start time is,

$$\langle t_s \rangle = \left\langle \frac{l^2(r)}{2D} \right\rangle = \frac{\int_{-a/\sqrt{2}}^{a/\sqrt{2}} \left(\frac{a^2}{2} - r^2 \right) dr}{2D \int_{-a/\sqrt{2}}^{a/\sqrt{2}} dr} = \frac{a^2}{6D} \tag{13}$$

For example, the calculated $\langle t_s \rangle$ is 0.3 s in a tube with 25 μm radius, which corresponds to 0.5 cm for a velocity of 1.7 cm/s. Qualitatively and approximately (*i.e.*, recognizing that the velocity is most easily described in a cylindrical coordinate system, but the diffusion field is Cartesian), this is the time at which the two reactant 'halves' of the flow stream have intermingled to a modest degree over a fraction of the capillary radius. The two halves have intermingled to a greater degree in lamina moving faster than the average velocity, and have intermingled virtually not at all for lamina near the wall.

The length required for the reaction, L_R, is the product of the sum of the chemical reaction time and the average start time and the mean fluid velocity unless this product is smaller then the homogenization length, L_H (*i.e.*, the reaction is fast*)*. In the latter case, the chemical reaction length is taken to be L_H.

$$L_R = \left(\langle t_s \rangle + \langle t_K \rangle\right) \cdot v = \left(\frac{a^2}{6D} + \langle t_K \rangle\right) \cdot v \qquad \text{when} \quad \frac{a^2}{6D} + \langle t_K \rangle > \frac{a^2}{D} \qquad (14)$$

$$= \frac{a^2}{D} v = L_H \qquad \text{otherwise.}$$

Figure 3-7 shows a plot of L_R as a function of rate constants for [A] = 1 μM and [B] = 0.5 μM reacting with 1:1 stoichiometry. The dotted line in Figure 3-7 shows the expected L_R with 2:1 stoichiometry for [A] = 1 μM and [B] = 5 μM. It predicts that the expected reaction length of 5 μM *p*-hydroquinone with 1 μM $\mathbf{1}^{3+}$ (k_2 of 8.04 x 10^5 $M^{-1} \cdot s^{-1}$ and 95% completion) occurs at around L_H (3.0 cm). This value corresponds to the experimentally determined reaction length.

Comparing the reaction length and the mixing length, the presence of a signal maximum in Figure 3-3(b) indicates that the reaction is complete much earlier than predicted. One possible reason for the short reaction length comes from the flow paths. The fluid streams from the postcolumn reagent and from the column effluent travel through 18 μm cylindrical channels. The Reynolds number is very near unity, so it is not possible to be sure that the flow is either inertial or viscous. It is possible that the two adjacent streams are constrained for a short time before they diffuse radially to fill a 50 μm diameter capillary. The homogenization could be completed in a shorter length than predicted because the diffusion distances are shorter than the 50 μm diameter of the reaction capillary. The signal decay with $\mathbf{1}^{2+}$, along with the presence of the signal maximum with $\mathbf{1}^{3+}$, suggests the radial relaxation of fluids occurs in a CTR. When $\mathbf{1}^{3+}$ is used,

the reaction increases the concentration of the product, while the radial relaxation process dilutes the product. If two processes have the same time scales, signal maximum would occur. A similar phenomenon was reported in a theoretical study of a coaxial mixer.[85] Another uncertainty comes from the laser focal point onto the capillary in association with the radially confined flow. The beam was focused to give a maximum signal during the experiment, but we do not know exactly where in the capillary we are measuring.

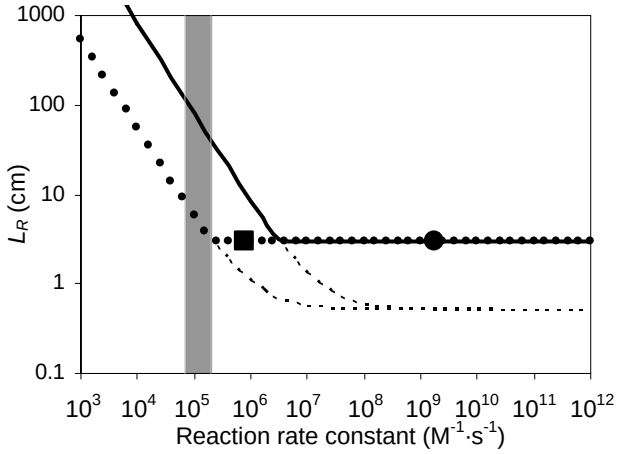

Figure 3–7. A plot of L_R as a function of second-order reaction rate constant, k.

For a reaction of A + B → P at [A] = 1 μM and [B] = 0.5 μM (solid line), and 2A + B → 2P at [A] = 1 μM and [B] = 5 μM (dotted line), where [C] denotes concentration of C in the mixed flow. The extent of reaction defining $\langle t_R \rangle$ (from equations (2) or (4)) is 95%. The dashed lines denote $\left(\langle t_s \rangle + \langle t_K \rangle\right) \cdot v$ for each reaction conditions (refer to equation (14)). The reaction rate constants of 5 (1.7 x 10^9 $M^{-1}\cdot s^{-1}$, calculated) is represented as a dot, and that of *p*-hydroquinone (8.04 x 10^5 $M^{-1}\cdot s^{-1}$, measured) as a square. Rate constants of catechols lie in the shaded area

Overlaying the measured reaction rate constants of catechols with $\mathbf{1}^{3+}$ onto the theoretical calculation in Figure 3-7 shows that the corresponding reactions are relatively slow and thus kinetically controlled. The corresponding photoluminescence signal intensity indeed depended on the rate constants at an intermediate reaction length as seen from the experimental results.

From the reaction rate constant, one can calculate the theoretical yields of the product, $\mathbf{1}^{2+}$. Lines in Figure 3-5 show the expected concentrations of products at different analyte concentrations at L = 8.0 cm. This length corresponds to 4.4 s reaction time plus 0.3 s start time. The experimentally measured concentrations of products are generally more than the calculated amounts when 2.0 μM of $\mathbf{1}^{3+}$ was used. As the reagent concentration increases to 6.0 μM and 10.0 μM, the amounts of products match the calculated amounts.

3.4.6. Comparison of a CTR with a chaotic mixer[91]

The chaotic mixer (staggered herringbone mixer, SHM) reported by the Whitesides group can mix fluids in a very short length, without adding significant axial dispersion compared to an open rectangular channel of similar dimensions. It is thus worthwhile to compare the axial dispersion in a CTR with that of an SHM, as a measure of mixer efficiency.

From basic chromatographic relations, the time equivalent of the plate height, H_t, is the ratio of the peak variance, σ_t, to the peak elution time, t_r, (second central moment/first moment) as in equation (15). By measuring the peak widths ($4\sigma_t$ at the baseline) and the retention time from Figure 4 (c),[91] H_t of the SHM was found to be 1 s.

$$H_t = \sigma_t^2 / t_r \qquad (15)$$

The linear velocity of the flow was 0.1 cm/s with given parameters (*Pe*: 1 x 10^4, *D*: 1 x 10^{-7} cm^2/s). The SHM mixes 90% of the fluids as it travels 1 cm. This takes 10 s and results in a band spreading, σ_t, of 3.2 s, sweeping a volume of 0.17 μL.

Let us compare this to a simple CTR. When a flow in a tube of radius a, is in the Taylor dispersion regime, H_t is a function of a and D (equation 16).

$$H_t = a^2 / 24D \qquad (16)^{11}$$

From this relation, a CTR with 16 μm radius is has H_t = 1 s for a solute with D = 1 x 10^{-7} cm^2/s. A flow in the CTR with the same *Pe* (1 x 10^4, v = 0.65 cm/s), is expected to be in the Taylor regime after it travels 16 cm (*Pe* < *L/a*). The corresponding residence time is 24 s, with expected σ_t of 4.9 s. The longer CTR has a smaller physical volume (0.12 μL) than the SHM, due to a small cross-sectional area of a capillary tube. However, this small area along with the long tube length does require backpressure. The Hagen-Poiseuille equation predicts an aqueous fluid traveling in a CTR will develop a backpressure of only 5~12 psi, which can be easily managed with conventional systems.

σ_t in a chromatographic sense is a measure of axial dispersion, and each dispersion contributes to a total peak broadening as follows,

$$\sigma^2_{TOTAL} = \sigma^2_{column} + \sigma^2_{postcolumn} + \sigma^2_{etc} \qquad (17)$$

Although σ_t from a CTR is about 1.5 times larger than that from an SHM, the actual contribution to total peak broadening in capillary HPLC is still comparable. Taking the actual chromatographic data from a similar study using a CTR (σ_{column} = 3.4 s, $\sigma_{postcolumn}$(CTR) = 0.88 s)[11] and assuming that σ_t value from a CTR is 1.5 times larger than that of an SHM in capillary HPLC conditions ($\sigma_{postcolumn}$(SHM) = 0.58 s), the extra peak broadening from the SHM is 1.5% of the capillary column band broadening, compared to that of the CTR being 3.2% . A similar calculation with a CTR of 50 μm diameter, however, predicts the travel time to be 60~160 s with expected σ_t of 13~20 s. Clearly, a 33 μm diameter CTR is comparable to the SHM, whereas the 50 μm diameter reactor is not. The sensitive efficiency change of a CTR to a small change in a diameter is explainable, considering that the major mixing process occurs by radial diffusion.

The above comparison was based on a slow-diffusing analyte with $D \sim 10^{-7}$ cm^2/s, and the diffusion coefficients of common analytes in HPLC are in the 10^{-5} to 10^{-6} cm^2/s range. Direct comparison of the SHM and the CTR using the conditions in the Whitesides work shows that the efficiency of an SHM is certainly a little better than that of a CTR. However, the CTR's figures of merit are much better when values of the diffusion coefficient are in the small solute range. Because the fabrication of a CTR does not need lithographic techniques and sophisticated facilities, a simple CTR with appropriate selection of flow conditions is thus very useful and effective for postcolumn reaction.

3.4.7. General considerations for applications to chromatographic systems

As a simple reactor, a CTR can mix fluid streams by radial diffusion without significant band broadening. However, certain analytes react more slowly than others, making the total time for the reaction longer. Since the extra time in a reactor causes extra band broadening, which is a major challenge for a postcolumn derivatization methods in chromatography, it is worthwhile to figure out how fast a reaction should be to maintain the separation efficiency.

Taking the actual chromatographic data again from the previous study (number of theoretical plates (N) = 14,000, σ_{column} = 3.4 s, D = 4.1 x 10^{-6} cm^2/s and a = 25 μm)[11] and equations (16) and (17), we can find out the residence time of a fluid in a CTR that adds 10% extra band broadening (*i.e.,* when σ_{TOTAL} is 3.7 s). The calculated residence time is on the order of 40 s.

In a PFET postcolumn chromatographic system, analyte concentrations are usually far less than the reagent concentration. The kinetics of such reactions follows a pseudo-first-order rate law, as in equations (18),

$$\mathbf{1}^{3+} + An \rightarrow \mathbf{1}^{2+} + An^{+} \quad (18a)$$

$$d[\mathbf{1}^{2+}]/dt = k_1 \cdot [\mathbf{1}^{3+}] \cdot [An] = k_3 \cdot [An] \quad (18b)$$

where k_3 is a pseudo-first-order reaction rate (= $k_1 \cdot [\mathbf{1}^{3+}]$) with units s^{-1}. Evaluating the solution of the differential equation with 95% extent of reaction at 40 s reaction time gives a k_3 value of 0.1 s^{-1}. Reactions with smaller pseudo-first-order rate constants thus are expected to suffer either more than 10% of extra column band broadening with full signal, or acceptable band spreading with less than full signal. When 10 μM $\mathbf{1}^{3+}$ is used as the reagent, the corresponding minimum second-order reaction rate constant, k_{min}, is about 2 x 10^4 $M^{-1} \cdot s^{-1}$. A similar calculation assuming 5% extra band broadening yields the residence time of ~ 20 s and k_{min} of 3 x 10^4 $M^{-1} \cdot s^{-1}$. However, it is always possible to make the derivatization reaction faster (*i.e.*, to decrease the extra column band broadening) by increasing the concentration of $\mathbf{1}^{3+}$. For example, using 1 mM $\mathbf{1}^{3+}$ as the reagent decreases k_{min} to 2 x 10^2 $M^{-1} \cdot s^{-1}$ for 10% band broadening. Generally k_{min} is inversely proportional to the concentration of $\mathbf{1}^{3+}$ at a given reaction time, thus increased reagent concentrations enable the reactions with small rate constants to be eligible for postcolumn reaction. Although these estimates are based on a specific chromatographic peak with σ_{column} of 3.4 s, in general, such estimate gives a simple method to optimize the reaction conditions and to predict the extent of band broadening based on basic kinetics laws.

3.5. Conclusions

A capillary Taylor reactor serves as a simple and effective postcolumn reactor for various analytes with different reaction rates. Two processes, homogenization and chemical kinetics, in the capillary reactor govern the reaction length. There is a minimum pseudo first-order reaction rate constant of about 0.1 s^{-1} necessary to avoid significant band broadening in capillary HPLC when using a 50 μm ID CTR.

4. Simultaneous Determination of Biogenic Monoamines in Rat Brain Dialysates using Capillary High-Performance Liquid Chromatography with Photoluminescence-Following Electron-Transfer

This work is published in *Anal. Chem.*, **2006**, *78*, 1755-1760;

4.1. Abstract

Simultaneous determination of biogenic monoamines such as dopamine, serotonin and 3-methoxytyramine in brain is important in understanding neurotransmitter activity. This study presents a sensitive determination of biogenic monoamines in rat brain striatum microdialysates using capillary high-performance liquid chromatography (HPLC) with the photoluminescence-following electron-transfer (PFET) detection technique. Separation conditions were optimized by changing the concentration of an ion-interaction agent and the percentage of an organic modifier. The high concentration of the ion-interaction agent enabled the amines as a class to be separated from interfering acids, but also made the separation very long. To shorten the separation time, 10% (v/v) acetonitrile was used as the organic modifier. Eight chromatographic runs during a 3-hour period were analyzed in terms of retention times, peak heights and peak widths. Chromatograms are very reproducible, with less than 1% changes in peak height over three hours.

Typical concentration detection limits at the optimum separation condition were less than 100 pM for metabolic acids and about 200 pM for monoamines. The injection volume of the sample was 500 nL. Thus, the mass detection limits were less than 50 amol for metabolic acids and around 100 amol for monoamines. Typical separation time was less than 10 minutes.

To validate the technique, the separation method was applied to the observation of drug-induced changes of monoamine concentrations in rat brain microdialysis samples. Local perfusion of tetrodotoxin, a sodium-channel blocker, into the striatum of an anesthetized rat decreased dopamine, 3-methoxytyramine and serotonin concentrations in dialysates. Successive monitoring of striatal dialysates at a temporal resolution of 7.7 min showed that the injection of

nomifensine transiently increased dopamine and 3-methoxytyramine concentration in rat brain dialysates.

4.2. Introduction

Biogenic monoamines in brain, such as dopamine (DA) and serotonin (5HT), play important roles as major neurotransmitters in the mammalian central nervous system.[100] Reliable measurement of extracellular neurotransmitter concentration is thus important in understanding the central nervous system and its underlying physiology.

Several methods have been used to monitor the extracellular level of neurotransmitters and their metabolites without separation.[15, 101-103] However, most neurons do not contain only one neurotransmitter, thus changes in the neurotransmitter concentrations are often interrelated. Moreover, the real biological response is more likely due to the interplay of all the released neurotransmitters. Therefore, it is highly desirable to monitor the level of several neurotransmitters simultaneously. Measuring extracellular concentrations of neurotransmitter metabolites including 3, 4-dihydroxyphenylacetic acid (DOPAC), 3-methoxytyramine (3MT), 5-hydroxyindole-3-acetic acid (5HIAA), homovanillic acid (HVA), is also important in understanding the metabolic pathways and their kinetics.[104]

Since the first successful combination of microdialysis and high-performance liquid chromatography (HPLC) in 1980s,[13] the technique has been most widely used to determine the extracellular levels of neurotransmitters and their metabolites. Typical detection methods are electrochemical detection (HPLC-ECD)[105, 106] and fluorescence detection(HPLC-FL).[107-109] The high sensitivity and selectivity of HPLC-ECD is beneficial, but its reliability is compromised due to electrode fouling. On the other hand, the utility of HPLC-FL is limited due to the availability

of suitable fluorescent labels. Analytes can be derivatized, but it requires multiple sample treatment steps and can induce extra band broadening if it is done after separation.

The photoluminescence-following-electron-transfer (PFET) technique,[9, 10] developed in our laboratory, is a useful detection scheme for electrochemically active molecules. A fluid stream containing a homogeneous oxidant is mixed with chromatographic effluent in a diffusion-controlled mixer. The oxidant is subsequently reduced allowing photoluminescence upon optical excitation, which is quantitatively measured and recorded. No surface reaction is involved in the PFET process, thus no electrode fouling can happen. Also, the PFET detection does not include derivatization steps, but rather an electron transfer reaction. As long as the analyte can be oxidized by the homogenous oxidant, which is true for many neurotransmitters and their metabolites, the PFET technique can be applied after separation with negligible band broadening.[11, 45]

In this chapter, we report a successful combination of a capillary HPLC with tris(2,2'-bipyridine)osmium(**1**) as the postcolumn PFET reagent. The capillary HPLC is especially suited for the analysis of biological samples due to its small sample load volume and high sensitivity.[56, 110] Rat brain microdialysis samples were analyzed to show the effectiveness of the system by monitoring the changes in neurotransmitter concentrations under previously characterized conditions. The PFET approach has competitive detection limits (both mass and concentration) and is rapid and reproducible.

4.3. Experimental Section

4.3.1. Reagents

All chemicals from commercial sources were used as received without further purification except where noted. Reagent and sources were as follows: trifluoroacetic acid (TFA) from Acros (Geel, Belgium); monochloroacetic acid from Mallinckrodt (St. Louis, MO); acetonitrile, 2-propanol, and sodium acetate from EMD (Gibbstown, NJ); 1-propanol, lead dioxide, sodium hydroxide, glacial acetic acid, and disodium EDTA from J.T. Baker (Phillipsburg, NJ); tetrodotoxin (with citrate) from Alomone Lab (Jerusalem, Israel); sodium perchlorate from Aldrich (Milwaukee, WI); chloral hydrate, nomifensine, dopamine (DA) hydrochloride, 3, 4-dihydroxyphenylacetic acid (DOPAC), serotonin (5HT) hydrochloride, 3-methoxytyramine (3MT) hydrochloride, 5-hydroxyindole-3-acetic acid (5HIAA), homovanillic acid (HVA) and sodium 1-octanesulfonate (SOS) from Sigma (St. Louis, MO). Sodium perchlorate was recrystallized from methanol once to remove chloride. All aqueous solutions were prepared with deionized water (18.2 MΩ resistivity) from a Millipore Milli-Q Synthesis A10 system (Billerica, MA).

4.3.2. Preparation of metal polypyridyl complexes

$Os(bpy)_3(PF_6)_2$ (**1**) was prepared and recrystallized in our laboratory according to previously reported procedures.[54] Crystals of the osmium complex were dissolved in acetonitrile to make a 1.0 mM stock solution. Aliquots of the stock solution were diluted in an acidic electrolyte solution (0.2% TFA and 0.1 M $NaClO_4$ in acetonitrile) to prepare the PFET reagent solution. The

resulting solution was used after filtering through a disposable 0.45 μm PTFE/PP syringe filter (Chrom Tech, Apple Valley, MN).

4.3.3. Chromatographic system

Two HPLC pumps (Waters 590 and 600/626S, Milford, MA) or a syringe pump (ISCO 100DM, Lincoln, NE) with simple tees as flow splits delivered solutions at ~1 μL/min. The Waters 600/626S pump was used to deliver the mobile phase and another to deliver the PFET reagent. The flow rate from each source was frequently checked by measuring the volume of solutions delivered in a specific time, to ensure the correct flow rate is maintained during experiments.

Homemade capillary columns were packed by previously described techniques[56] using 100 μm i.d., 360 μm o.d. fused-silica capillaries (Polymicro Technologies, Phoenix, AZ) as the column blank. The column was slurry packed with reversed-phase particles at 3000-4000 psi using a constaMetric III metering pump (LDC Analytical, Riveria Beach, FL)[11] and was connected directly to an Upchurch loop microinjector (Oak Harbor, WA), which introduced 500 nL of each sample into the column.

A capillary Taylor reactor (CTR) was used to mix the chromatographic effluents and the postcolumn PFET solution. They were prepared according to the previously reported procedure.[11, 45, 57] The ends of two 18-μm tungsten wires (Goodfellow, Devon, PA) were each threaded into two 50-μm fused-silica capillaries (Polymicro Technologies). The other ends were both threaded into another 50-μm fused-silica capillary to form a Y-shaped device. The third capillary was coated with a transparent polymer (Polymicro Technologies). The junction between three capillaries was placed in a piece of dual shrink/melt tubing (Small Parts, Miami

Lakes, FL). After sufficient heat was applied and the device was allowed to cool, the tungsten wires were removed to create fluid conduits of 18-μm diameter between 50-μm capillaries. The reaction length was set at 8 cm from the confluence according to the previous study.[45]

4.3.4. Optical detection setup

A laser beam from a 30-mW variable-power blue-line argon ion laser (Cyonics/Uniphase 2201-30BL, San Jose, CA) passed through a 488-nm band-pass filter and was focused onto an optically transparent capillary. Photoluminescence from $\mathbf{1}^{2+}$ was measured using an epifluorescence optical setup: a microscopic objective lens (Carl-Zeiss Plan Neofluar 20x, NA 0.5, Thornwood, NY) focused the optical emission from the capillary and a combination of a dichroic mirror (cutoff at 500 nm) and optical filters (a 600-nm long-pass filter and a 750-nm band-pass filter, angle tuned) allowed the photoluminescence into an IR-sensitive photomultiplier tube (Hamamatsu R374, Bridgewater, NJ). A Keithley 6485 picoammeter (Cleveland,OH) converted photocurrent from the photomultiplier tube to a dc voltage signal. An IBM-compatible computer with a PeakSimple Chromatographic Data System (SRI Instruments, Torrance, CA) collected the dc signal after a 0.4-Hz eight-pole low-pass filter (Wavetek 852 Dual filter, San Diego, CA).

4.3.5. Chromatographic conditions for separation of monoamines

The capillary column was slurry packed to 7.6 cm with 2.6 μm XTerra MS-C_{18} (Waters, Milford, MA) reversed phase particles. Aqueous buffers containing 100 mM sodium acetate or a mixture of sodium acetate and monochloroacetic acid (total concentration of 100 mM), 0.15 mM disodium EDTA, and SOS (pH was adjusted with glacial acetic acid or concentrated NaOH solution) were mixed with organic modifiers, such as acetonitile or methanol. The mobile phase was passed through a Nylon filter with 0.45 μm pores (Osmonics, Minnetonka, MN).

4.3.6. Chromatographic standard samples

Stock solutions of 1.0 mM analytes were prepared in 0.1 M acetic acid and stored frozen. The frozen stock solutions were thawed before each use and were diluted to desired concentrations in degassed solutions. Typically, successive 10-fold dilutions were made using 0.1 M acetic acid except the final dilution, where artificial cerebrospinal fluid (aCSF), was used to mimic the sample matrix of the microdialysis samples. The aCSF contained 145.0 mM NaCl, 2.7 mM KCl, 1.0 mM $MgCl_2$, 1.2 mM $CaCl_2$, 0.45 mM NaH_2PO_4 and 1.55 mM Na_2HPO_4 at pH 7.40.

4.3.7. Animal and surgical procedures

All procedures involving animals were conducted with approval of the Institutional Animal Care and Use Committee of the University of Pittsburgh. Male Sprague–Dawley rats (250–375 g, Hilltop, Scottdale, PA) were anesthetized with chloral hydrate (initial dose of 300 mg/kg i.p.

with additional doses of 50 mg/kg i.p. as needed to maintain anesthesia) and wrapped in a homeothermic blanket (EKEG Electronics, Vancouver, BC, Canada). The rats were placed in a stereotaxic frame (David Kopf Instruments, Tujunga, CA) with the incisor bar set at 5 mm above the interaural line[58] and appropriately placed holes were drilled through the skull.

4.3.8. Microdialysis

Vertical concentric microdialysis probes (220 μm o.d., 4 mm long) were constructed with hollow fiber dialysis membrane (Spectra-Por RC Hollow Fiber, MWCO: 13,000, 160 μm i.d., Spectrum Laboratories Inc., Rancho Dominguez, CA) and fused silica outlet lines (150 μm o.d., 75μm i.d., Polymicro Technologies). The microdialysis probe was implanted into the brain over a period of 30 min to the following coordinates: 2.5 mm anterior to bregma, 2.5 mm lateral from midline and 7.0 mm below dura. The probe was perfused at 0.586 μL/min. For drug-induced changes of the monoamine concentrations, tetrodotoxin (TTX) and nomifensine were used. 100 μM of TTX was dissolved in aCSF, and perfused locally. Nomifensine (20 mg/kg, i.p.) was prepared in a phosphate buffered saline (PBS). All brain dialysates were collected in vials containing 10%(v/v) 0.1 M acetic acid, where typical volume of the dialysis samples was 5 μL unless otherwise noted. For nomifensine experiments, 4 consecutive dialysates were collected from an anesthetized rat brain striatum at an interval of 15 minutes to monitor basal levels of monoamines. After the i.p. injection of nomifensine, the sampling interval was reduced to 7.7 min to increase the temporal resolution. All collected dialysates were stored in an ice bath for immediate analysis, or frozen for future use.

4.4. Results and Discussion

4.4.1. Optimizing the separation conditions

The separation conditions for the biogenic monoamines were optimized using three parameters: pH of the mobile phase, the SOS (ion-interaction agent) concentration and the percentage of organic modifier. The major technical problem in the separation was that the brain dialysates contained interfering compounds, including amines and acids. Retention times of solutes usually depend on pH, according to their pK_a values. However, a previous study proved that the PFET system works best at acidic conditions.[10, 111] The pH values of the mobile phases tested were thus limited to a range of pH from 3.0 to 5.0. Generally in this range, acids are retained less at higher pH while the retention of amines is not influenced much by changes in pH.

A more effective optimization could be achieved by changing the SOS concentration and the organic modifier contents. SOS is known to retain ammonium ions electrostatically. Thus, a high concentration of SOS makes monoamines as a class separate from acids. The SOS concentrations of the mobile phases were from 0 to 10 mM. Successful separations of monoamines and metabolic acids in standard samples (DA, DOPAC, HVA, 3MT, 5HT and 5HIAA) were achieved with a mobile phase at low or intermediate concentrations of SOS. However, application of the same separation condition to the rat brain dialysates was not successful. The concentrations of uric acid, ascorbic acid and the acidic metabolites in the brain dialysates are much higher than the concentrations of monoamines, typically a few orders of magnitude higher. Thus monoamine peaks were usually buried by huge peaks of metabolic acids, and quantification of the peaks was difficult. This problem was solved by using a high

concentration of SOS to retain the monoamines even longer in the column: the monoamines were eluted even later than the typical late runner, HVA. The use of SOS at high concentration, however, resulted in a very long chromatographic run and band broadening of the more retained monoamines. Thus organic modifiers, methanol and acetonitrile in this study, were used to shorten the chromatographic run time. The optimum organic modifier was 10% (v/v) acetonitrile. A typical isocratic chromatographic run time for a standard mixture was less than 7 minutes. Using organic modifiers did not only shorten the chromatographic run times, but also achieved on-line preconcentration of analytes: since the injection solution did not contain any organic solvents, injected analytes were concentrated at the front of the column until the more hydrophobic mobile phase eluted the analytes. Thus, peak volumes of analytes are smaller than the injection volume. Figure 4-1 shows a typical optimized separation of standard analytes.

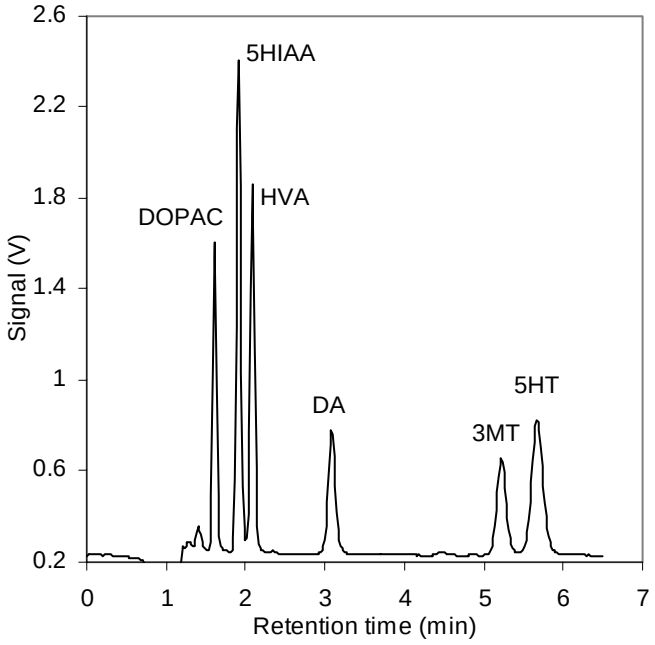

Figure 4−1. A typical chromatogram of a standard injection sample.

Sample contained DA, DOPAC, 3MT, HVA, 5HT and 5HIAA, each at 100 nM. Separation conditions were as follows. Column: 100 μm i.d., 7.6 cm length capillary column packed with XTerra MS-C_{18} reversed phase particles. Mobile phase: pH 4.00 aqueous buffer containing 100 mM sodium acetate, 0.15 mM disodium EDTA and 10.0 mM SOS, mixed with 10% (v/v) acetonitrile. Flow rate: 1 μL/min. Injection volume: 500 nL.

4.4.2. Reproducibility, linearity and detection limits

The chemistry of the detection is more thoroughly explained in the chapter 2. For the determination of monoamines the reproducibility of a method is very important. Table 4-1 shows the variability of the retention times, the peak heights and the peak widths (full-width at half-maximum, FWHM) for 8 chromatographic runs during a 3-hour period. Some of the 8 chromatograms are consecutive. Chromatograms are very reproducible, with changes in peak height less than 1% over the three hour period. This is remarkable reproducibility for a nominally electrochemical detection technique.

Table 4–1. Reproducibility of the chromatographic retention and the detector sensitivity.

Eight chromatographic runs of 50 nM mixture samples were analyzed. Values in the parentheses are standard errors of the mean for 8 repeats. Separation conditions were slightly different from Figure 4-1. Mobile phase contained the aqueous buffer of 100 mM sodium acetate, 0.15 mM disodium EDTA and 7.0 mM of SOS at pH 4.00, mixed with 87.5:12.5 (v/v) acetonitrile. Capillary column was slurry packed to 9.5 cm with 3 μm AlltimaC_{18}.

Analytes	Retention time (min)	Peak Height (mV)	FWHM (s)
DOPAC	1.78 (0.00)	546 (3)	3.48 (0.00)
5HIAA	2.31 (0.00)	811 (5)	4.10 (0.09)
HVA	2.56 (0.00)	494 (3)	4.23 (0.10)
DA	3.07 (0.00)	183 (1)	7.86 (0.08)
3MT	5.45 (0.00)	133 (1)	7.86 (0.12)
5HT	5.95 (0.01)	291 (2)	9.42 (0.11)

A calibration fit revealed the linearity of the detector and the detection limits. Standard solutions containing DA, 3MT and 5HT from 0 to 100 nM were injected, and the resulting peak heights were analyzed. Typical regression equations for peak heights versus concentrations (mV/nM) were: $y = 4.88 x + 0.06$ ($r^2 = 1.000$) for DA, $y = 3.64 x – 5.06$ ($r^2 = 0.997$) for 3MT, $y = 5.99 x – 2.37$ ($r^2 = 0.999$) for 5HT.

The concentration detection limits for monoamines were calculated from the calibration fit, and those of metabolic acids were from a standard injection containing 100 nM analytes using a signal to noise ratio of 3. Typical concentration detection limits were 62 pM for DOPAC, 41 pM for 5HIAA, 55 pM for HVA, 180 pM for DA, 250 pM for 3MT and 150 pM for 5HT. The injection volume of the sample was 500 nL. Thus the mass detection limits were 31 amol for DOPAC, 21 amol for 5HIAA, 27 amol for HVA, 92 amol for DA, 120 amol for 3MT and 75 amol for 5HT.

4.4.3. Analysis of rat brain microdialysates

The optimized chromatographic conditions were used to determine monoamine concentrations in rat brain dialysates. Figure 4-2 shows the chromatograms of dialysates from a rat brain striatum before and after local infusion of TTX for ~60 min. Local infusion of TTX, a voltage-sensitive sodium channel blocker, caused a significant decrease of extracellular monoamine concentrations: basal levels of DA, 3MT and 5HT were 10.6, 3.6 and 1.2 nM respectively, while concentrations of monoamines after local infusion of TTX were 3.1, 1.6 and 0.6 nM. All concentrations are not corrected for *in vitro* probe recovery. Generally accepted literature values for basal concentrations of DA and 5HT in rat brain striatum are 5 – 12 nM and 0.2 – 6 nM.[15, 112, 113]

The small injection volume of the capillary HPLC, combined with a short HPLC analysis time enabled the consecutive analysis of the samples. Our optimized HPLC-PFET method was applied to monitor the drug-induced changes of the monoamine concentrations. Figure 4-3 shows the concentration changes of the monoamines upon the injection of nomifensine, a dopamine

reuptake blocker. The dopamine level increased by ~10 times soon after nomifensine was injected and gradually relaxed to a value, still higher than the basal level of dopamine. The concentration of 3MT changed with the same time course as that of DA. Typical chromatograms from the analysis are presented in Figure 4-4. All the solutes were eluted in 9 min, thus the total analysis time for all 16 chromatographic runs was less than 2.5 hours. (9 min x 16 = 144 min)

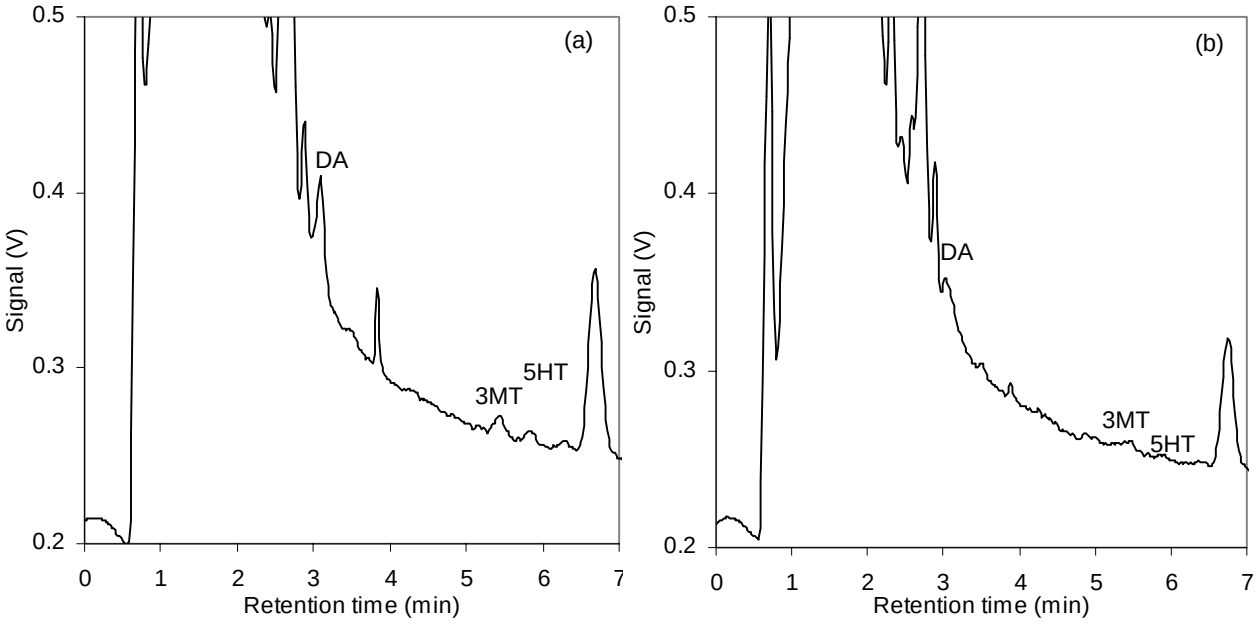

Figure 4–2. Chromatograms of rat brain dialysates (a) before and (b) after local infusion of TTX for 60 min. TTX decreased the DA concentration to ~30% of basal level and other monoamines to ~50%.[109] Separation conditions were same as in Figure 4-1.

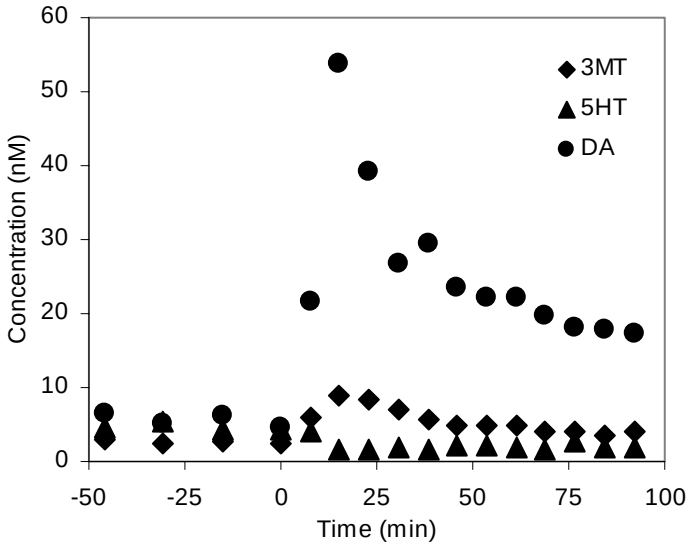

Figure 4–3. Concentration changes of the monoamines in the rat brain striatum dialysates after injection of nomifensine.

Injection time of nomifensine is marked as time = 0.

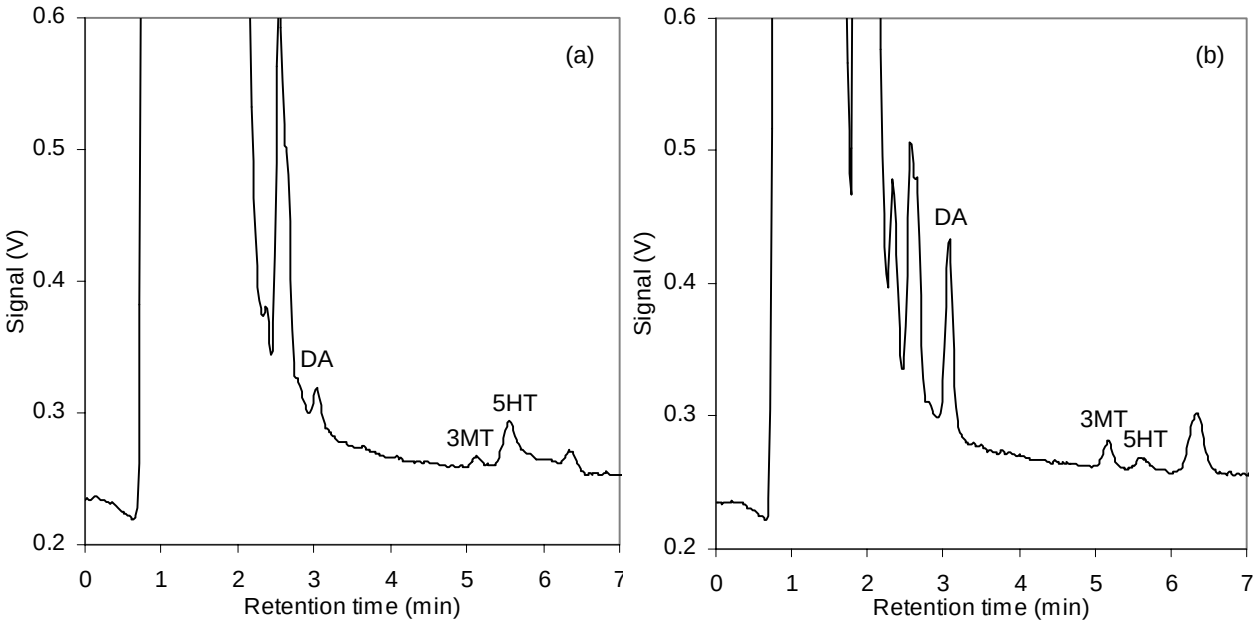

Figure 4–4. Typical chromatograms of rat brain dialysis (a) before and (b) after the injection of nomifensine.

Separation conditions were same as in Figure 4-1.

4.4.4. Comparison with other techniques

The utility of the detection method can be assessed by several factors: (1) concentration and/or mass detection limits, (2) sample requirements, (3) variety of detectable analytes and (4) the analysis time. The capillary electrophoresis (CE) combined with laser-induced fluorescence (LIF) technique generally showed good mass detection sensitivity, typically ~300 amol of catecholamines.[114-117] This is mainly due to the small sample volume for CE. Non-fluorescent catecholamine analytes were successfully derivatized with naphthalene-2,3-dicarboxaldehyde (NDA) before separation. The relatively fast reaction of NDA, on the order of few minutes, was successfully combined with an on-line derivatization technique to achieve continuous detection of catecholamines with a temporal resolution of 20 s.[116] However, the NDA-derivatization technique is highly selective: DOPAC, a very important dopamine metabolite, cannot be derivatized due to the lack of a primary amine.[118] Serotonin could not be derivatized either. Thus simultaneous detection of catecholamines and indoleamines with their metabolites is not possible. Serotonin was reported to be derivatized with fluorescein isothiocyanate (FITC),[119] but its detection limit was on the order of 20 nM with a 2-hour derivatization time.

Table 4-2 shows a summary of the comparison of PFET to the best fluorescence approach and the most recent electrochemical detector approaches. Yamaguchi, Kehr and coworkers presented a successful two-step precolumn derivatization technique for catecholamines and indoleamines combined with HPLC.[109, 120, 121] The two-step derivatization involves reactions of benzylamine (BA) and 1,2-diphenylethylenediamine (DPE). This technique enabled simultaneous detection of many neurotransmitters and their metabolites with very good detection sensitivity. Typical mass detection limits are ~100 amol with 10 – 20 μL injections. However,

the technique is limited due to the long analysis time and pretreatment steps. The derivatization step takes ~20 min at elevated temperature (50 °C), and the chromatographic run time is about 50 min.

HPLC-ECD is one of the most widely used techniques for neurotransmitter detection, because there is no need for sample pretreatment. Simultaneous detection of various neurotransmitters and their metabolites is possible in ~20 min depending on the separation conditions.[104, 122] Typical detection limits are ~1 nM, but careful optimization of the separation/detection conditions[123-125] and modification of an electrode surface[126] enabled the even higher detection sensitivity of subnanomolar concentrations. Innovations in cell design[113, 127] also improved the detection sensitivity to lower than 100 pM. The typical sample injection volume was 10 μL. In one case, the injection volume was 200 nL,[127] however the technique uses redox recycling thus it is limited to reversible couples. Furthermore, it was not applied to real samples.

The performance of PFET combined with a capillary HPLC system is comparable to that of the best HPLC-ECD or HPLC-FL: its typical detection limits of ~100 pM (with 500 nL injection volume) with a short analysis time of less than 10 minutes. Aside from the good detection performance, the technique is remarkably robust. Chromatographic parameters (retention, peak shape, sensitivity) are reproducible. There is no electrode fouling problem and no need for a pretreatment step before sample injection.

Table 4–2. Comparison of detection limits, separation time and detectable analytes for HPLC detection.

FL: fluorescence detection, ECD: electrochemical detection, PFET: photoluminescence-following electron-transfer, DA: dopamine, 5HT: 5-hydroxytyramine (serotonin), 3MT: 3-methoxytyramine, DOPAC: 3, 4-dihydroxyphenylacetic acid, 5HIAA: 5-hydroxyindole-3-acetic acid, HVA: homovanillic acid, NE: norepinephrine and E: epinephrine.

Det. method	Analytes	Analysis time	Injection volume	Mass detection limit	Concentration detection limit
FL[109]	DA, 5HT, NE	22 + 50 min	10 μL	42 amol (DA) 76 amol (5HT)	4.2 pM (DA) 7.6 pM (5HT)
FL[121]	DA, 5HT, NE, 5HIAA, DOPAC, *l*-DOPA	22 + 50 min	20 μL	130 amol (DA) 200 amol (5HT)	19.5 pM (DA) 30 pM (5HT)[a]
ECD[b, 127]	DA, NE, E	10 min	200 nL	25 amol (DA, NE)	120 pM (DA, NE)
ECD[124]	DA	11 min	10 μL	600 amol (DA)	60 pM (DA)
ECD[123]	DA, 5HT, NE	25 min	10 μL	3 – 6 fmol	300 – 600 pM
ECD[128]	DA, 5HT, NE, DOPAC, HVA, 5HIAA	30 min	50 μL	110 fmol (DA) 28 fmol (5HT)	2.2 nM (DA) 560 pM (5HT)
ECD[c, 113]	DA, 5HT, DOPAC, HVA, 5HIAA	25 min	15 μL	0.5 – 1 fmol	30 – 70 pM
ECD[d, 126]	DA, 5HT, NE, E, DOPAC	25 min	20 μL	50 fmol (DA) 20 fmol (5HT) 10 fmol (NE, E)	2.5 nM (DA) 1.0 nM (5HT) 500 pM (NE, E)
PFET[e]	DA, 5HT, 3MT, HVA, DOPAC, 5HIAA	< 10 min	500 nL	92 amol (DA) 120 amol (3MT) 75 amol (5HT)	180 pM (DA) 250 pM (3MT) 150 pM (5HT)

[a] due to dilution during derivatization, [b] electrochemical detection with redox-cycling, [c] electrochemical detection with the thin-layer amperometric cell, [d] electrochemical detection with the modified dual electrodes, [e] this work.

4.5. Conclusions

The capillary HPLC system with tris(2,2'-bipyridine)osmium as the postcolumn PFET reagent achieved selective and sensitive detection of biogenic monoamines. Dopamine, serotonin, 3-hydroxytyramine and other metabolites were determined at subnanomolar concentrations. Concentrations of biogenic monoamines in the rat brain striatum were monitored while nomifensine was injected to an anesthetized rat. Temporal resolution of 7.7 min was short enough to show the rise and decay of the dopamine concentration, and the chromatographic system was sensitive enough to follow the changes.

5. Chromatographic Determination of Carbidopa and Dopamine in Rat Brain Microdialysates with Detection by Photoluminescence-Following Electron-Transfer

5.1. Abstract

Brain microdialysis combined with high-performance liquid chromatography is a widely used method to investigate the extracellular space of living brain tissues. However, the microdialysis probe damages brain tissue. Carbidopa, co-prescribed with levodopa, is an enzyme inhibitor that is excluded from brain by the blood-brain barrier in normal circumstances. We hypothesize that damage in the brain tissue will allow carbidopa to enter into the brain.

Striatal microdialysis samples from anesthetized rats were investigated by high-performance liquid chromatography (HPLC) combined with photoluminescence-following electron-transfer (PFET) technique at a temporal resolution of 10 min. Separation of carbidopa in brain microdialysates was achieved using a reversed-phase, 100 μm i.d. capillary column at 1 μL/min flowrate. The mobile phase contained aqueous acetate-monochloroacetate buffer at pH 2.30, with 0.15 mM disodium EDTA and 13 mM sodium 1-octanesulfonate as an ion-interaction agent, mixed with 12.5% (v/v) acetonitrile. A typical separation required 8 min. The pH of the mobile phase was a very effective variable for carbidopa separation. The concentration detection limits of dopamine and carbidopa were 570 pM and 320 pM, respectively at 500 nL injection.

Striatal microdialysates from three rats, which were given carbidopa by i.p. injection, contained approximately 100 nM carbidopa in dialysates. Microdialysates from three control rats, which were given saline buffer, did not contain any carbidopa.

5.2. Introduction

Brain microdialysis is a useful technique to monitor the local extracellular environment in the brain tissues. Since it has the ability to sample continuously from the tissue of a living animal,[14] the technique has been widely used in conjunction with conventional separation techniques such as high-performance liquid-chromatography.[13] However, many studies report that the microdialysis probe causes damage to the brain as a result of the implantation.[15]

Carbidopa is a common therapeutic co-prescription with levodopa (*l*-DOPA) for Parkinson's disease (PD), a degenerative nervous system disorder. The causes of PD are still not clear, but its symptoms such as progressive tremor, bradykinesia and muscular rigidity are effectively treated by medication that increases the concentration of dopamine in brain.[129, 130] However, the administration of dopamine is not successful, because it cannot cross the blood-brain barrier (BBB). Thus levodopa, the precursor for a dopamine, is orally administered for PD patients. Levodopa, after crossing the BBB, is decarboxylated to form dopamine in the brain. However, levodopa can be also decarboxylated outside the brain. A high concentration of dopamine outside the BBB causes adverse side effects such as nausea, anorexia and cardiac abnormalities.[131] Side effects can be reduced by administering levodopa with carbidopa. Carbidopa inhibits decarboxylation of levodopa outside the BBB, allowing more levodopa to be transported into the brain. Furthermore, carbidopa does not pass the BBB, thus it does not inhibit decarboxylation of levodopa in the brain.

If, however, the blood-brain barrier is damaged by any means, the carbidopa may be found in the extracellular space of brain tissue. In this study, we used carbidopa as a probe molecule to monitor the damage to brain tissues caused by microdialysis probe. Carbidopa was

administered during the continuous microdialysis sampling. The rat brain dialysates were subsequently analyzed by high-performance liquid-chromatography with photoluminescence-following electron-transfer (HPLC-PFET) technique,[9, 10] to monitor dopamine and carbidopa concentrations.

5.3. Experimental Section

5.3.1. Reagents

All commercial chemicals were used as received without further purification except where noted. Reagent and sources were as follows: trifluoroacetic acid (TFA) from Acros (Geel, Belgium); monochloroacetic acid from Mallinckrodt (St. Louis, MO); acetonitrile, 2-propanol, and sodium acetate from EMD (Gibbstown, NJ); 1-propanol, lead dioxide, sodium hydroxide, glacial acetic acid, and disodium EDTA from J.T. Baker (Phillipsburg, NJ); sodium perchlorate from Aldrich (Milwaukee, WI); chloral hydrate, dopamine (DA) hydrochloride, 3, 4-dihydroxyphenylacetic acid (DOPAC), serotonin (5HT) hydrochloride, 3-methoxytyramine (3MT) hydrochloride, 5-hydroxyindole-3-acetic acid (5HIAA), homovanillic acid (HVA), S-(-)-carbidopa and sodium salt of 1-octanesulfonic acid (SOS) from Sigma (St. Louis, MO). Sodium perchlorate was recrystallized from methanol once to remove chloride. All aqueous solutions were prepared with deionized water (18.2 MΩ resistivity) from a Millipore Milli-Q Synthesis A10 system (Billerica, MA).

5.3.2. Preparation of metal polypyridyl complexes

$Os(bpy)_3(PF_6)_2$ (**1**) was prepared and recrystallized in our laboratory according to previously reported procedures.[54] Crystals of osmium complex were dissolved in acetonitrile, to make a 1.0 mM stock solution. Aliquots of the stock solution were diluted in an acidic electrolyte solution (0.2% TFA and 0.1 M $NaClO_4$ in acetonitrile) to prepare the PFET reagent solution. The resulting solution was used after filtering through a disposable 0.45 μm PTFE/PP syringe filter (Chrom Tech, Apple Valley, MN).

5.3.3. Chromatographic system

Two HPLC pumps (Waters 590 and 600/626S, Milford, MA) or a syringe pump (ISCO 100DM, ISCO, Lincoln, NE) with simple tees as flow splits delivered solutions at ~1 μL/min. The Waters 600/626S pump was used to deliver the mobile phase and another to deliver the PFET reagent. The flow rate from each source was frequently checked by measuring the volume of solutions delivered in a specific time, to ensure the correct flow rate is maintained during experiments.

Homemade capillary columns were packed by previously described techniques[11] using 100 μm i.d., 360 μm o.d. fused-silica capillaries as the column blank. The column was slurry packed with reversed-phase particles at 3000-4000 psi using a constaMetric III metering pump (LDC Analytical, Riveria Beach, FL). It was connected directly to an Upchurch loop microinjector (Oak Harbor, WA), which introduced 500 nL of each sample into the column.

A capillary Taylor reactor (CTR) was used to mix the chromatographic effluents and the postcolumn PFET solution. They were prepared according to the previously reported

procedure.[11, 45, 57] The ends of two 18-μm tungsten wires (Goodfellow, Devon, PA) were each threaded into two 50-μm fused-silica capillaries (Polymicro Technologies, Phoenix, AZ). The other ends were both threaded into another 50-μm fused-silica capillary to form a Y-shaped device. The third capillary was transparent coated. The junction between three capillaries was placed in a piece of dual shrink/melt tubing (Small Parts, Miami Lakes, FL). After heat-shrinking the device was allowed to cool, the tungsten wires were removed to create fluid conduits of 18-μm diameter between 50-μm capillaries. The reaction length was set at 8 cm from the confluence according to the previous study.[45]

5.3.4. Optical detection setup

A laser beam from a 30-mW variable-power blue-line argon ion laser (Cyonics/Uniphase 2201-30BL, San Jose, CA) passed through a 488-nm band-pass filter and was focused onto an optically transparent capillary. Photoluminescence from $\mathbf{1}^{2+}$ was measured using an epifluorescence optical setup: a microscopic objective lens (Carl-Zeiss Plan Neofluar 20x, NA 0.5, Thornwood, NY) focused the optical emission from the capillary and a combination of a dichroic mirror (cutoff at 500 nm) and optical filters (a 600-nm long-pass filter and a 750-nm band-pass filter, angle tuned) allowed the photoluminescence into an IR-sensitive photomultiplier tube (R374, Hamamatsu, Bridgewater, NJ). A Keithley 6485 picoammeter (Cleveland,OH) converted photocurrent from the photomultiplier tube to a

dc voltage signal. An IBM-compatible computer with a PeakSimple Chromatographic Data System (SRI Instruments, Torrance, CA) collected the dc signal after a 0.4-Hz eight-pole low-pass filter (Wavetek 852 Dual filter, San Diego, CA).

5.3.5. Chromatographic conditions for determination of carbidopa and dopamine

Chromatographic conditions for carbidopa separation were optimized by changing the mobile phase composition. Aqueous buffers containing a mixture of monochloroacetic acid and sodium acetate (total concentration of 100 mM), 0.15 mM disodium EDTA, and SOS (pH was adjusted with concentrated NaOH solution) was mixed with acetonitrile, the organic modifier. The mobile phase was passed through a Nylon filter with 0.45 μm pores (Osmonics, Minnetonka, MN). The capillary column at the optimized condition was slurry packed to 7.6 cm with 2.6 μm XTerra MS-C_{18} (Waters, Milford, MA) reversed-phase particles.

5.3.6. Chromatographic standard samples

Stock solutions of 1.0 mM catechols and carbidopa were prepared in 0.1 M acetic acid and stored frozen. The frozen stock solutions were thawed before each use and were diluted to desired concentrations in degassed solutions. Typically, successive 10 fold dilutions were made using 0.1 M acetic acid except the final dilution. The final dilution which made injection solutions, were 10% of stock solution (in 0.1 M acetic acid) in 80% of artificial cerebrospinal fluid (aCSF) and 10% of 1 M acetic acid. The aCSF contained 145.0 mM NaCl, 2.7 mM KCl, 1.0 mM $MgCl_2$, 1.2 mM $CaCl_2$, 0.45 mM NaH_2PO_4 and 1.55 mM Na_2HPO_4 at pH 7.40.

5.3.7. Temperature effect on detection sensitivity

A homemade heating block controlled the temperature of the CTR. A Minco PID controller (Model CT15122, Minneapolis, MN) drove two square-shaped silicon rubber heaters (SRFG-202/10, 5 x 5 cm^2, 2.5 W/in^2, Omega, Stamford, CT). An aluminum block directly on top of the heaters transferred heat to the confluence end of the CTR. Between the CTR and the aluminum block were silicon rubber sheets (0.10" thickness, McMaster-Carr, Cleveland, OH) to enhance the thermal contact. All the heating assembly is placed inside of insulator blocks made from calcium silicate (McMaster-Carr). The insulator assembly helped to stabilize the temperature of the heating block. An elastomer-coated temperature sensor (Minco, S665PDZ24A) in the insulator assembly monitored the actual temperature, and this information was used as a feedback to the PID controller.

For each new temperature setting, enough thermal equilibration time was given. Once the temperature became stable, a blank injection with aCSF was made to determine the baseline noise level. The baseline signal from 1 to 4 minutes was analyzed with Microsoft Excel's REGRESSION function. After a linear regression was made for a given data set, the standard deviation of Y-residual values was taken as the noise level. Thus the noise measurement does not include linear changes in the baseline.

5.3.8. Animal and surgical procedures

All procedures involving animals were conducted with approval of the Institutional Animal Care and Use Committee of the University of Pittsburgh. Male Sprague–Dawley rats (250–375 g,

Hilltop, Scottdale, PA, USA) were anesthetized with chloral hydrate (initial dose of 300 mg/kg i.p. with additional doses of 50 mg/kg i.p. as needed to maintain anesthesia) and wrapped in a homeothermic blanket (EKEG Electronics, Vancouver, BC, Canada). The rats were placed in a stereotaxic frame (David Kopf Instruments, Tujunga, CA, USA) with the incisor bar set at 5 mm above the interaural line[58] and appropriately placed holes were drilled through the skull.

5.3.9. Microdialysis

Vertical concentric microdialysis probes (220 μm o.d., 4 mm long) were constructed with hollow fiber dialysis membrane (Spectra-Por RC Hollow Fiber, MWCO: 13,000, 160 μm i.d., Spectrum Laboratories Inc., Rancho Dominguez, CA) and fused silica outlet lines (150 μm o.d., 75μm i.d., Polymicro Technologies, Phoenix, AZ). The microdialysis probe was implanted into the brain over a period of 30 min to the following coordinates: 2.5 mm anterior to bregma, 2.5 mm lateral from midline and 7.0 mm below dura. The probe was perfused at 0.586 μL/min for 2 hours before the initial sample collection. Five consecutive 10-min dialysis samples were collected in vials containing 0.65 μL of 1 M acetic acid (10% of total volume). After collecting 5 pre-drug dialysis samples, the rat was given a single i.p. injection. Three rats received carbidopa (150 mg/kg, i.p.) in phosphate buffered saline (PBS) and another three received volume-matched PBS. Six additional 10-min dialysis samples were collected as described above. All collected dialysates were stored in an ice bath for immediate analysis, or frozen for future use. Concentrations of dopamine and carbidopa were determined by HPLC-PFET using a blind testing format.

5.4. Results and Discussion

5.4.1. Optimizing separation conditions

There are several studies on chromatographic separation of carbidopa in biological fluids. However, the sample matrices of the studies were mainly human plasma[132-135] or urine,[134, 135] which differ greatly from brain dialysates. Thus separation conditions for carbidopa were selected based on the previous conditions for monoamine separation.[136] Changing the pH of the mobile phase was most effective in achieving a successful separation of carbidopa from interfering peaks. The carboxylic acid end of carbidopa was deprotonated in weakly acidic conditions. Carbidopa was not retained well in a reversed-phase stationary phase due to the hydrophilic nature of the carboxylate. However, the pH of the mobile phase changed the hydrophilicity of carbidopa: decreasing the pH of the mobile phase protonated the carboxylate, thus making carbidopa more hydrophobic. The pH of the mobile phase was lowered to 2.30 at the optimal condition for the carbidopa separation. The very low pH of the mobile phase, however, was not compatible with the injection sample matrix. Carbidopa and dopamine dissolved in aCSF, a phosphate buffer at pH 7.40, showed split or broadened peak shape. On the other hand, same analytes in 0.1 M acetic acid gave very sharp peaks. Thus 10% of 1 M acetic acid was included in the injection sample in aCSF to make the injection sample more acidic. The acidic sample showed sharp and reproducible peaks upon injection. Figure 5-1 shows a typical chromatogram for a standard separation using a pH 2.30 aqueous buffer (90 mM monochloroacetic acid and 10 mM sodium acetate) with 0.15 mM disodium EDTA and 13 mM SOS, mixed with 12.5% (v/v) acetonitrile.

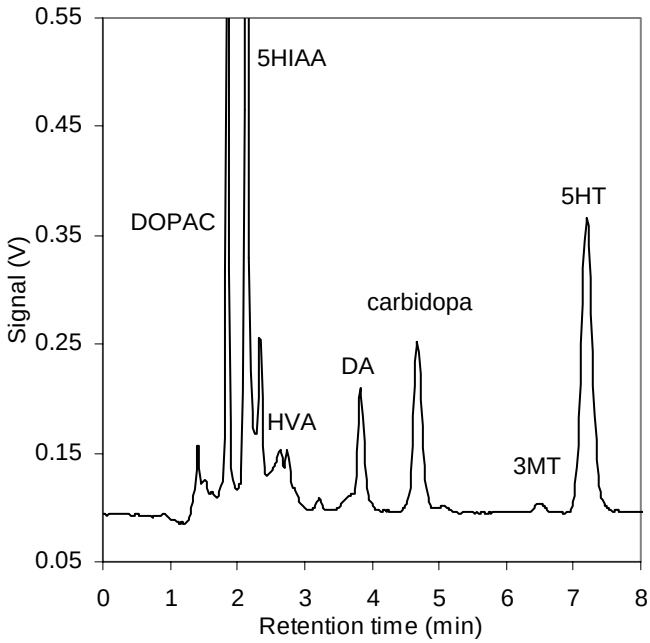

Figure 5–1. Separation of standards.

Concentrations of the analytes were ~100 nM. Separation conditions were as follows. Column: 100 μm i.d., 7.6 cm length capillary column packed with XTerra MS-C_{18} reversed phase particles. Mobile phase: pH 2.30 aqueous buffer containing 90 mM monochloro acetic acid, 10 mM sodium acetate, 0.15 mM disodium EDTA and 13.0 mM SOS, mixed with 12.5% (v/v) acetonitrile. Flow rate: 1 μL/min. Injection volume: 500 nL.

The PFET system is also influenced by the pH of the mobile phase. As reported previously, the reaction rates of the PFET reagent with catechols are pH dependent.[45, 111] Direct comparison of chromatograms of the standards revealed that the peak heights at pH 2.30 were much smaller than those from a previous report[136] at pH 4.00. The small peak height is a result of slower kinetics. To increase the reaction rate, the reactor tubing of the CTR was heated in a homemade heater, as reported previously.[111] The results are in Figure 5-2. Increasing the reactor temperature increased the peak area and height by speeding up the reaction kinetics; however, the noise level increased accordingly. Therefore there was no overall benefit in detection sensitivity by heating the reactor. The reactor was maintained at 25°C at the optimal condition.

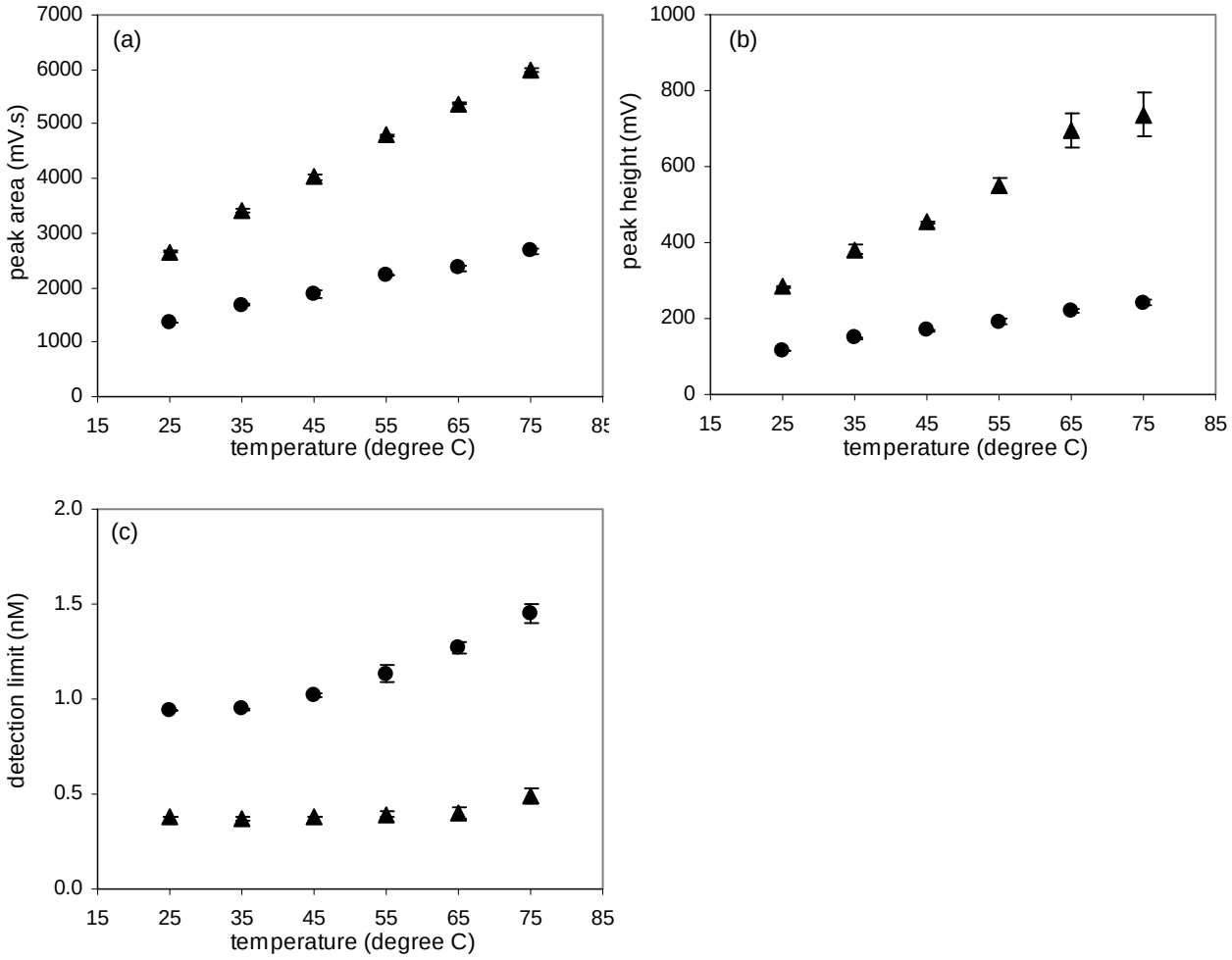

Figure 5–2. Reaction of 1^{3+} with dopamine and carbidopa at various temperatures.

(a) Peak area, (b) peak height and (c) detection limit are compared for chromatographic peaks of dopamine (●) and carbidopa (▲).The error bars on the figure represents the standard errors of the mean. Separation conditions were as follows. Column: 100 μm i.d., 7.6 cm length capillary column packed with XTerra MS-C_{18} reversed phase particles. Mobile phase: pH 2.40 aqueous buffer containing 85 mM monochloroacetic acid, 15 mM sodium acetate, 0.15 mM disodium EDTA and 10.0 mM SOS, mixed with acetonitrile (89:11, v/v). Flow rate: 1 μL/min. Injection volume: 500 nL.

5.4.2. Analysis of rat brain microdialysis

The rat brain microdialysis samples were analyzed at the optimal separation conditions to determine the carbidopa and dopamine concentrations. Calibration fits were constructed using standard solutions containing 0 – 100 nM carbidopa and dopamine before analyzing each set of

rat brain dialysates. Typical regression equations for peak heights versus concentrations (mV/nM) were: $y = 1.58 x + 1.63$ ($r^2 = 0.9993$) for dopamine and $y = 2.84 x + 1.99$ ($r^2 = 0.9997$) for carbidopa. The concentration detection limits were calculated from the calibration fit using signal to noise ratio of 3. Typical concentration detection limits were 570 pM for dopamine and 320 pM for carbidopa. Corresponding mass detection limits based on 500 nL injection were 290 amol for dopamine and 160 amol for carbidopa.

Figure 5-3 and 5-4 show typical chromatograms of dialysates before and after the injection of PBS and carbidopa, respectively. The error bars on the figure represent the standard errors of the means. Concentration changes of dopamine and carbidopa with time are in Figure 5-5. We observed that the concentration of carbidopa increased just after the injection of carbidopa, while there was no observable change upon injection of PBS. It is thus clear that the carbidopa in the extracellular space of the brain came from the i.p. injection of carbidopa, possibly as a result of the traumatic injury caused by the microdialysis probe. The relatively big error bars on measured carbidopa concentrations might also be evidence of traumatic injury. Since the extent of the breach at the BBB by the microdialysis probes cannot be quantitatively measured nor repeated, the level of carbidopa is expected to vary.

It has to be noted from Figure 5-5, it appears as though there was carbidopa in the brain dialysates even before carbidopa was injected. This was due to the unidentified transient peak overlapping the carbidopa peak. The unidentified peaks were not always found in dialysates. Even dialysates from a same set showed different responses. However, the height of the unidentified peak was always negligible compared to that of carbidopa peak. Thus it is unlikely that the large increase of the peak height after the injection was due to the unidentified peak. Moreover, the huge increase in the peak height was never observed when the rat was given PBS.

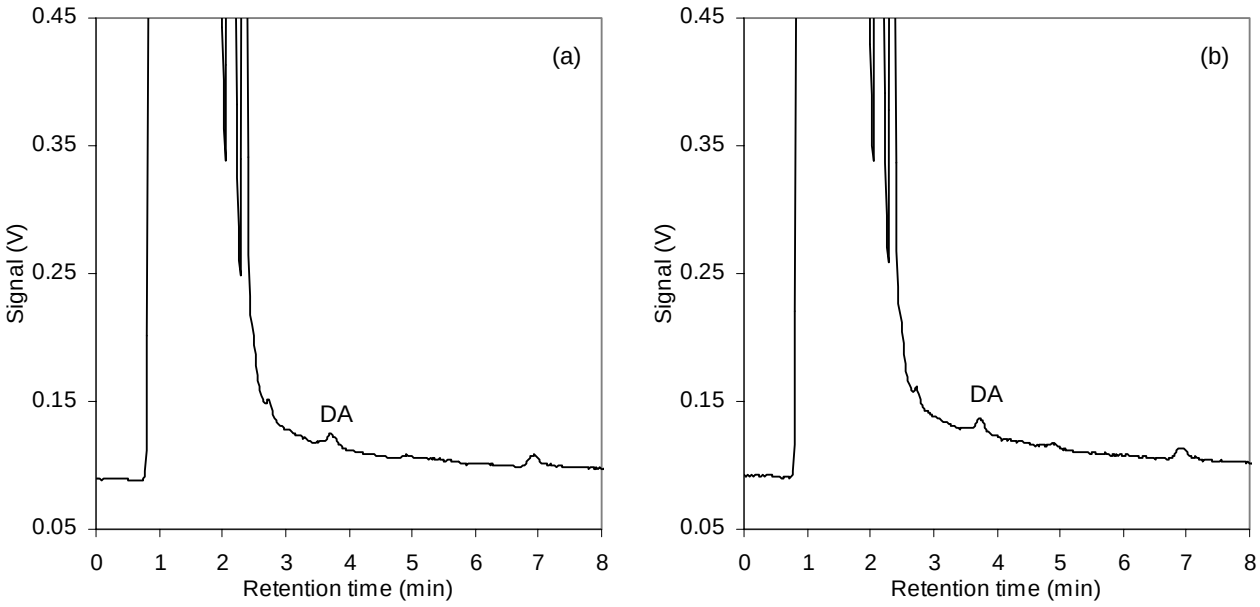

Figure 5–3. Typical chromatograms (a) before and (b) after the administration of PBS. Separation conditions were same as in Figure 5-1.

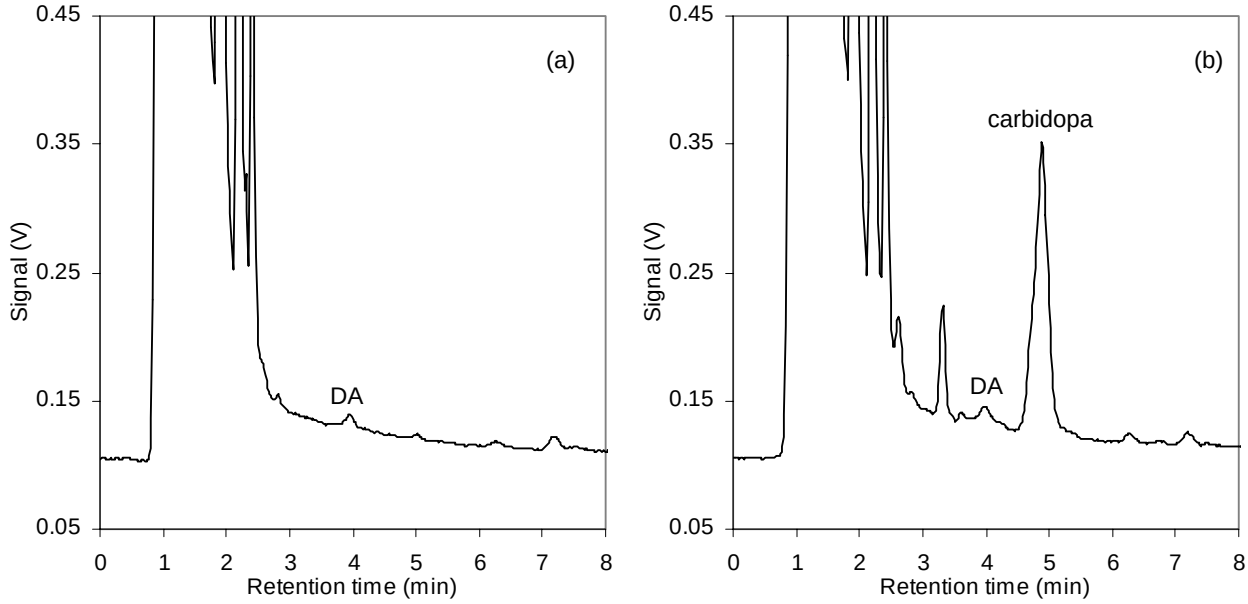

Figure 5–4. Typical chromatograms of (a) before and (b) after the administration of carbidopa. Separation conditions were same as in Figure 5-1.

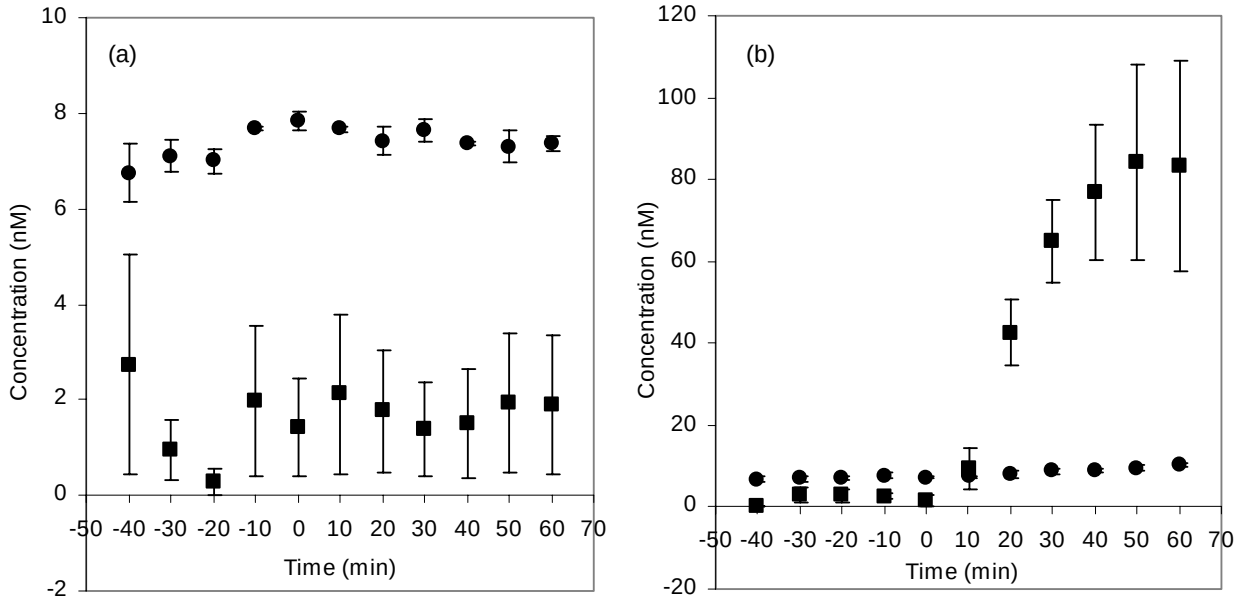

Figure 5–5. Concentration of dopamine(●) and carbidopa (■) after administration of (a) PBS (control) and (b) carbidopa.

The error bars on the figure represents the standard errors of the mean (n=3).

APPENDIX

PFET optics alignment procedures

The optical setup of the PFET system needs to be optimized to obtain a maximum efficiency. It is especially important when the photoluminescence from the PFET is not strong. $\mathbf{1}^{2+}$, the PFET reagent used in this study, is an example.

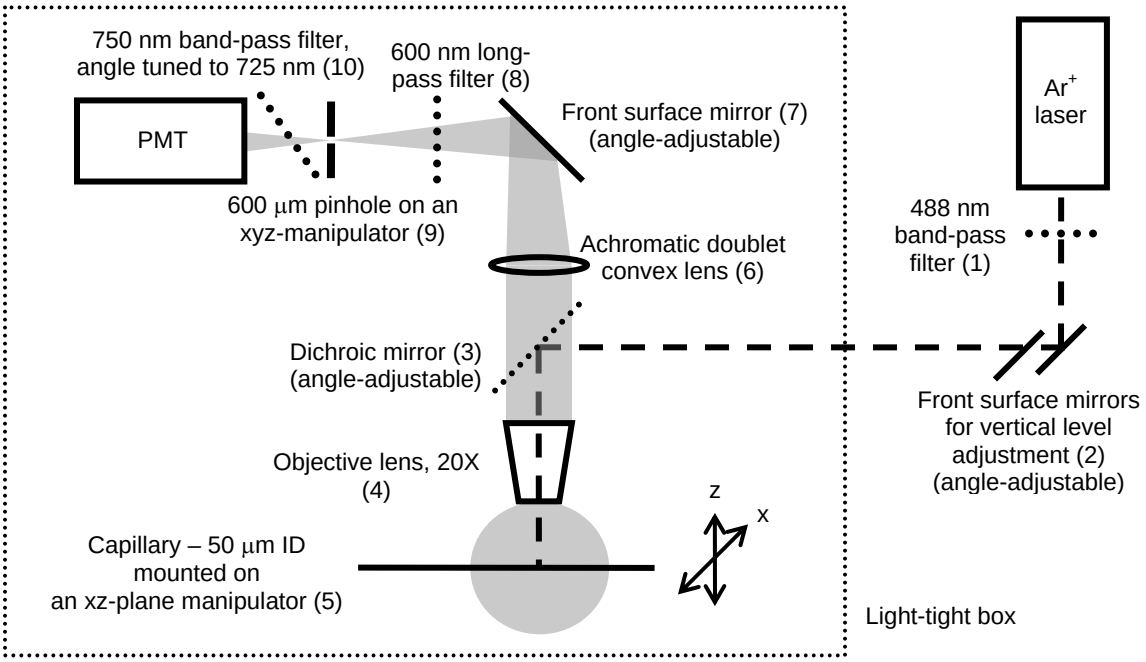

Figure A–1. The layout of the optical setup. Each optical part is labeled with numbers.

A slight move of the laser beam position changes the entire beam path, thus total alignment of the system starts from the argon ion laser. Such a complete alignment is normally not necessary for routine use. Daily focusing should be limited to fine-tuning the capillary position under the objective lens (5). Further focusing can be achieved by adjusting the pinhole position (9). Such pinhole position adjustments are expected only once in several months. If another PFET reagent or a luminophore with a different maximum emission wavelength is used, the emission optics (parts after the front-surface mirror (7) above the dichroic mirror (3)) should be replaced to accommodate the new wavelength. Any alignment procedure requires proper protective eyewear to protect eyes from the strong laser beam.

A.1. Alignment of the excitation laser beam

The laser system used in this study is a Cyonics/Uniphase 30-mW variable power blue-line laser. The laser beam consists of several monochromic lights with wavelengths around 480 nm. Previous experiments found that the excitation of $\mathbf{1}^{2+}$ with only 480 nm is most effective in the PFET application: the photoluminescence intensity was the largest with small optical background noises. Thus a 488 nm band-pass filter (1) is placed after the argon ion laser to attenuate other wavelengths. The filter was slightly angle-tuned. The exact angle of the filter was found from a spectrophotometer placed after the filter.

The clean 488 nm laser beam is directed to the dichroic mirror (3). Since an objective lens (4) and an xz-plane manipulator (with a capillary holder, 5) are attached directly beneath the dichroic mirror, the vertical position of the dichroic mirror is higher than that of the laser unit. A couple of front surface mirrors (2) bring the laser beam to the height of the dichroic mirror (3).

The xz-plane manipulator (5) is removed temporarily. A dark-colored paper is placed under the objective lens so that the image of the beam can be seen on the paper. A distinguishable image can only be seen when the distance between the paper and the objective lens is much larger than the focal length of the objective lens. (Figure A-2 (a)) The beam is positioned on the dichroic mirror so that it is a little apart from the center. At the same time, the beam image on the paper should form an oval. An eclipsed oval tells that the beam is hitting a non-reflective surface such as the inner barrel of the objective lens: the angle of the dichroic mirror is adjusted so that the image is no longer eclipsed.

After the excitation beam is aligned in the objective lens, a front-surface mirror is placed under the objective lens with an xz-plane manipulator (Figure A-2 (b)). The mirror on the manipulator is adjusted so that the laser beam is focused on the mirror. The reflection of the laser beam can be seen on the surface of the dichroic mirror (3) or on the front surface mirror (2). It is easier to view the reflections on the front surface mirror. The two reflections should not overlap: overlapping the excitation beam and its reflection results in a noisy optical background.

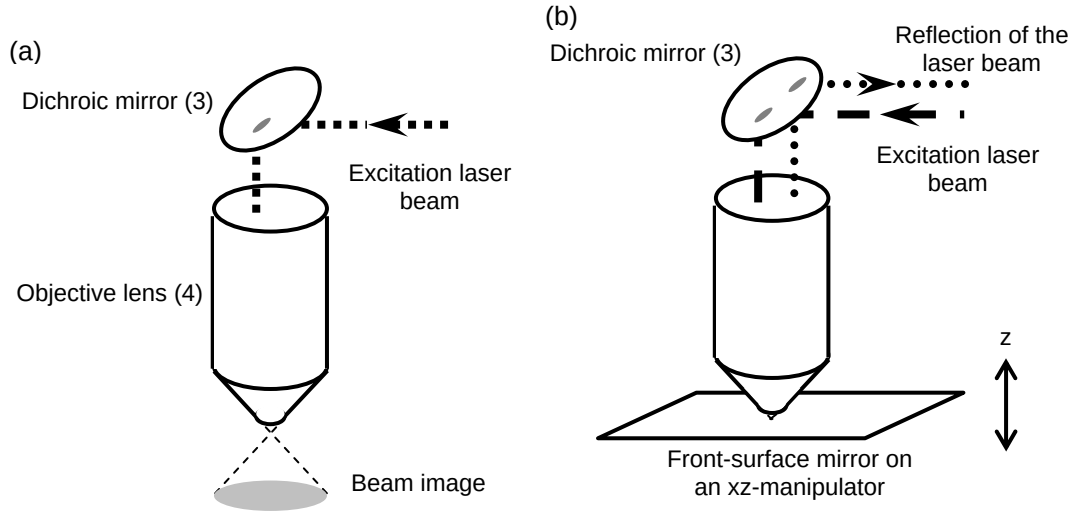

Figure A–2. The alignment of the excitation beam.
(a) The excitation beam through the objective lens should form an oval image. (b) The excitation laser beam and its reflection should not overlap at the dichroic mirror (3).

A.2. Rough alignment of the emission optics using Rhodamine 590

The emission optics mainly consists of the objective lens (the same objective lens used to focus the excitation beam), a convex lens and a photomultiplier tube assembly. The emission optics is roughly aligned using a bright fluorophore, Rhodamine 590. The emission from a PFET reagent could be used, but the emission from $\mathbf{1}^{2+}$ is colorless (λ_{max} ~ 723 nm). The bright green fluorescence from Rhodamine is useful in visualizing the emission beam path.

The front surface mirror on the xz-manipulator (5) is replaced with a capillary filled with the ethanol solution of Rhodamine (~ 10 μM). A 1-cm section of the capillary is burnt to remove the opaque polyimide coating on the capillary, thus serving as a detection window. The excitation laser beam is focused on the detection window. The objective lens captures the fluorescence from Rhodamine, as well as the reflected laser beam. Most of the reflection does not pass the dichroic mirror (3) but a fraction does, resulting in a background noise: optical filters are placed later in front of the photomultiplier tube to filter out the reflected beam.

The emission beam after the objective (4) lens is rather large in its size. Thus a convex lens (6) was placed above the dichroic mirror to condense the beam. The convex lens used in this study has a focal length of 20 cm. Another front surface mirror (7) was placed with an angle so that the emission is directed to the photomultiplier tube (PMT). An IR-sensitive PMT from Hamamatsu (R374) was used to measure the photoluminescence from $\mathbf{1}^{2+}$. However, a PMT detects the photons from the photoluminescence as well as the fraction of excitation beam passing the dichroic mirror (3). Thus a band-pass filter (10) was tightly attached in front of the PMT. A 750 nm band-pass filter was angle-tuned to adjust the transmittance maximum to be around 725 nm, which is close to the emission maximum of $\mathbf{1}^{2+}$ (λ_{max} ~ 723 nm). The exact angle

was found by trial-and-error using a conventional UV spectrometer. A 600 μm pinhole was mounted on a xyz-manipulator (9) and placed in front of the PMT/band-pass filter assembly. This pinhole serves as the only opening allowing photons to be directed into the PMT.

The position of the PMT assembly is adjusted so that the focus of the emission beam is directed through the pinhole. Beside the green fluorescence from Rhodamine, reflection of the excitation laser is focused as a blue dot. The position of the blue dot does not overlap the fluorescence focus as long as the objective lens is aligned as shown in Figure A-2(b). The PMT assembly position is fine-adjusted so that only green focus from Rhodamine is directed into the pinhole (9) by changing the angle of the front-surface mirror (7) and the position of the pinhole.

A.3. Fine alignment with the PFET reagent

The emission from PFET reagent has different wavelength from that from Rhodamine. The exact beam path differs slightly due to the chromatic aberration. Therefore, the emission optics requires fine tuning using the actual PFET reagent. The capillary filled with Rhodamine is replaced with the PFET detection capillary. The detection capillary is either made with a transparent-coated capillary or a polyimide coated capillary with a detection window.

A 600 nm long-pass filter (8) is then attached between the PMT assembly and the front surface reflector (7), but this filter can often be omitted without increasing the background noise. A homemade light-tight box houses the optics as shown in Figure A-1. A small opening accommodates the path of the excitation laser beam into the light-tight box. As the PFET reagent solution is pumped through the capillary, the laser beam is focused onto the detection capillary by adjusting the xz-manipulator (5). The PMT is powered up to monitor the signal. The position

of the pinhole is also fine-tuned using the xyz-manipulator (9). Both the detection capillary position and the pinhole position are repeatedly adjusted to maximize the PMT signal.

A.4. Checking for the stray light

Once the PMT signal is maximized, the supply of the PFET reagent is stopped and the acetonitrile is pumped. Acetonitrile does not give any photoluminescence at this wavelength window. Thus the PMT signal should drop quickly close to zero. The signal is the optical background noise of the system. Optical noise is a result of stray light from the excitation laser or outside light reaching the PMT.

BIBLIOGRAPHY

(1) Tswett, M. S. *Ber. Bot. Ges.* **1906**, *24*, 316-332.

(2) Simoni, R. D.; Hill, R. L.; Vaughan, M. *J. Biol. Chem.* **2002**, *277*, 28.

(3) Martin, A. J. P.; Randall, S. S. *Biochem. J.* **1951**, *49*, 293.

(4) Tiselius, A.; Clasesson, D. *Arkiv. Kemi Mineral. Geol.* **1942**, *18*, 15B.

(5) Scott, R. P. W. *Liquid chromatography detectors*; Elsevier: New York, NY, 1986.

(6) Jorgenson, J. W.; Lukacs, K. D. *Science (Washington, D.C.)* **1983**, *222*, 266-272.

(7) Nickerson, B.; Jorgenson, J. W. *J. Chromatogr.* **1989**, *480*, 157-168.

(8) Jung, M. C. *PittCon 2003*, Orlando, FL 2003.

(9) Woltman, S. J.; Even, W. R.; Sahlin, E.; Weber, S. G. *Anal. Chem.* **2000**, *72*, 4928-4933.

(10) Woltman, S. J.; Even, W. R.; Weber, S. G. *Anal. Chem.* **1999**, *71*, 1504-1512.

(11) Beisler, A. T.; Sahlin, E.; Schaefer, K. E.; Weber, S. G. *Anal. Chem.* **2004**, *76*, 639-645.

(12) Beisler, A. T.; Schaefer, K. E.; Weber, S. G. *J. Chromatogr., A* **2003**, *986*, 247-251.

(13) Ungerstedt, U.; Herrera-Marschitz, M.; Jungnelius, U.; Stahle, L.; Tossman, U.; Zetterstroem, T. *Adv. Biosci.* **1982**, *37*, 219-231.

(14) Robinson, T. E.; Justice, J. B. *Microdialysis in the Neurosciences*; Elsevier: Amsterdam, 1991.

(15) Khan, A. S.; Michael, A. C. *Trends Anal. Chem.* **2003**, *22*, 503-508.

(16) Watson, C. J.; Venton, B. J.; Kennedy, R. T. *Anal. Chem.* **2006**, *78*, 1391-1399.

(17) Chen, J.-G.; Woltman, S. J.; Weber, S. G. *Adv. Chromatogr.* **1996**, *36*, 273-313.

(18) Sahlin, E.; Beisler, A. T.; Sandberg, M.; Weber, S. G. In *Electroanalytical Methods for Biological Materials*; Brajter-Toth, A., Chambers, J. Q., Eds.; Marcel Dekker, Inc: NY, 2002, pp 367-398.

(19) Albery, W. J.; Svanberg, L. R.; Wood, P. *J. Electroanal. Chem. Interfacial Electrochem.* **1984**, *162*, 45-53.

(20) Dou, L.; Krull, I. S. *Anal. Chem.* **1990**, *62*, 2599-2606.

(21) Kissinger, P. T. *J. Pharm. Biomed. Anal.* **1996**, *14*, 871-880.

(22) Al-Arfaj, N. A. *Talanta* **2004**, *62*, 255-263.

(23) Monji, H.; Yamaguchi, M.; Aoki, I.; Ueno, H. *J. Chromatogr., B* **1997**, *690*, 305-313.

(24) Wei, S.; Zhao, L.; Cheng, X.; Lin, J.-M. *Anal. Chim. Acta* **2005**, *545*, 65-73.

(25) Holeman, J. A.; Danielson, N. D. *J. Chromatogr., A* **1994**, *697*, 277-284.

(26) Xi, J.; Shi, B. A.; Ai, X.; He, Z. *J. Pharm. Biomed. Anal.* **2004**, *36*, 237-241.

(27) Bolden, M. E.; Danielson, N. D. *J. Chromatogr., A* **1998**, *828*, 421-430.

(28) Noffsinger, J. B.; Danielson, N. D. *J. Chromatogr.* **1987**, *387*, 520-524.

(29) Kim, Y.-S.; Park, J. H.; Choi, Y.-S. *Bull. Kor. Chem. Soc.* **2004**, *25*, 1177-1181.

(30) Saito, K.; Murakami, S.; Yamazaki, S.; Muromatsu, A.; Hirano, S.; Takahashi, T.; Yokota, K.; Nojiri, T. *Anal. Chim. Acta* **1999**, *378*, 43-46.

(31) Tsukagoshi, K.; Miyamoto, K.; Nakajima, R.; Ouchiyam, N. *J. Chromatogr., A* **2001**, *919*, 331-337.

(32) Ishida, J.; Takada, M.; Hitoshi, N.; Iizuka, R.; Yamaguchi, M. *J. Chromatogr., B* **2000**, *738*, 199-206.

(33) Takezawa, K.; Tsunoda, M.; Watanabe, N.; Imai, K. *Anal. Chem.* **2000**, *72*, 4009-4014.

(34) Yakabe, T.; Yoshida, H.; Nohta, H.; Yamaguchi, M. *Anal. Sci.* **2002**, *18*, 1375-1378.

(35) Chen, X.; Sato, M. *Anal. Sci.* **1995**, *11*, 749-754.

(36) Zorzi, M.; Pastore, P.; Magno, F. *Anal. Chem.* **2000**, *72*, 4934-4939.

(37) Guo, Z.; Dong, S. *Electroanalysis* **2005**, *17*, 607-612.

(38) Morita, H.; Konishi, M. *Anal. Chem.* **2002**, *74*, 1584-1589.

(39) Uchikura, K. *Chem. Pharm. Bull.* **2003**, *51*, 1092-1094.

(40) Miao, W.; Bard, A. J. *Anal. Chem.* **2004**, *76*, 5379-5386.

(41) Miao, W.; Bard, A. J. *Anal. Chem.* **2004**, *76*, 7109-7113.

(42) Miao, W.; Choi, J.-P.; Bard, A. J. *J. Am. Chem. Soc.* **2002**, *124*, 14478-14485.

(43) Wightman, R. M.; Forry, S. P.; Maus, R.; Badocco, D.; Pastore, P. *J. Phys. Chem. B* **2004**, *108*, 19119-19125.

(44) Zhan, W.; Alvarez, J.; Sun, L.; Crooks, R. M. *Anal. Chem.* **2003**, *75*, 1233-1238.

(45) Jung, M. C.; Weber, S. G. *Anal. Chem.* **2005**, *77*, 974-982.

(46) Juris, A.; Balzani, V.; Barigelletti, F.; Campagna, S.; Belser, P.; Von Zelewsky, A. *Coord. Chem. Rev.* **1988**, *84*, 85-277.

(47) Zhang, C.; Haruyama, T.; Kobatake, E.; Aizawa, M. *Anal. Chim. Acta* **2000**, *408*, 225-232.

(48) Zakeeruddin, S. M.; Fraser, D. M.; Nazeeruddin, M. K.; Graetzel, M. *J. Electroanal. Chem.* **1992**, *337*, 253-283.

(49) Weaver, M. J. *J. Phys. Chem.* **1990**, *94*, 8608-8613.

(50) Nakabayashi, Y.; Nakamura, K.; Kawachi, M.; Motoyama, T.; Yamauchi, O. *J. Biol. Inorg. Chem.* **2003**, *8*, 45-52.

(51) Abruna, H. D. *J. Electroanal. Chem. Interfacial Electrochem.* **1984**, *175*, 321-326.

(52) Abruna, H. D. *J. Electrochem. Soc.* **1985**, *132*, 842-849.

(53) Sutin, N.; Creutz, C. *Adv. Chem. Ser.* **1978**, *168*, 1-27.

(54) Gaudiello, J. G.; Bradley, P. G.; Norton, K. A.; Woodruff, W. H.; Bard, A. J. *Inorg. Chem.* **1984**, *23*, 3-10.

(55) Watts, R. J.; Crosby, G. A. *J. Am. Chem. Soc.* **1971**, *93*, 3184-3188.

(56) Kennedy, R. T.; Jorgenson, J. W. *Anal. Chem.* **1989**, *61*, 1128-1135.

(57) Sahlin, E.; Beisler, A. T.; Woltman, S. J.; Weber, S. G. *Anal. Chem.* **2002**, *74*, 4566-4569.

(58) Pellegrino, L. J.; Pellegrino, A. S.; Cushman, A. J. *A Stereotaxic Atlas of the Rat Brain*, 2nd ed.; Plenum Press: New York, 1979.

(59) Chen, D. Y.; Dovichi, N. J. *J. Chromatogr., B* **1994**, *657*, 265-269.

(60) Harriman, A. *J. Phys. Chem.* **1987**, *91*, 6102-6104.

(61) Wardman, P. *J. Phys. Chem. Ref. Data* **1989**, *18*, 1637-1755.

(62) Abbaspour, A.; Mehrgardi, M. A. *Talanta* **2005**, *67*, 579-584.

(63) Rubinstein, I.; Bard, A. J. *J. Am. Chem. Soc.* **1981**, *103*, 512-516.

(64) Kalyanasundaram, K. *Photochemistry of polypyridine and porphyrin complexes*; Academic Press Inc.: San Diego, CA, 1992.

(65) Nord, G.; Wernberg, O. *J. Chem. Soc. Dalton Trans.* **1975**, *845-849*.

(66) Shi, M.; Anson, F. C. *Langmuir* **1996**, *12*, 2068-2075.

(67) Deakin, M. R.; Wightman, R. M. *J. Electroanal. Chem.* **1986**, *206*, 167-177.

(68) Laviron, E. *J. Electroanal. Chem.* **1983**, *146*, 15-36.

(69) Laviron, E. *J. Electroanal. Chem.* **1984**, *164*, 213-227.

(70) Lebeau, E. L.; Binstead, R. A.; Meyer, T. J. *J. Am. Chem. Soc.* **2001**, *123*, 10535-10544.

(71) Freeman, K.; Lin, P.; Lin, L.; Blank, C. L. In *High Performance Liquid Chromatography in Neuroscience Research*; Holman, R. B., Cross, A. J., Joseph, M. H., Eds.; John Wiley & Sons: Chichester, 1993, pp 27-55.

(72) Zahniser, N. R.; Larson, G. A.; Gerhardt, G. A. *J. Pharm. Exp. Ther.* **1999**, *289*, 266-277.

(73) Tsuda, T.; Novotny, M. *Anal. Chem.* **1978**, *50*, 271-275.

(74) Folestad, S.; Johnson, L.; Josefsson, B.; Galle, B. *Anal. Chem.* **1982**, *54*, 925-929.

(75) Huber, J. F. K.; Jonker, K. M.; Poppe, H. *Anal. Chem.* **1980**, *52*, 2-9.

(76) Fultz, M. L.; Durst, R. A. *Anal. Chim. Acta* **1982**, *140*, 1-18.

(77) Hupp, J. T.; Weaver, M. J. *Inorg. Chem.* **1983**, *22*, 2557-2564.

(78) Zhang, L.; Yeung, E. S. *J. Chromatogr., A* **1996**, *734*, 331-337.

(79) Emmer, A.; Roeraade, J. *J. Chromatogr., A* **1994**, *662*, 375-381.

(80) Kostel, K. L.; Lunte, S. M. *J. Chromatogr., B* **1997**, *695*, 27-38.

(81) Zhu, R.; Kok, W. T. *J. Chromatogr., A* **1995**, *716*, 123-133.

(82) Oldenburg, K. E.; Sweedler, J. V. *Analyst (Cambridge, U.K.)* **1997**, *122*, 1581-1585.

(83) Coble, P. G.; Timperman, A. T. *J. Chromatogr., A* **1998**, *829*, 309-315.

(84) Ye, M.; Hu, S.; Quigley, W. W. C.; Dovichi, N. J. *J. Chromatogr., A* **2004**, *1022*, 201-206.

(85) Andreev, V. P.; Koleshko, S. B.; Holman, D. A.; Scampavia, L. D.; Christian, G. D. *Anal. Chem.* **1999**, *71*, 2199-2204.

(86) Scampavia, L. D.; Blankenstein, G.; Ruzicka, J.; Christian, G. D. *Anal. Chem.* **1995**, *67*, 2743-2749.

(87) Oak, J.; Pence, D. V.; Liburdy, J. A. *Microscale Thermophys. Eng.* **2001**, *5*, 233-246.

(88) Bessoth, F. G.; deMello, A. J.; Manz, A. *Anal. Commun.* **1999**, *36*, 213-215.

(89) Weigl, B. H.; Bardell, R. L.; Kesler, N.; Morris, C. J. *Fresenius' J. Anal. Chem.* **2001**, *371*, 97-105.

(90) Choban, E. R.; Markoski, L. J.; Wieckowski, A.; Kenis, P. J. A. *J. Power Sources* **2004**, *128*, 54-60.

(91) Stroock, A. D.; Dertinger, S. K. W.; Ajdari, A.; Mezit, I.; Stone, H. A.; Whitesides, G. M. *Science (Washington, D.C.)* **2002**, *295*, 647-651.

(92) Marcus, R. A.; Sutin, N. *Biochim. Biophys. Acta* **1985**, *811*, 265-322.

(93) Yang, E. S.; Chan, M.-S.; Wahl, A. C. *J. Phys. Chem.* **1980**, *84*, 3094-3099.

(94) DuVall, S. H.; McCreery, R. L. *J. Am. Chem. Soc.* **2000**, *122*, 6759-6764.

(95) Hawley, M. D.; Tatwawadi, S. V.; Piekarski, S.; Adams, R. N. *J. Am. Chem. Soc.* **1967**, *89*, 447-450.

(96) Probstein, R. F. *Physicochemical Hydrodynamics*; John Wiley & Sons: New York, 1994.

(97) Rodriguez, M.; Bard, A. J. *Anal. Chem.* **1990**, *62*, 2658-2662.

(98) Shankar, A.; Lenhoff, A. M. *J. Chromatogr.* **1991**, *556*, 235-248.

(99) Nord, G.; Pedersen, B.; Farver, O. *Inorg. Chem.* **1978**, *17*, 2233-2238.

(100) Nestler, E. J.; Hyman, S. E.; Malenka, R. C. *Molecular Neuropharmacology*; McGraw-Hill: New York, 2001.

(101) Troyer, K. P.; Heien, M. L. A. V.; Venton, B. J.; Wightman, R. M. *Curr. Opinion Chem. Biol.* **2002**, *6*, 696-703.

(102) Michael, D.; Travis, E. R.; Wightman, R. M. *Anal. Chem.* **1998**, *70*, 586A-592A.

(103) Perez, X. A.; Andrews, A. M. *Anal. Chem.* **2005**, *77*, 818-826.

(104) Kumar, A. M.; Fernandez, J. B.; Schneiderman, N.; Goodkin, K.; Eisdorfer, C.; Kumar, M. *J. Liq. Chrom. & Rel. Technol.* **1999**, *22*, 2211-2223.

(105) Nagatsu, T. *J. Chromatogr.* **1991**, *566*, 287-307.

(106) Kissinger, P. T.; Bruntlett, C. S.; Shoup, R. E. *Life Sci.* **1981**, *28*, 455-465.

(107) Kehr, J. *J. Chromatogr., A* **1994**, *661*, 137-142.

(108) Parrot, S.; Bert, L.; Mouly-Badina, L.; Sauvinet, V.; Colussi-Mas, J.; Lambas-Senas, L.; Robert, F.; Bouilloux, J.-P.; Suaud-Chagny, M.-F.; Denoroy, L.; Renaud, B. *Cell. Mol. Biol.* **2003**, *23*, 793-804.

(109) Yoshitake, T.; Yoshitake, S.; Fujino, K.; Nohta, H.; Yamaguchi, M.; Kehr, J. *J. Neurosci. Methods* **2004**, *140*, 163-168.

(110) Chervet, J. P.; Van Soest, R. E. J.; Salzmann, J. P. *LC-GC* **1992**, *10*, 866, 868-871.

(111) Jung, M. C.; Munro, N.; Shi, G.; Michael, A. C.; Weber, S. G. *Anal. Chem.* **2006**, *78*, 1761-1768.

(112) Trabace, L.; Cassano, T.; Tucci, P.; Steardo, L.; Kendrick, K. M.; Cuomo, V. *Brain Res.* **2004**, *1008*, 293.

(113) Chaurasia, C. S.; Chen, C.-E.; Ashby, C. R., Jr. *J. Pharm. Biomed. Anal.* **1999**, *19*, 413-422.

(114) Bert, L.; Robert, F.; Denoroy, L.; Renaud, B. *Electrophoresis* **1996**, *17*, 523-525.

(115) Bert, L.; Robert, F.; Denoroy, L.; Stoppini, L.; Renaud, B. *J. Chromatogr., A* **1996**, *755*, 99-111.

(116) Parrot, S.; Sauvinet, V.; Riban, V.; Depaulis, A.; Renaud, B.; Denoroy, L. *J. Neurosci. Methods* **2004**, *140*, 29.

(117) Robert, F.; Bert, L.; Lambas-Senas, L.; Denoroy, L.; Renaud, B. *J. Neurosci. Methods* **1996**, *70*, 153.

(118) Desvignes, C.; Bert, L.; Vinet, L.; Denoroy, L.; Renaud, B.; Lambas-Senas, L. *Neurosci. Lett.* **1999**, *264*, 5-8.

(119) Roman, D. A.; Carretero, A. S.; Blanco, C. C.; Gutierrez, A. F. *Biomed. Chromatogr.* **2004**, *18*, 422-426.

(120) Fujino, K.; Yoshitake, T.; Kehr, J.; Nohta, H.; Yamaguchi, M. *J. Chromatogr., A* **2003**, *1012*, 169-177.

(121) Yoshitake, T.; Kehr, J.; Yoshitake, S.; Fujino, K.; Nohta, H.; Yamaguchi, M. *J. Chromatogr., B* **2004**, *807*, 177-183.

(122) Duine, J. M.; Floch, F.; Cann-Moisan, C.; Mialon, P.; Caroff, J. *J. Chromatogr., B* **1998**, *716*, 350-353.

(123) Heidbreder, C. A.; Lacroix, L.; Atkins, A. R.; Organ, A. J.; Murray, S.; West, A.; Shah, A. J. *J. Neurosci. Methods* **2001**, *112*, 135-144.

(124) Virag, L.; Whittington, R. A. *J. Chromatogr., B* **2002**, *772*, 267-272.

(125) Sabbioni, C.; Saracino, M. A.; Mandrioli, R.; Pinzauti, S.; Furlanetto, S.; Gerra, G.; Raggi, M. A. *J. Chromatogr., A* **2004**, *1032*, 65-71.

(126) Zhang, W.; Cao, X.; Xie, Y.; Ai, S.; Jin, L.; Jin, J. *J. Chromatogr., B* **2003**, *785*, 327-336.

(127) Cullison, J. K.; Waraska, J.; Buttaro, D. J.; Acworth, I. N.; Bowers, M. L. *J. Pharm. Biomed. Anal.* **1999**, *19*, 253-259.

(128) Vicente-Torres, M. A.; Gil-Loyzaga, P.; Carricondo, F.; Bartolome, M. V. *J. Neurosci. Methods* **2002**, *119*, 31-36.

(129) Calne, D. B. *N. Engl. J. Med.* **1993**, *329*, 1021-1027.

(130) Cooper, J. R.; Bloom, F. E.; Roth, R. H. *The Biochemical Basis of Neuropharmacology*, 8th ed.; Oxford University Press: Oxford, UK, 2003.

(131) Reynolds, J. E. F. *Martindale: the extra pharmacopoeia*, 31st ed.; Royal Pharmaceutical Society: London, 1996.

(132) Michotte, Y.; Moors, M.; Deleu, D.; Herregodts, P.; Ebinger, G. *J. Pharm. Biomed. Anal.* **1987**, *5*, 659-664.

(133) Nissinen, E.; Taskinen, J. *J. Chromatogr.* **1982**, *231*, 459-462.

(134) Sagar, K. A.; Smyth, M. R. *J. Pharm. Biomed. Anal.* **2000**, *22*, 613-624.

(135) Titus, D. C.; August, T. F.; Yeh, K. C.; Eisenhandler, R.; Bayne, W. F.; Musson, D. G. *J. Chromatogr.* **1990**, *534*, 87-100.

(136) Jung, M. C.; Shi, G.; Borland, L.; Michael, A. C.; Weber, S. G. *Anal. Chem.* **2006**, *78*, 1755-1760.